A Thesis for the Degree of Ph.D. in Engineering

Detection, Contamination Assessment, and Human Exposure Protection Measure of Aerosol Particle-Bound Polycyclic Aromatic Hydrocarbons Collected by the Cyclone Sampler

January 2024

Graduate School of Science and Technology

Keio University

JING, Weidong

Detection, Contamination Assessment, and Human Exposure Protection Measure of Aerosol Particle-Bound Polycyclic Aromatic Hydrocarbons Collected by the Cyclone Sampler

サイクロンサンプラーを用いて採取したエアロゾル粒子に含まれる多環芳香族炭化水素類の測定と汚染評価および健康影響防止対策

Jing Weidong
景 偉東

School of Science for Open and Environmental System, Graduate School of Science and Technology, Keio University
Environmental Chemistry Laboratory, Department of Applied Chemistry, Faculty of Science and Technology, Keio University
3-14-1 Hiyoshi, Kohoku Ward, Yokohama, Kanagawa 223-8522, Japan

Contents

Chapter 1: General Introduction to Particulate Matter Environmental Characteristics, and Particle-bound Polycyclic Aromatic Hydrocarbons (PAHs) Behaviors

1.1 Ambient particulate matter 1
1.1.1 Particulate matter environmental effect 1
1.1.2 Particulate matter toxicity 2
1.1.3 Particulate matter collection methods 3
1.2 Background of PM-bound polycyclic aromatic hydrocarbons 4
1.2.1 General information 4
1.2.2 Extracting and detecting methods of PM-bound PAHs 8
1.2.3 Emission sources of PM-bound PAHs 9
1.2.4 Human health risk 11
1.3 Objective of the research 13
1.4 References 16

Chapter 2: Optimization of the QuEChERS Extraction Method to Determine Polycyclic Aromatic Hydrocarbons (PAHs) in Powder Aerosol Particles Collected by Cyclone

2.1 Introduction 24
2.2 Materials and methods 27
2.2.1 Reagents and materials 27
2.2.2 Experimental design 28
2.2.3 Sample pre-treatment 29
2.2.4 PAHs analysis 30
2.2.5 Environmental powder aerosol sample 32
2.2.6 Statistical analysis 33
2.3 Results and discussion 34
2.3.1 I-optimal design results 34
2.3.2 Extraction parameters optimization 42
2.3.3 Actual sample extraction 47
2.4 Summary 49
2.5 Reference 50

Chapter 3: Pollution Characteristics, Sources, and Risk Assessment of Powder $PM_{2.5}$-bound Polycyclic Aromatic Hydrocarbons (PAHs) Collected at Yokohama, Japan between Pre- and Post-COVID-19

3.1 Introduction 59

3.2 Materials and methods 61
3.2.1 Sample collection 61
3.2.2 Chemical analysis 62
3.2.3 Meteorological conditions 67
3.2.4 Health risk assessments 67
3.3 Results and discussion 69
3.3.1 Pollution trends of PAHs in PM from 2018 to 2023 69
3.3.2 Meteorological conditions impact on PAHs contamination 71
3.3.3 Source identification 74
3.3.4 Health risk assessment 76
3.4 Summary 78
3.5 References 79

Chapter 4: Protective Effect of Astaxanthin Enriched in Japanese Raw Fish Diet Against PM-bound PAHs Induces Cell Damage

4.1 Introduction 85
4.2 Materials and methods 88
4.2.1 Chemical reagents 88
4.2.2 A549 cell culture 89
4.2.3 Cell viability 89
4.2.4 Reactive oxygen species (ROS) 90
4.2.5 RT-PCR 90
4.2.6 Atmospheric aerosol samples 91
4.2.7 Statistical analysis 92
4.3 Results and discussion 92
4.3.1 Harmful effects of ATX on cells viability 92
4.3.2 Cell hazard testing for PAHs solutions 95
4.3.3 Protection effect of ATX for PAHs exposed A549 cells 96
4.3.4 ATX cell protection validation experiments 97
4.3.5 ROS 99
4.3.6 ATX protection effect for actual aerosol exposure to A549 cell 102
4.4 Summary 106
4.5 References 107

Chapter 5: Characterization of elemental compositions and valence states of cyclone-collected aerosol particles using EDXRF and XAFS at three sites in Japan

5.1 Introduction 112
5.2 Experimental 115
5.2.1 Sample collection 115

5.2.2 EDXRF analysis....116
5.2.3 XAFS spectra analysis....118
5.2.4 Indices of source identification....120
5.3 Results and discussion....121
5.3.1 Metallic element concentration in aerosol particles....121
5.3.1.1 Cr....121
5.3.1.2 Mn....122
5.3.1.3 Fe....122
5.3.1.4 Cu....122
5.3.1.5 Zn....123
5.3.2 Valence state of target elements....126
5.3.2.1 Mn....126
5.3.2.2 Fe....126
5.3.2.3 Cu....127
5.3.2.4 Zn....127
5.3.3 Source identification....129
5.3.3.1 Enrichment factors (EFs)....129
5.3.3.2 Correlation analysis....130
5.3.3.3 Principal component analysis (PCA) and cluster analysis (CA)....136
5.3.4 Potential contribution for PAHs photocatalytic and PM oxidative potential....139
5.4 Summary....141
5.5 References....142

Chapter 6: General conclusions and future outlook

6.1 General conclusions....150
6.2 Future outlook....152

List of publications....156

ACKNOWLEDGMENTS....157

Chapter 1: General Introduction to Particulate Matter Environmental Characteristics, and Particle-bound Polycyclic Aromatic Hydrocarbons (PAHs) Behaviors

1.1 Ambient particulate matter

1.1.1 Particulate matter environmental effect

Atmospheric aerosol is a relatively stable homogeneous dispersion system of solid or liquid particles suspended in the air with a particle size of 0.01 μm ~ 100 μm together with a gas carrier, and the solid or liquid particles in this multiphase system are usually referred to as particulate matter [1]. According to the correlation between the chemical components, sources and health hazards of atmospheric particulate matter and particle size, atmospheric particulate matter can be divided into total suspended particulate matter (TSP, aerodynamic equivalent diameter ≥ 100 μm), respirable particulate matter (PM_{10}, aerodynamic equivalent diameter ≤ 10 μm), and PM_{10} can be divided into coarse particulate matter (2.5 μm ≤ aerodynamic equivalent diameter < 10 μm) and fine particulate matter ($PM_{2.5}$, aerodynamic equivalent diameter ≤ 2.5 μm) [2], [3]. Compared with coarse particulate matter, fine particulate matter has smaller particle size, larger specific surface area, relatively slow deposition rate, and longer stay in the atmosphere. It is more likely to carry airborne toxic and harmful pollutants such as heavy metals and PAHs, thus having greater chemical activity and toxicity [4], [5]. The smaller the particle size, the deeper the entry into the respiratory system area, such as TSP will be filtered by the nasal mucosa, between 2.5 μm and 10 μm particles can enter the upper respiratory tract, but $PM_{2.5}$ can be deposited in the bronchial tubes and alveoli through the upper respiratory tract (**Fig. 1.1**).

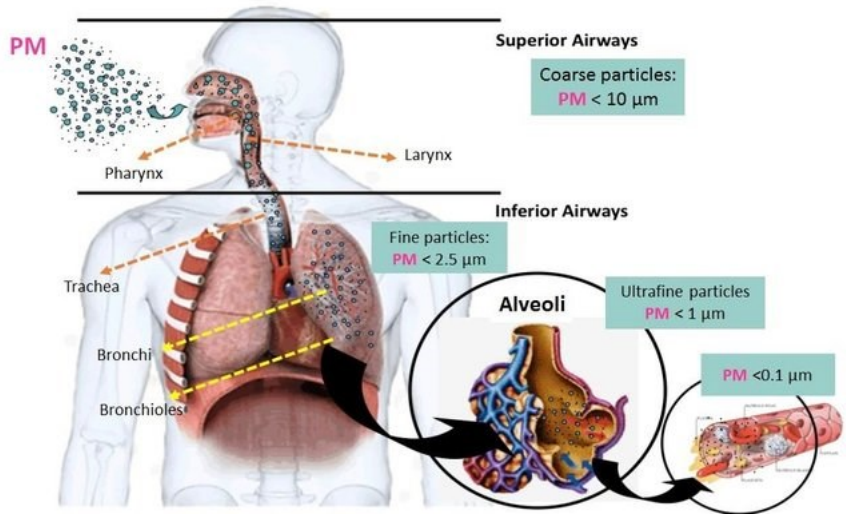


Fig. 1.1 Respiratory tract and particulate matter (PM) size classification [6]

This work © 2 by Fiorella F. Barraza Castelo is licensed under CC BY-NC-SA 4.0.
To view a copy of this license, visit http://creativecommons.org/licenses/by-nc-sa/4.0/

1.1.2 Particulate matter toxicity

Atmospheric particulate matter exposure can induce or exacerbate respiratory diseases, cardiovascular diseases, diabetes, and diseases due to early childhood [7]. $PM_{2.5}$ first enters the lungs through the respiratory tract and is deposited on the surfaces of the pulmonary bronchioles and alveoli, causing respiratory infections and decreased lung function, which can lead to chronic obstructive pulmonary disease (COPD), asthma, pulmonary fibrosis, and even lung cancer [6], [8]–[10]. $PM_{2.5}$ alters subclinical indices of cardiovascular function, which correlates with the rate of cardiovascular. Long-term exposure to $PM_{2.5}$ promotes the incidence of diabetes, induces diversification of the pathogenesis of type 2 diabetes, and may increase the risk of death from diabetes even when exposed to low concentrations of $PM_{2.5}$ [11], [12]. In addition, $PM_{2.5}$ exposure during pregnancy is strongly associated with preterm birth, low birth weight and neonatal death, and the adverse health effects continue into childhood and adulthood [13]. In October 2013, the International Agency for Research on Cancer (IARC) reported that $PM_{2.5}$ was identified as a Group I carcinogen [14]. The World Health Organization (WHO) stated that air pollution is the second highest risk factor for non-communicable diseases and that 99% of the world's population as of 2019 live

in places that do not meet the standards of the WHO's air quality guidelines [15]. Cohen et al. (2005) pointed out that around 0.8 million premature deaths and 6.4 million years of life lost (YLL) per year globally are closely linked to $PM_{2.5}$ pollution in 2005, and this burden occurred predominantly in developing countries; 65% in Asia alone. By 2017, 4.58 million deaths were attributed to $PM_{2.5}$ exposure worldwide with 142.52 million disability-adjusted life years (DALYs), and the deaths rose to 6.7 million in 2019 [15], [17].

Particulate matter-induced oxidative stress is considered as one of the important mechanisms of atmospheric particulate matter toxicity [18]. Some of the organic matter in particulate matter can be activated to electrophilic reactive metabolites, which can increase or generate intracellular reactive oxygen species (ROS), and transition metals such as Fe, Cu, Vn, and Mn in PM can induce the generation of ROS through the Fenton reaction [19], [20]. Increased intracellular ROS may disrupt the balance between ROS and antioxidant functions already present in the cell, which may result in the generation of additional ROS. ROS can disrupt the balance between ROS and antioxidant functions already present in the cell, resulting in more oxidative stress and negative health responses, thus damaging the cells through lipid peroxidation, oxidative modification of proteins, and DNA mutation [21].

1.1.3 Particulate matter collection methods

Airborne PM_{10} as well as $PM_{2.5}$ samples with smaller particle sizes are usually collected using filters prepared from different materials, such as glass fiber filters (GFF), quartz fiber filters (QFF), Teflon filters, and combinations thereof, and some studies use filters made from other materials, such as cellulose membranes [19], [22]–[24]. Still, because of the low porosity or strength of such filtration materials, they cannot be guaranteed at high flow rates without damaging or clogging the filters [24]. These filters allow large volumes of air to pass through while trapping and concentrating aerosol particles of specific sizes that have already been separated on their surfaces for the

purpose of collecting particles of different sizes.

However, there are two potential problems with using methods that trap particulate matter in the gas stream and enrich it on the filter surface. First, the organic pollutants contained in the particulate matter immobilized on the filter surface are more readily degraded by oxides in the sampled air (e.g., ozone, nitrogen dioxide), which can result in a significant underestimation of pollutant concentrations in the ambient air [25], [26]. Adding an ozone eliminator to the front of the sampler removes ozone from the air sampled, effectively preventing oxidative degradation of pollutants during the sampling process, but this sampling combination is less effective in humid conditions and can increase sampling costs [27]. Secondly, unlike powder samples collected directly by the cyclone, particulate samples adhering to the filter surface require additional pre-processing to separate them from the filter matrix. In cytological studies exploring the hazards of particulate matter, ultrasound is mainly used to separate particulate matter from the filter surface by mechanical oscillation, but this process does not ensure complete stripping of particulate matter, and repeated solvent oscillation might affect the concentration of the attached contaminants [28]–[30].

1.2 Background of PM-bound polycyclic aromatic hydrocarbons

1.2.1 General information

Polycyclic aromatic hydrocarbons (PAHs) are compounds formed by condensing two or more benzene rings or cyclopentadiene, with stable benzene ring structure, belonging to semi-volatile substances. PAHs generally have high melting and boiling points, so they can exist in solid form at room temperature. PAHs with three or more rings are colorless or yellowish crystals, and some are dark in color. Most PAHs have high octanol-water partition coefficients, so they are generally insoluble in water, but are soluble in organic solvents.

PAHs of the same molecular weight have multiple isomers, resulting in a wide variety of PAHs. According to the connecting way of the aromatic rings, PAHs can be divided

into two categories: the first category is polynuclear aromatics hydrocarbons, i.e., PAHs in which the adjacent benzene ring has at least two shared carbon atoms, such as naphthalene (Nap). The second category is hydrocarbons in which the benzene rings are directly united by a single bond, or connected by one or several carbon atoms, called isolated PAHs. The term PAHs is usually used to refer mainly to condensed aromatic hydrocarbons. According to the difference in the number of benzene rings, PAHs can be divided into three groups: the first group contains 2-3 benzene rings of low molecular weight PAHs (L-PAHs), such as phenanthrene (Phe); the second group contains 4 benzene rings of medium molecular weight PAHs (M-PAHs), such as fluoranthene (Flt); and the third group is high molecular weight PAHs (H-PAHs) containing 5-7 benzene rings, such as benzo(a)pyrene (BaP). In general, as the molecular weight and the number of benzene rings of PAHs increase, they become less volatile, less water-soluble, and more lipophilic [31], [32]. In the natural environment, L-PAHs show high volatility because of relatively high vapor pressure, exist mainly in gaseous form in the atmosphere, are easier to be transported over long distances, and have a high rate of biodegradation. H-PAHs usually have a lower vapor pressure and lower volatility, and are mainly adsorbed and bound to fine particulate matter in the atmosphere. H-PAHs have a high octanol-water partition coefficient and show strong lipophilicity, which makes it easier to penetrate the defense barriers of organisms for bioconcentration and lower biodegradation rate [33]. The U.S. Environmental Protection Agency (USEPA) has listed 16 main PAHs as priority control pollutants in 1978, and the structural formulas and physical and chemical properties of the 16 PAHs are shown in **Fig. 1.2** and **Table 1.1** [34].

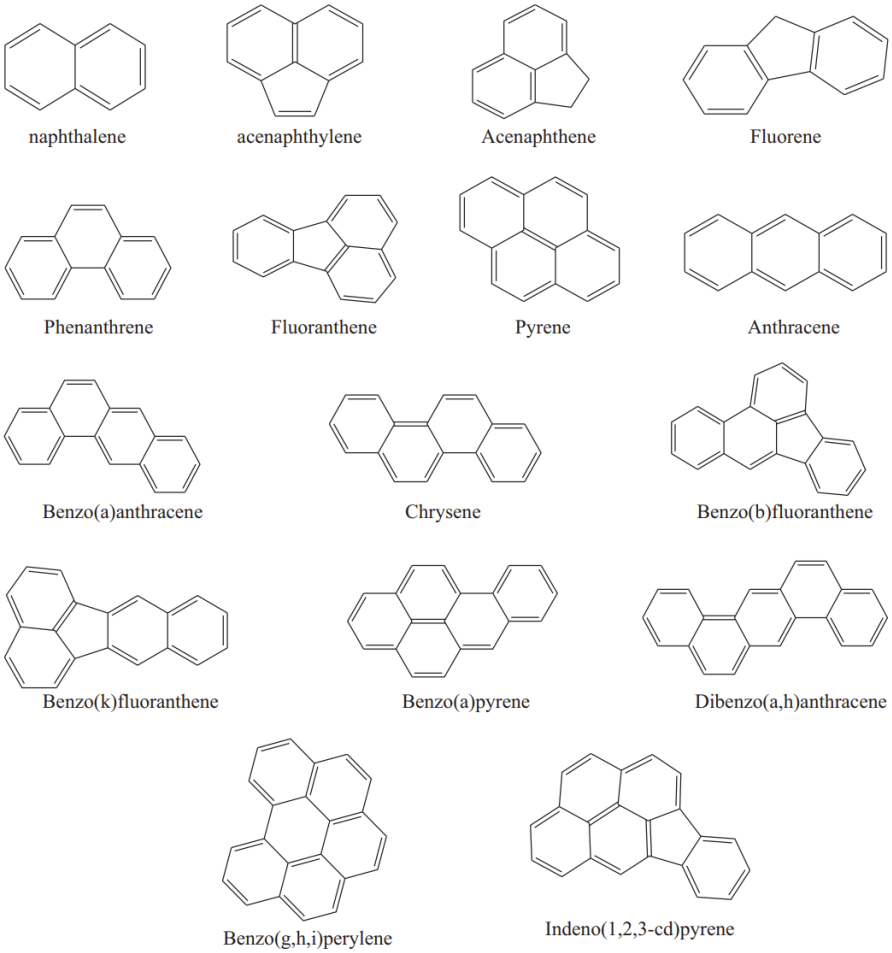


Fig. 1.2 Molecular structure of 16 PAHs

Table 1.1 Physical and chemical properties of 16 PAHs [34]

Compound	Number of rings	Molecular weight	Melting point, ℃	Boiling point, ℃	Vapor pressure, kPa	Solubility in water (mg/L)	Octanol-Water Partition Coefficient, LogKow	IARC Classification*
Naphthalene, Nap	2	128.18	80.2	218	1.1×10^{-2}	3.93	3.4	2B
Acenaphthylene, Acy	2	152.20	92-93	265-280	3.9×10^{-3}	3.93	3.85	Not evaluated
Acenaphthene, Ace	2	154.20	90-96	278-279	2.1×10^{-3}	1.93	3.95	3
Fluorene, Fl	2	166.23	116-118	293-295	8.7×10^{-5}	1.68-1.98	4.11	3
Phenanthrene, Phe	3	178.24	96-101	339-340	2.3×10^{-5}	1.2	4.47	3
Anthracene, Ant	3	178.24	216-219	340	3.6×10^{-6}	0.076	4.57	3
Fluoranthene, Flt	3	202.26	107-111	375-393	6.5×10^{-7}	0.2-2.6	4.97	3
Pyrene, Pyr	4	202.26	150-156	360-404	3.1×10^{-6}	0.077	5.01	3
Benzo(a)anthracene, BaA	4	228.30	157-167	435	1.5×10^{-8}	0.01	5.83	2B
Chrysene, Chr	4	228.30	252-256	441-448	5.7×10^{-10}	0.0028	5.67	2B
Benzo(b)fluoranthene, BbF	4	252.32	167-168	481	6.7×10^{-8}	0.0012	5.86	2B
Benzo(k)fluoranthene, BkF	4	252.32	198-217	471-480	2.1×10^{-8}	0.00076	5.86	2B
Benzo(a)pyrene, BaP	5	252.32	1980217	493-496	7.3×10^{-10}	0.0023	6.05	1
Dibenzo(a,h)anthracene, DbA	5	278.35	266-270	524	1.3×10^{-11}	0.0005	6.57	2B
Benzo(g,h,i)perylene, BgP	5	276.34	275-278	525	1.3×10^{-11}	0.00026	6.51	2A
Indeno(1,2,3-cd)pyrene, InP	6	276.34	162-163	530	$Ca\times10^{-11}$	0.062	6.63	3

*IARC (International Agency for Research and Cancer) Classification

Group 1: The agent is carcinogenic to humans.

Group 2A: The agent is probably carcinogenic to humans.

Group 2B: The agent is possibly carcinogenic to humans.

Group 3: The agent is not classifiable as to its carcinogenicity to humans [35].

1.2.2 Extracting and detecting methods of PM-bound PAHs

PAHs in the particulate phase are usually collected by direct collection of particulate media (PM_{10} or $PM_{2.5}$). After the collection of airborne PAHs particles, PM samples are treated individually or in combination using a range of organic solvents (e.g., hexane, methylene chloride, acetone, methanol, etc.). Meanwhile, extraction methods such as Soxhlet extraction, microwave extraction, ultrasonic extraction, or other techniques (e.g., pressurized liquid extraction) are often used to extract PAHs from filter samples to improve its recovery rates.

Soxhlet extraction is considered as the standard, and it is a recommended extraction method by USEPA. It is simpler than microwave-assisted extraction (MAE), pressurized liquid extraction (PFE), and accelerated solvent extraction (ASE), and has high recovery and low equipment requirements [36]. However, this method has a long extraction time, requires a large volume of organic solvent, and the high extraction temperature can lead to labile compounds being degraded thermally. Ultrasonic extraction is a simple, low-cost method that requires a small amount of organic solvent and can extract comparable or even greater amounts of hydrocarbons than other methods, but this method provided lower recoveries [37].

After extracting and separating PAHs from particulate media, how to detect their concentration is also a very important part. Chromatography is the most method for PAHs detection. High performance liquid chromatography with UV detector (HPLC-UV) and gas chromatography with mass detector (GC-MS) are the main methods recommended by the USEPA for the detection of PAHs in water, particulate matter, and sediments [38]–[41]. HPLC with diode array detector (DAD) and fluorescence detector (FLD) are also widely used for the detection of PAHs due to their higher detection sensitivity and selectivity [42]–[44].

1.2.3 Emission sources of PM-bound PAHs

The main sources of PAHs in the environment can be divided into two categories: natural and anthropogenic sources. PAHs from natural sources make up the environmental background value of PAHs. They mainly include terrestrial, aquatic, and microbial biosynthetic releases as well as various environmental processes caused by natural factors, such as volcanic eruptions, forest fires, and sediment diagenetic evolution [45], [46]. However, emissions of PAHs from natural sources contribute only a small fraction of PAHs to the environment compared to emissions of PAHs from anthropogenic sources.

Anthropogenic sources are the main sources of PAHs in the environment. Anthropogenic PAHs are mostly formed from saturated hydrocarbon under oxygen-deficient conditions. Pyrosynthesis and pyrolysis are two major mechanisms leading to PAHs formation, in which reactions or production processes are mainly contained in incomplete combustion and pyrolysis of material containing carbon and hydrogen, such as coal, oil, wood, and petroleum products [46]–[48]. Therefore, the contribution from different sources such as residential heating, automobile exhaust, industrial power generation, incinerators, and the production of coal tar, coke, and asphalt is difficult to separate clearly [33]. According to the emitting characteristics of different sources, they can be divided into three main groups, mainly include point sources, such as chemical and coking sources; line sources, such as transportation sources; and surface sources, such as domestic sources and agricultural sources [48], [49].

- **Chemical production pollution source**

Various production activities in factories produce large quantities of PAHs. For example, burning 1 kg of coal usually emits 10 mg of BaP, and burning 1 kg of petroleum emits 40 mg of BaP. The statistics in Canada in 1994 showed that 21% of its PAHs emissions were generated by the aluminum refining industry [50]. In Germany, the results of a survey showed that coke from industrial activities contributed 30% to

PAHs emissions, and PAHs emissions from coal heating and combustion processes contributed up to 56% to the total [51]. China's statistics in 2012 showed that coke combustion contributed 34% to the total PAHs emissions [52]. Yang et al. [53] studied the exhaust gases from different factories and combustion furnace stacks and showed that the consumption of 1 kg of raw materials can produce 77-3970 μg PAHs, of which 2-16 μg of BaP, and mainly were 3-4 rings PAHs.

- **Transportation pollution source**

Vehicle engine fuel emissions have become the largest source of PAHs in cities, with gasoline vehicles emitting mainly L-PAHs from unburned gasoline and diesel vehicles emitting relatively high levels of particulate-phase PAHs [54]. The United Kingdom's 2008 air quality report noted that PAHs from light duty vehicles and heavy duty vehicles (buses and coaches) accounted for 41% of the total PAHs emissions [55]. In addition, PAHs are generated from asphalt pavement volatilization and vehicle tires. Shimada et al. [56] indicated that vehicles were the main sources of the PAHs (accounting for 40% to 80%) in Tokyo, Japan, and there was no significant change in the contribution of vehicle emissions to PAHs concentrations during the period from 2007 to 2016. And sampling data from a roadside air pollution monitoring station in Kanazawa, Japan, shows that local PAHs concentrations have dropped by 33% in 2019 compared to 2017 since the implementation of new emissions regulations [57].

- **Domestic Pollutants**

Domestic sources of PAHs mainly refer to PAHs produced by people through emissions from activities such as home cooking and heating. Oil fumes from cooking are the main source of PAHs in kitchen air [58]. The cooking method, the type of cooking oil, the fat content of the ingredients, the fuel used, and the cooking temperature all affect the emission of PAHs [59]–[61]. Cooking and the burning of coal and biomass fuels for residential heating are also major domestic sources of PAHs, and

this source of emissions is most prominent in most developing countries [62]. Shen et al. [62] estimated that the total global emissions of PAHs in 2007 were about 504 Gg, with more than half of these emissions coming from residential biomass combustion. Li's study points out that due to the use of cleaner energy sources such as natural gas for cooking and heating, China's national population-weighted indoor BaP concentration has dropped significantly from 46.1 ng/m^3 in 1992 to 6.60 ng/m^3 in 2017 [63].

- **Agricultural pollution source**

Agricultural pollution sources mainly refer to the large amounts of PAHs produced by the open burning of agricultural straw and other biomass. On average, open burning of straw and other biomass can emit about 5-683 mg of PAHs per kg, and the emission of PAHs increases with the emission of particulate matter [64]. Korenage et al. [65] also noted that the emission of PAHs from particulate matter produced by burning rice straw varied between 1-38 mg/kg, and that the moisture content in rice straw significantly affected the production of PAHs during combustion.

1.2.4 Human health risk

The main health hazards of PAHs are carcinogenicity, immunotoxicity, and reproductive developmental toxicity. PAHs are metabolized into other compounds and excreted from the body, or they form PAHs-deoxyribonucleic acid adducts (PAHs-DNA adducts). The presence of PAHs-DNA adducts is considered as the initial stage of chemical carcinogenesis [66]. A study by the IARC found a significant increase in the risk of lung cancer among coke production workers, which may be attributed to the presence of PAHs in coke oven mixtures [67]. Epidemiologic studies have shown that occupational exposure to PAHs increases the incidence of diseases such as lung and bladder cancer [68], [69]. One research showed the PAHs and their halogenated derivatives (HPAHs) concentration in workers' serum in coal-fired power plants were

higher than in people without occupational exposure, and the total concentration of PAHs and HPAHs in males were positively correlated with pulmonary hypofunction and hypertension [70]. In addition, dietary intake of PAHs, which produced in cooking process such as meat grilling and roasting, increases the risk of cancers such as prostate cancer in some individuals [71]–[73].

Besides, PAHs can cause immunosuppressive effects. Cytotoxicology study results based on rodent model show B[α]P-mediated immunotoxic effects such as suppressing the antibody production of T-dependent antigen, alloantigen-specific mixed-lymphocyte reactions, and mitogen-induced T cell and B cell proliferative responses [74]–[77]. Meland et al. [78] found that Salmo trutta showed a large of molecular changes in its liver after 4 h of exposure to particulate matter of traffic origin, which persisted for several hours after exposure. Moreover, data from human in vivo and in vitro research also indicate that PAHs can cause immunosuppression by inhibiting differentiation and maturation of innate immune cells and B-cells resulting in the inhibition of T-cell function [79], [80].

PAHs can also produce reproductive developmental toxicity by interfering with the secretion of sex hormones, affecting the physiological function of the gonads and the process of reproductive development. A large amount of research data suggests that PAHs can cross the placental barrier [81]. Cytochrome P450 enzymes (CYP1A1 and CYP1B1) can metabolize PAHs into intermediates at placenta, and these intermediates can cause cellular damage by forming DNA and protein adducts or by generating ROS [82]. PAH-DNA adducts levels in umbilical cord blood or placental tissue had correlation with a lot of adverse birth outcomes such as aberrant child behavior and impaired fetal growth [83], [84]. More importantly, the negative effects of PAHs can be seen later in life as well, such as lowered intelligence quotient (IQ), allergies, and asthma [85], [86].

1.3 Objective of the research

As mentioned in Section 1.3, the problem with the traditional sampling method of using filters to trap airborne particulate matter is the degradation of pollutants during sampling, and the inability to separate particulate matter attached on the filters completely for subsequent cell and animal exposure experiments. Aiming to solve these problems, our laboratory developed a sampling device that collects $PM_{2.5}$ in powder form using a cyclone instead of a filter. The device has a real impactor having an impaction plate at the inlet of the airflow for separating $PM_{2.5}$ particles from the air, and then the airflow containing $PM_{2.5}$ flows into the cyclone along the tangential direction and makes a rotary motion, and with the help of the centrifugal force, the $PM_{2.5}$ particles are separated from the airflow and captured in the inner wall, then the $PM_{2.5}$ particles will fall into the lower sample bottle with the help of gravity [28], [29]. The schematic diagram and each device photograph of the high-volume cyclone sampler are shown in **Fig. 1.3**. To overcome the problem of large volume and inconvenient handling and installation of high-volume cyclone device, our lab has successfully realized the miniaturization of the cyclone device by optimizing the design and structure of the device, named Keio-Transportable Real impactor with Cyclone (K-TRiC) (**Fig. 1.4**).

Unlike $PM_{2.5}$ samples collected using filters, the physical appearance of powdered particulate matter samples collected directly using cyclone is more similar as those of dust and soil samples. The cyclone-collected samples are smaller in volume because there is no filter membrane as a support structure, so less organic solvent is needed to extract PAHs from particulate matter using conventional methods such as Soxhlet extraction, but the disadvantages, such as time-consuming, costly, and pollutants thermal decomposition of the contaminants and evaporation loss of solvents by high-temperature extraction still cannot be avoided.

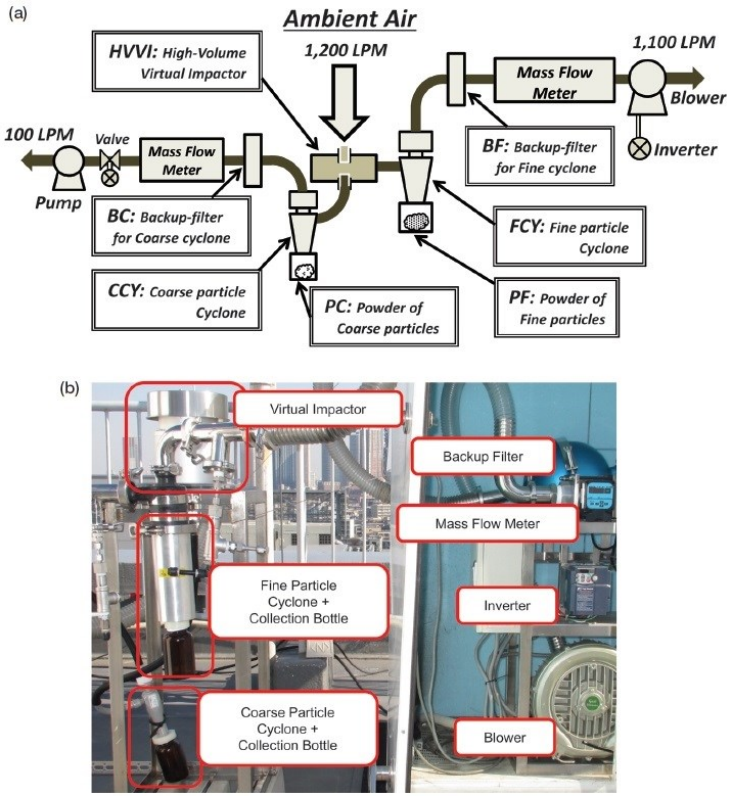


Fig. 1.3 (a) Schematic diagram and (b) each device photograph of the high-volume cyclone sampler [29]

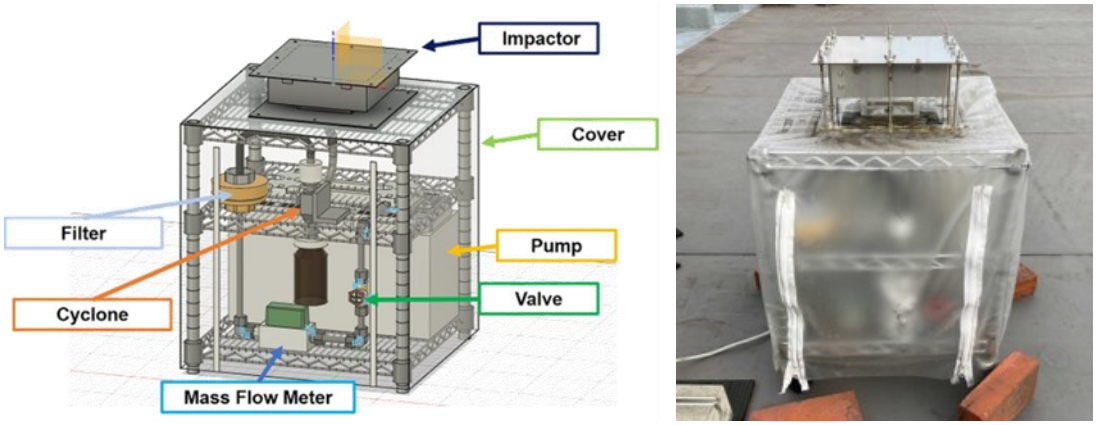


Fig. 1.4 Photograph of miniaturized cyclone device, K-TRiC

To solve the above problem with the PM-bound PAHs collection, extraction, pollution, and human health damage, this thesis aims to develop one extraction method for rapid extraction of PAHs from powder aerosol samples based on the cyclone sampler, analyze the pollution characteristics and human exposure risk of PAHs in atmospheric

particulate matter in Japan during the COVID-19 epidemic, and investigate the feasibility of ameliorating the PAHs exposure risk to humans through daily dietary intake (**Fig. 1.5**).

In Chapter 1, background knowledge of particulate matter and the PAHs attached to it is described. Particularly, problems with conventional filter sampling devices and PAHs extraction methods that have existed in previous studies are noted. Targeting our attempts to solve these problems using a novel cyclone sampler. After that, the aims of this thesis are also presented and briefly describes the content structure of the thesis.

In Chapter 2, the QuEChERS (quick, easy, cheap, effective, rugged, and safe) extraction method, which had been used for pesticide and organic pollutants extraction in soil, was optimized for the extracting and detecting of PAHs in powder-from aerosol samples. Firstly, the environmental standard material (SRM1944 sample) was used for testing the PAHs extraction effect of different extracting factors combination designed by response surface method, then the parameters were optimized based on the boundary condition with the 2-factor interaction model to get the best PAHs extraction result. Finally, cyclone-collected environmental aerosol samples were used to verify the theoretical optimal conditions application effect for PM-bound PAHs extraction.

In Chapter 3, the PAHs concentration in 30 cyclone-collected aerosol samples over a long period at Yokohama, Japan from 2018 to 2023 using the QuEChERS extraction method and HPLC-FLD detection system. The PAHs concentration trend, correlation with meteorological and other contaminant factors, and changing emission sources were discussed over the COVID-19 outbreaking period. In addition, the human health risk of PM-bound PAHs through inhalation, ingestion, and dermal routes were assessed.

In Chapter 4, The feasibility of preventing and mitigating the exposure hazards of PM-bound PAHs in humans by means of daily dietary intake was investigated. Astaxanthin (ATX) was used to investigate its protective effects on PAHs-exposed cells due to its potent antioxidant properties, comparing the survival of PAHs-exposed A549 cells with that of ATX-added controls in terms of the amount of ROS produced and the

expression of inflammatory cytokines.

In Chapter 5, the energy dispersive X-ray fluorescence spectroscopy (EDXRF) and X-ray absorption fine structure (XAFS) assays were used to analyze the concentrations and valence compositions of metals in powdered particulate matter samples collected by cyclone at three locations in Japan, and the differences in metal contaminants adhering to particulate matter between sampling seasons and regions are discussed.

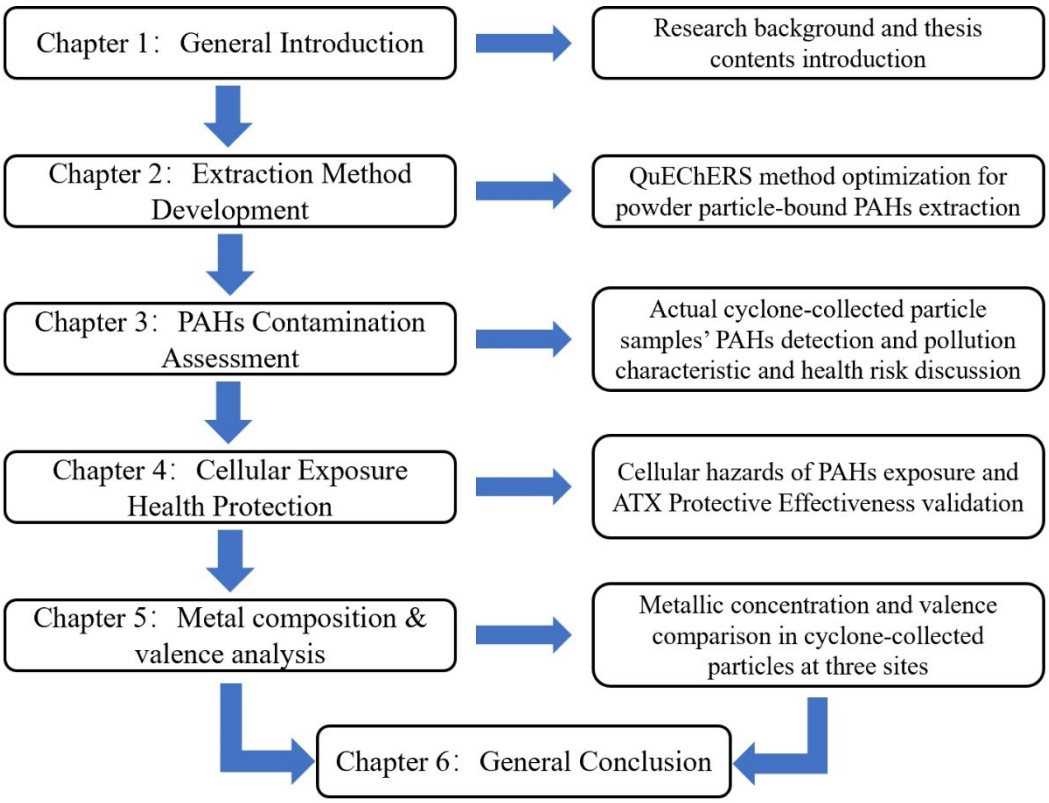


Fig. 1.5 Thesis conceptual framework

1.4 References

[1] USEPA, "Continuous measurement of PM10 suspended particulate matter (SPM) in ambient air." [Online]. Available: https://www.epa.gov/sites/default/files/2019-11/documents/overvw1.pdf

[2] B. Fang *et al.*, "PM2.5-Bound Polycyclic Aromatic Hydrocarbons: Sources and Health Risk during Non-Heating and Heating Periods (Tangshan, China)," *IJERPH*, vol. 17, no. 2, p. 483, Jan. 2020, doi: 10.3390/ijerph17020483.

[3] W. Hill *et al.*, "Lung adenocarcinoma promotion by air pollutants," *Nature*, vol.

616, no. 7955, pp. 159–167, Apr. 2023, doi: 10.1038/s41586-023-05874-3.

[4] S. Palleschi *et al.*, "Toxicity of the readily leachable fraction of urban PM2.5 to human lung epithelial cells: Role of soluble metals," *Chemosphere*, vol. 196, pp. 35–44, Apr. 2018, doi: 10.1016/j.chemosphere.2017.12.147.

[5] H. Wang *et al.*, "Cytotoxicity and inflammatory effects in human bronchial epithelial cells induced by polycyclic aromatic hydrocarbons mixture," *J Appl Toxicol*, vol. 41, no. 11, pp. 1803–1815, Nov. 2021, doi: 10.1002/jat.4164.

[6] B. Fiorella, "Human exposure assessment related to oil activities in Ecuador: from the air quality monitoring to the study of metallic contaminants transfer in the soil-plant continuum," Universite Toulouse 3 Paul Sabatier (UT3 Paul Sabatier), 2017. This work © 2 by Fiorella F. Barraza Castelo is licensed under CC BY-NC-SA 4.0. To view a copy of this license, visit http://creativecommons.org/licenses/by-nc-sa/4.0/.

[7] B.-J. Lee, B. Kim, and K. Lee, "Air Pollution Exposure and Cardiovascular Disease," *Toxicological Research*, vol. 30, no. 2, pp. 71–75, Jun. 2014, doi: 10.5487/TR.2014.30.2.071.

[8] C. I. Falcon-Rodriguez, A. R. Osornio-Vargas, I. Sada-Ovalle, and P. Segura-Medina, "Aeroparticles, Composition, and Lung Diseases," *Front. Immunol.*, vol. 7, Jan. 2016, doi: 10.3389/fimmu.2016.00003.

[9] S. Majewski and W. J. Piotrowski, "Air Pollution—An Overlooked Risk Factor for Idiopathic Pulmonary Fibrosis," *JCM*, vol. 10, no. 1, p. 77, Dec. 2020, doi: 10.3390/jcm10010077.

[10] T. Wang *et al.*, "Combustion-Derived Particulate PAHs Associated with Small Airway Dysfunction in Elderly Patients with COPD," *Environ. Sci. Technol.*, p. acs.est.2c00797, Jul. 2022, doi: 10.1021/acs.est.2c00797.

[11] M. Romanello *et al.*, "Tracking progress on health and climate change in Europe," *The Lancet Public Health*, vol. 6, no. 11, pp. e858–e865, Nov. 2021, doi: 10.1016/S2468-2667(21)00207-3.

[12] Z. Liu *et al.*, "Combined Effects of Ambient PM2.5 and Cold Exposure on the Development of Metabolic Disorder," *Atmosphere*, vol. 14, no. 7, p. 1157, Jul. 2023, doi: 10.3390/atmos14071157.

[13] S. Steinle *et al.*, "In Utero Exposure to Particulate Air Pollution during Pregnancy: Impact on Birth Weight and Health through the Life Course," *IJERPH*, vol. 17, no. 23, p. 8948, Dec. 2020, doi: 10.3390/ijerph17238948.

[14] D. Loomis *et al.*, "The carcinogenicity of outdoor air pollution," *The Lancet Oncology*, vol. 14, no. 13, pp. 1262–1263, Dec. 2013, doi: 10.1016/S1470-2045(13)70487-X.

[15] WHO, "Ambient (outdoor) air pollution." [Online]. Available: https://www.who.int/news-room/fact-sheets/detail/ambient-(outdoor)-air-quality-and-health

[16] A. J. Cohen *et al.*, "The Global Burden of Disease Due to Outdoor Air Pollution," *Journal of Toxicology and Environmental Health, Part A*, vol. 68, no. 13–14, pp.

1301–1307, Jul. 2005, doi: 10.1080/15287390590936166.
[17] X. Bu *et al.*, "Global PM2.5-attributable health burden from 1990 to 2017: Estimates from the Global Burden of disease study 2017," *Environmental Research*, vol. 197, p. 111123, Jun. 2021, doi: 10.1016/j.envres.2021.111123.
[18] F. Ren *et al.*, "PM2.5 induced lung injury through upregulating ROS-dependent NLRP3 Inflammasome-Mediated Pyroptosis," *Immunobiology*, vol. 227, no. 3, p. 152207, May 2022, doi: 10.1016/j.imbio.2022.152207.
[19] S. Lu *et al.*, "A characterization of HULIS-C and the oxidative potential of HULIS and HULIS-Fe(II) mixture in PM2.5 during hazy and non-hazy days in Shanghai," *Atmospheric Environment*, vol. 219, p. 117058, Dec. 2019, doi: 10.1016/j.atmosenv.2019.117058.
[20] Y. Wang, S. Salana, H. Yu, J. V. Puthussery, and V. Verma, "On the Relative Contribution of Iron and Organic Compounds, and Their Interaction in Cellular Oxidative Potential of Ambient PM $_{2.5}$," *Environ. Sci. Technol. Lett.*, vol. 9, no. 8, pp. 680–686, Aug. 2022, doi: 10.1021/acs.estlett.2c00316.
[21] T. Xiao *et al.*, "NF-κB-regulation of miR-155, via SOCS1/STAT3, is involved in the PM2.5-accelerated cell cycle and proliferation of human bronchial epithelial cells," *Toxicology and Applied Pharmacology*, vol. 377, p. 114616, Aug. 2019, doi: 10.1016/j.taap.2019.114616.
[22] M. Liu *et al.*, "Measurements of Gross α- and β-Activities of Archived PM $_{2.5}$ and PM $_{10}$ Teflon Filter Samples," *Environ. Sci. Technol.*, vol. 54, no. 19, pp. 11780–11788, Oct. 2020, doi: 10.1021/acs.est.0c02284.
[23] Y. Zhang, E. Guo, H. Hu, H. Wang, and X. Liu, "Experimental Study on PM2.5 Purification Characteristics of Different Filter Units in Enclosed Environments," *Aerosol Air Qual. Res.*, vol. 22, no. 11, p. 220184, 2022, doi: 10.4209/aaqr.220184.
[24] L. Chen, Y. Guo, and X. Peng, "Hydrophobic and porous cellulose nanofibrous screen for efficient particulate matter (PM2.5) blocking," *J. Phys. D: Appl. Phys.*, vol. 50, no. 40, p. 405304, Oct. 2017, doi: 10.1088/1361-6463/aa82af.
[25] C. Schauer, R. Niessner, and U. Pöschl, "Polycyclic Aromatic Hydrocarbons in Urban Air Particulate Matter: Decadal and Seasonal Trends, Chemical Degradation, and Sampling Artifacts," *Environ. Sci. Technol.*, vol. 37, no. 13, pp. 2861–2868, Jul. 2003, doi: 10.1021/es034059s.
[26] M. Tsapakis and E. G. Stephanou, "Diurnal Cycle of PAHs, Nitro-PAHs, and oxy-PAHs in a High Oxidation Capacity Marine Background Atmosphere," *Environ. Sci. Technol.*, vol. 41, no. 23, pp. 8011–8017, Dec. 2007, doi: 10.1021/es071160e.
[27] S. K. Pandey, K.-H. Kim, and R. J. C. Brown, "A review of techniques for the determination of polycyclic aromatic hydrocarbons in air," *TrAC Trends in Analytical Chemistry*, vol. 30, no. 11, pp. 1716–1739, Dec. 2011, doi: 10.1016/j.trac.2011.06.017.
[28] T. Okuda, R. Isobe, Y. Nagai, S. Okahisa, K. Funato, and K. Inoue, "Development of a High-Volume PM2.5 Particle Sampler Using Impactor and Cyclone Techniques," *Aerosol Air Qual. Res.*, vol. 15, no. 3, pp. 759–767, 2015, doi:

10.4209/aaqr.2014.09.0194.
[29] T. Okuda *et al.*, “Development of a High-Volume Simultaneous Sampler for Fine and Coarse Particles using Virtual Impactor and Cyclone Techniques,” *ajae*, vol. 12, no. 1, pp. 78–86, Mar. 2018, doi: 10.5572/ajae.2018.12.1.078.
[30] A. Honda, T. Okuda, M. Nagao, N. Miyasaka, M. Tanaka, and H. Takano, “PM2.5 collected using cyclonic separation causes stronger biological responses than that collected using a conventional filtration method,” *Environ Res*, vol. 198, p. 110490, Jul. 2021, doi: 10.1016/j.envres.2020.110490.
[31] Y.-G. Ma, Y. D. Lei, H. Xiao, F. Wania, and W.-H. Wang, “Critical Review and Recommended Values for the Physical-Chemical Property Data of 15 Polycyclic Aromatic Hydrocarbons at 25 °C,” *J. Chem. Eng. Data*, vol. 55, no. 2, pp. 819–825, Feb. 2010, doi: 10.1021/je900477x.
[32] H. Dop , P. Fabian , H. Güsten , J. M. Hales , A. Wint, *The Handbook of Environmental Chemistry*. Springer, 1986.
[33] H. Valli, “Cancer risk assessment, indicators, and guidelines for polycyclic aromatic hydrocarbons in the ambient air.,” *Environmental Health Perspectives*, vol. 110, p. 38, 2002.
[34] K. Hussain *et al.*, “Monitoring and Risk Analysis of PAHs in the Environment,” in *Handbook of Environmental Materials Management*, C. M. Hussain, Ed., Cham: Springer International Publishing, 2018, pp. 1–35. doi: 10.1007/978-3-319-58538-3_29-2.
[35] IARC, “IARC. IARC monographs on the identification of carcinogenic hazards to humans.” [Online]. Available: https://monographs.iarc.who.int/agents-classified-by-the-iarc/
[36] J. P. Robinson, S. W. Kingman, C. E. Snape, H. Shang, R. Barranco, and A. Saeid, “Separation of polyaromatic hydrocarbons from contaminated soils using microwave heating,” *Separation and Purification Technology*, vol. 69, no. 3, pp. 249–254, Oct. 2009, doi: 10.1016/j.seppur.2009.07.024.
[37] T. Oluseyi, K. Olayinka, B. Alo, and R. M. Smith, “Comparison of extraction and clean-up techniques for the determination of polycyclic aromatic hydrocarbons in contaminated soil samples,” *African Journal of Environmental Science and Technology*, vol. 5, no. 7, pp. 482–493, Jul. 2011, doi: 10.1088/1742-6596/1819/1/012061.
[38] M. Mahmoudpour, J. Mohtadinia, M. Ansarin, and M. Nemati, “Dispersive Liquid–Liquid Microextraction for HPLC-UV Determination of PAHs in Milk,” *Journal of AOAC INTERNATIONAL*, vol. 99, no. 2, pp. 527–533, Mar. 2016, doi: 10.5740/jaoacint.15-0169.
[39] J. Tang *et al.*, “The pollution profiles and human exposure risks of chlorinated and brominated PAHs in indoor dusts from e-waste dismantling workshops: Comparison of GC–MS, GC–MS/MS and GC × GC–MS/MS determination methods,” *Journal of Hazardous Materials*, vol. 394, p. 122573, Jul. 2020, doi: 10.1016/j.jhazmat.2020.122573.

[40] A. Khan, M. Imran, A. Hashmi, W. Shehzad, and M. Abbas, “Quantification of Selected Polycyclic AromaticHydrocarbons (PAHs) in Soil, Water and Bloodby an Optimized and Validated HPLC –UV–DADMethod,” *Pol. J. Environ. Stud.*, vol. 31, no. 4, pp. 3633–3644, Jul. 2022, doi: 10.15244/pjoes/145994.

[41] Z. Zeng *et al.*, “Liquid-liquid extraction combined with online cleanup for the simultaneous determination of PAHs by GC–MS/MS and their hydroxylated metabolites by LC-MS/MS in human fingernails,” *Journal of Chromatography B*, vol. 1188, p. 123057, Jan. 2022, doi: 10.1016/j.jchromb.2021.123057.

[42] A. Onopiuk, K. Kołodziejczak, M. Marcinkowska-Lesiak, and A. Poltorak, “Determination of polycyclic aromatic hydrocarbons using different extraction methods and HPLC-FLD detection in smoked and grilled meat products,” *Food Chemistry*, vol. 373, p. 131506, Mar. 2022, doi: 10.1016/j.foodchem.2021.131506.

[43] P. Świt, J. Orzeł, and S. Maślanka, “Monitoring of PAHs in simulated natural and artificial fires by HPLC-DAD-FLD with the application of Multi-Component Integrated calibration method to improve quality of analytical results,” *Measurement*, vol. 196, p. 111242, Jun. 2022, doi: 10.1016/j.measurement.2022.111242.

[44] H. Vistnes *et al.*, “The Determination of Polycyclic Aromatic Hydrocarbons (PAHs) with HPLC-DAD-FLD and GC-MS Techniques in the Dissolved and Particulate Phase of Road-Tunnel Wash Water: A Case Study for Cross-Array Comparisons and Applications,” *Toxics*, vol. 10, no. 7, p. 399, Jul. 2022, doi: 10.3390/toxics10070399.

[45] E. Manoli and C. Samara, “Polycyclic aromatic hydrocarbons in natural waters: sources, occurrence and analysis,” *TrAC Trends in Analytical Chemistry*, vol. 18, no. 6, pp. 417–428, Jun. 1999, doi: 10.1016/S0165-9936(99)00111-9.

[46] N.-D. Dat and M. B. Chang, “Review on characteristics of PAHs in atmosphere, anthropogenic sources and control technologies,” *Science of The Total Environment*, vol. 609, pp. 682–693, Dec. 2017, doi: 10.1016/j.scitotenv.2017.07.204.

[47] K. Ravindra, R. Sokhi, and R. Vangrieken, “Atmospheric polycyclic aromatic hydrocarbons: Source attribution, emission factors and regulation,” *Atmospheric Environment*, vol. 42, no. 13, pp. 2895–2921, Apr. 2008, doi: 10.1016/j.atmosenv.2007.12.010.

[48] A. M. Mastral and M. S. Callén, “A Review on Polycyclic Aromatic Hydrocarbon (PAH) Emissions from Energy Generation,” *Environ. Sci. Technol.*, vol. 34, no. 15, pp. 3051–3057, Aug. 2000, doi: 10.1021/es001028d.

[49] A. T. Lawal, “Polycyclic aromatic hydrocarbons. A review,” *Cogent Environmental Science*, vol. 3, no. 1, p. 1339841, Jan. 2017, doi: 10.1080/23311843.2017.1339841.

[50] Canada, “Priority substances list assessment report-polycyclic aromatic hydrocarbons.” [Online]. Available: https://publications.gc.ca/collections/collection_2018/eccc/En40-215-42-eng.pdf

[51] G. Fu, “Study on the Emission Characteristic of Polycyclic Aromatic Hydrocarbons from Coal Combustion,” Zhejiang University, 2002.
[52] X. Xu, “Polycyclic Aromatic Hydrocarbons Air Pollution Generated from Human Activity and Its Human Health Impact in China,” Shandong University, 2014.
[53] H.-H. Yang, W.-J. Lee, S.-J. Chen, and S.-O. Lai, “PAH emission from various industrial stacks,” *Journal of Hazardous Materials*, vol. 60, no. 2, pp. 159–174, Jun. 1998, doi: 10.1016/S0304-3894(98)00089-2.
[54] J. Li, G. Zhang, X. Li, S. Qi, G. Liu, and X. Peng, “Source seasonality of polycyclic aromatic hydrocarbons (PAHs) in a subtropical city, Guangzhou, South China,” *Science of The Total Environment*, vol. 355, no. 1–3, pp. 145–155, Feb. 2006, doi: 10.1016/j.scitotenv.2005.02.042.
[55] UK, “UK Emissions of Air Pollutants 1970 to 2008.” [Online]. Available: https://uk-air.defra.gov.uk/assets/documents/reports/cat07/1009030925_2008_Report_final270805.pdf
[56] K. Shimada *et al.*, “Effects of changes in polycyclic aromatic hydrocarbons (PAHs) emissions and degradation on their concentrations in Tokyo from 2007 and 2016,” *Sci Rep*, vol. 12, no. 1, p. 4249, Mar. 2022, doi: 10.1038/s41598-022-08138-8.
[57] W. Xing *et al.*, “Variations in traffic-related polycyclic aromatic hydrocarbons in PM2.5 in Kanazawa, Japan, after the implementation of a new vehicle emission regulation,” *Journal of Environmental Sciences*, vol. 121, pp. 38–47, Nov. 2022, doi: 10.1016/j.jes.2021.08.046.
[58] K.-P. Yu *et al.*, “Indoor air pollution from gas cooking in five Taiwanese families,” *Building and Environment*, vol. 93, pp. 258–266, Nov. 2015, doi: 10.1016/j.buildenv.2015.06.024.
[59] Y.-C. Li *et al.*, “Characteristics of polycyclic aromatic hydrocarbons in PM2.5 emitted from different cooking activities in China,” *Environ Sci Pollut Res*, vol. 25, no. 5, pp. 4750–4760, Feb. 2018, doi: 10.1007/s11356-017-0603-0.
[60] C. Li, Z. Li, and H. Wang, “Characterization and risk assessment of polycyclic aromatic hydrocarbons (PAHs) pollution in particulate matter in rural residential environments in China-A review,” *Sustainable Cities and Society*, vol. 96, p. 104690, Sep. 2023, doi: 10.1016/j.scs.2023.104690.
[61] X. Xu *et al.*, “Formation, migration, derivation, and generation mechanism of polycyclic aromatic hydrocarbons during frying,” *Food Chemistry*, vol. 425, p. 136485, Nov. 2023, doi: 10.1016/j.foodchem.2023.136485.
[62] H. Shen *et al.*, “Global Atmospheric Emissions of Polycyclic Aromatic Hydrocarbons from 1960 to 2008 and Future Predictions,” *Environ. Sci. Technol.*, vol. 47, no. 12, pp. 6415–6424, Jun. 2013, doi: 10.1021/es400857z.
[63] S. Li *et al.*, “Indoor exposure to polycyclic aromatic hydrocarbons associated with solid fuel use in rural China,” *Environ Geochem Health*, Sep. 2023, doi: 10.1007/s10653-023-01751-0.
[64] H.-H. Yang and C.-M. Chen, “Emission inventory and sources of polycyclic

aromatic hydrocarbons in the atmosphere at a suburban area in Taiwan," *Chemosphere*, vol. 56, no. 10, pp. 879–887, Sep. 2004, doi: 10.1016/j.chemosphere.2004.05.031.

[65] T. Korenaga, X. Liu, and Z. Huang, "The influence of moisture content on polycyclic aromatic hydrocarbons emission during rice straw burning," *Chemosphere - Global Change Science*, vol. 3, no. 1, pp. 117–122, Jan. 2001, doi: 10.1016/S1465-9972(00)00045-3.

[66] B. Ewa and M.-Š. Danuta, "Polycyclic aromatic hydrocarbons and PAH-related DNA adducts," *J Appl Genetics*, vol. 58, no. 3, pp. 321–330, Aug. 2017, doi: 10.1007/s13353-016-0380-3.

[67] Centre international de recherche sur le cancer, Ed., *A review of human carcinogens*. in IARC monographs on the evaluation of carcinogenic risks to humans, no. 100. Lyon: International agency for research on cancer, 2012.

[68]A. Singh *et al.*, "PAH exposure-associated lung cancer: an updated meta-analysis," *Occupational Medicine*, vol. 68, no. 4, pp. 255–261, May 2018, doi: 10.1093/occmed/kqy049.

[69] J. P. Costantino, C. K. Redmond, and A. Bearden, "Occupationally Related Cancer Risk Among Coke Oven Workers: 30 Years of Follow-Up:," *Journal of Occupational and Environmental Medicine*, vol. 37, no. 5, pp. 597–604, May 1995, doi: 10.1097/00043764-199505000-00009.

[70] C. Zhao *et al.*, "Parent and Halogenated Polycyclic Aromatic Hydrocarbons in the Serum of Coal-Fired Power Plant Workers: Levels, Sex Differences, Accumulation Trends, and Risks," *Environ. Sci. Technol.*, vol. 56, no. 17, pp. 12431–12439, Sep. 2022, doi: 10.1021/acs.est.2c03099.

[71] M. Stacewicz-Sapuntzakis, G. Borthakur, J. L. Burns, and P. E. Bowen, "Correlations of dietary patterns with prostate health," *Mol. Nutr. Food Res.*, vol. 52, no. 5, pp. 624–624, May 2008, doi: 10.1002/mnfr.200890018.

[72] V. Sánchez-Martín *et al.*, "Protective Effect of Thyme and Chestnut Honeys Enriched with Bee Products against Benzo(a)pyrene-Induced DNA Damage," *IJERPH*, vol. 19, no. 24, p. 16969, Dec. 2022, doi: 10.3390/ijerph192416969.

[73] S. Bulanda and B. Janoszka, "Polycyclic Aromatic Hydrocarbons (PAHs) in Roasted Pork Meat and the Effect of Dried Fruits on PAH Content," *IJERPH*, vol. 20, no. 6, p. 4922, Mar. 2023, doi: 10.3390/ijerph20064922.

[74] K. L. White, H. H. Lysy, and M. P. Holsapple, "Immunosuppression by polycyclic aromatic hydrocarbons: A structure-activity relationship in B6C3F1 and DBA/2 mice," *Immunopharmacology*, vol. 9, no. 3, pp. 155–164, Jun. 1985, doi: 10.1016/0162-3109(85)90011-6.

[75] M. Liamin *et al.*, "Genome-Wide Transcriptional and Functional Analysis of Human T Lymphocytes Treated with Benzo[α]pyrene," *IJMS*, vol. 19, no. 11, p. 3626, Nov. 2018, doi: 10.3390/ijms19113626.

[76] S. P. Mudzinski, "Effects of Benzo[a]pyrene on Concanavalin A-Stimulated Human Peripheral Blood Mononuclear cells in Vitro: Inhibition of Proliferation

but No Effect on Parameters Related to the G1 Phase of the Cell Cycle," *Toxicology and Applied Pharmacology*, vol. 119, no. 2, pp. 166–174, Apr. 1993, doi: 10.1006/taap.1993.1057.

[77] M. T. Schellenberger, N. Grova, S. Willième, S. Farinelle, E. J. F. Prodhomme, and C. P. Muller, "Modulation of Benzo[a]pyrene induced immunotoxicity in mice actively immunized with a B[a]P-diphtheria toxoid conjugate," *Toxicology and Applied Pharmacology*, vol. 240, no. 1, pp. 37–45, Oct. 2009, doi: 10.1016/j.taap.2009.06.019.

[78] S. Meland *et al.*, "Hepatic gene expression profile in brown trout (Salmo trutta) exposed to traffic related contaminants," *Science of The Total Environment*, vol. 409, no. 8, pp. 1430–1443, Mar. 2011, doi: 10.1016/j.scitotenv.2011.01.013.

[79] F. V. Andrews, E. Smit, B. M. Welch, S. M. Ahmed, and M. L. Kile, "Urinary polycyclic aromatic hydrocarbons concentrations and hepatitis B antibody serology in the United States (NHANES, 2003–2014)," *Environmental Research*, vol. 195, p. 110801, Apr. 2021, doi: 10.1016/j.envres.2021.110801.

[80] L. L. Allan and D. H. Sherr, "Disruption of human plasma cell differentiation by an environmental polycyclic aromatic hydrocarbon: a mechanistic immunotoxicological study," *Environ Health*, vol. 9, no. 1, p. 15, Dec. 2010, doi: 10.1186/1476-069X-9-15.

[81] E. Drwal, A. Rak, and E. L. Gregoraszczuk, "Review: Polycyclic aromatic hydrocarbons (PAHs)—Action on placental function and health risks in future life of newborns," *Toxicology*, vol. 411, pp. 133–142, Jan. 2019, doi: 10.1016/j.tox.2018.10.003.

[82] T. Shimada and Y. Fujii-Kuriyama, "Metabolic activation of polycyclic aromatic hydrocarbons to carcinogens by cytochromes P450 1A1 and1B1," *Cancer Science*, vol. 95, no. 1, pp. 1–6, Jan. 2004, doi: 10.1111/j.1349-7006.2004.tb03162.x.

[83] F. P. Perera *et al.*, "A Summary of Recent Findings on Birth Outcomes and Developmental Effects of Prenatal ETS, PAH, and Pesticide Exposures," *NeuroToxicology*, vol. 26, no. 4, pp. 573–587, Aug. 2005, doi: 10.1016/j.neuro.2004.07.007.

[84] F. P. Perera *et al.*, "Polycyclic Aromatic Hydrocarbons–Aromatic DNA Adducts in Cord Blood and Behavior Scores in New York City Children," *Environ Health Perspect*, vol. 119, no. 8, pp. 1176–1181, Aug. 2011, doi: 10.1289/ehp.1002705.

[85] F. P. Perera *et al.*, "Relationships among Polycyclic Aromatic Hydrocarbon–DNA Adducts, Proximity to the World Trade Center, and Effects on Fetal Growth," *Environ Health Perspect*, vol. 113, no. 8, pp. 1062–1067, Aug. 2005, doi: 10.1289/ehp.7908.

[86] P. Yang *et al.*, "Urinary Polycyclic Aromatic Hydrocarbon Metabolites and Human Semen Quality in China," *Environ. Sci. Technol.*, vol. 51, no. 2, pp. 958–967, Jan. 2017, doi: 10.1021/acs.est.6b04810.

Chapter 2: Optimization of the QuEChERS Extraction Method to Determine Polycyclic Aromatic Hydrocarbons (PAHs) in Powder Aerosol Particles Collected by Cyclone

This chapter is based on the manuscript submitted for publication in Environmental Technology and Innovation (ET&I) (Jing W.D., Nakano K., Shen Z.X., Okuda T. Optimization of the QuEChERS extraction method to determine polycyclic aromatic hydrocarbons (PAHs) in powder aerosol particles collected by cyclone, accepted on 6 April 2023 [1]) with some addition. This study aims to optimize an extraction method used for powder-from aerosol samples PAHs extraction by parameters design and theoretical calculation of response surface method, resulting in simpler operation, higher extraction effect, and lower cost.

2.1 Introduction

Polycyclic aromatic hydrocarbons (PAHs) are emitted in significant amounts from various anthropogenic sources, including diesel and gasoline vehicles, industrial processes, and solid fuel combustion [2]–[6]. Particle-bound PAHs are a crucial research topic in the fields of air pollution and human health effect because they can enter the body through the respiratory tract and induce inflammatory processes and DNA damage, which can be carcinogenic and mutagenic [7]–[9].

Particle-bound PAHs are generally collected using high-volume air sampler with different media, such as quartz and glass fiber filters. After sample pretreatment such as Soxhlet, ultrasonication, microwave-assisted extraction (MAE), pressurized liquid extraction or accelerated solvent extraction (PLE or ASE), and supercritical fluid extraction (SFE), they are detected using HPLC or GC-MS [10]–[20]. Nevertheless,

traditional aerosol sample collection and pretreatment methods have drawbacks in terms of accurately characterizing particle-bound contaminant pollution and assessing health damage. Firstly, adsorption enrichment of gaseous compounds on the filter can cause a positive/negative bias for contaminant concentration in the filter-collected sample [21]–[23]. Moreover, the PAHs present in the particles collected on the filter may undergo degradation as a result of their reaction with gaseous oxidants present in the air flowing through the membrane [24], [25]. Secondly, using filters to collect particulate matter (PM) samples raises questions regarding potential extraction artifacts, such as compositional biases in the extracted PM, volatilization losses, and contamination by filter material. The high temperature used for Soxhlet and ASE extraction can also lead to potential degradation of some non-thermolabile compounds in the extraction process. Additionally, traditional extraction methods are time- and energy-consuming, labor-intensive, and require large volumes of toxic and costly organic extraction solvents [26]–[28]. As a result, errors in concentration caused by filter sampling and pretreatment methods, as well as the inability of filter-collected samples to accurately mimic the in vivo cellular exposure reactions of inhaled PM in the human body, underscore the importance of developing a direct aerosol particle collection method that allows for simple and efficient extraction.

A cyclone is a sampling device that directly collects aerosol particles in "powder form" by using the principle of the cyclone dust collector. In brief, PM is classified by an impactor and enters the cyclone device, where $PM_{2.5}$ with an aerodynamic diameter of 2.5 μm gradually settles in the cyclone due to vortex and centrifugal force onto the inner wall of the cyclone or into the collection bottle connected to the cyclone [29]–[31]. Honda et al. [32] found that cyclone-collected powder $PM_{2.5}$ could stimulate airway epithelial cells to produce more interleukins 6 and 8 (IL-6, IL-8) and promote the secretion of IL-6, IL-1β, tumor necrosis factor-α (TNF-α), and the significant expression of cluster of differentiation 86 (CD86) and dendritic and epithelial cells 205 (DEC205) on antigen-presenting cells compared with filter-$PM_{2.5}$. Another study also

demonstrated that $PM_{2.5}$ collected using a cyclone device could significantly induce IL-33 expression in human THP-1 macrophages which might be related to the concentration of PAHs and endotoxins in PM [30]. These findings suggest that cyclone-collected powder aerosol samples are suited for characterizing the biochemical responses of human cells in vivo/vitro exposure experiments than samples collected using filters.

Given the limitations of traditional extraction methods as mentioned previously, we chose a milder extraction method for powder aerosol sample pretreatment, namely QuEChERS (quick, easy, cheap, effective, rugged, and safe). The QuEChERS extraction method was initially developed for extracting pesticides in food [33]–[35]. It is an effective sample preparation approach that involves organic solvent extraction (such as acetonitrile (ACN) and dichloromethane (DCM)) based on the dispersion of salts for extraction (salting-out effect), followed by the addition of salts and clean-up reagents to remove residual water and clean up. This method can isolate a wide range of analytes from complex matrices [36]–[38]. The primary advantage of this extraction technique is simplification of sample extraction and purification. The total extraction and clean-up time is usually approximately 10 min, and less quantity of extraction solvent is used, while still achieving high recoveries (>90%) for both polar and basic pesticides [36], [39]. In environmental pollutant analysis, the QuEChERS method has been widely used for contaminant extraction, such as pesticides, PCBs, PBDEs, and PAHs in wastewater, polluted soils, and sediments with high recoveries ranging from 60% to 110% [40]–[45]. Although the method has demonstrated a good extraction effect for PAHs and their derivatives in filter-collected aerosol samples [46], [47], it is not widely used in air pollution studies due to limitations with the filter carrier structure for particulate samples.

The extraction solvent, type of salt to improve the salting-out effect, and type of clean-up reagent can be optimized to achieve better extraction effects for different contaminant extractions from different sample matrices using the QuEChERS method.

In the original QuEChERS procedure, ACN was chosen as the extraction solvent, followed by a mixture of ACN with other solvents, such as water, methanol, ethyl acetate, and DCM, for the extraction of various target contaminants [48]–[50]. The salts commonly used in QuEChERS were a mixture of magnesium sulfate ($MgSO_4$) and sodium chloride (NaCl) in different ratios [37], [51]–[55]. However, a mixture of sodium sulfate (Na_2SO_4) and sodium acetate (NaOAc) with NaCl was also selected [33], [56], [57], especially Zhou et al. [56] demonstrated that the complexing interaction between the target extract and Mg^{2+} (from $MgSO_4$) may hinder the extraction procedure. Various clean-up reagents can be used because commonly used reagents have overlapping impurities that they can adsorb. For example, primary secondary amine (PSA), octadecyl silica (C18), graphitized carbon black (GCB), and Florisil can all be used to remove fatty acids, carbohydrates, organic acids, lipid, and pigments [58]–[60].

The objectives of this research were to use an I-optimal design of experiments with the response surface method to optimize the QuEChERS extraction method for detecting PAHs in the standard material SRM1944 sample and to investigate its application for the extraction of actual atmospheric powder particle-bound PAHs collected by cyclone. This combination of "powder aerosol particle collection and modified QuEChERS extraction" approach enables the analysis of PAHs bound to particulate matter with minimal use of organic solvents, while still achieving a high extraction yield. This optimized method is not only quick and low-cost, but also environmentally friendly.

2.2 Materials and methods

2.2.1 Reagents and materials

Acetonitrile (ACN, HPLC grade), methanol (MeOH, HPLC grade), Florisil (150-250 μm), C18 (30-50 μm), sodium acetate (NaOAc), sodium sulfate (Na_2SO_4), and magnesium sulfate heptahydrate ($MgSO_4 \cdot 7H_2O$) were purchased from Fujifilm Wako Pure Chemical Co. (Yokohama, Kanagawa, Japan). Dichloromethane (DCM, HPLC

grade) and sodium chloride (NaCl) were purchased from Junsei Chemical Co., Ltd (Tokyo, Japan). Dimethyl sulfoxide (DMSO) was purchased from Dojindo Molecular Technologies, Inc (Kawasaki, Kanagawa, Japan). Primary and secondary amine (PSA, 40μm) were purchased from Agilent Technologies (Santa Clara, CA, USA). NaOAc, Na_2SO_4, and NaCl were heated at 120 ℃ for 4 h to dry, whereas $MgSO_4 \cdot 7H_2O$ was heated at 200 ℃ for 6 h to remove the crystal water.

Ultrapure water was obtained using a water purification system (ELGA LabWater, Lane End, UK). The powder form standard reference material sample (SRM1944) was purchased from NIST (Gaithersburg, Maryland, USA). Sixteen PAHs mixture standard of naphthalene (Nap), acenaphthylene (Acy), acenaphthene (Ace), fluorene (Fl), phenanthrene (Phe), anthracene (Ant), fluoranthene (Flt), pyrene (Pyr), benz[a]anthracene (BaA), chrysene (Chr), benzo[b]fluoranthene (BbF), benzo[k]fluoranthene (BkF), benzo[a]pyrene (BaP), dibenz[a,h]anthracene (DbA), benzo[g,h,i]perylene (BgP), and indeno[1,2,3-cd]pyrene (InP) in a DCM: MeOH solution (1:1, v/v) were purchased from AccuStandard (200 μg/ml, 1 ml, AccuStandard, Inc., New Haven, CT, USA).

2.2.2 Experimental design

Extraction solvents, salts, and clean-up reagents are the primary influencing factors of the extraction effect of the QuEChERS method [61]–[63]. In the preliminary experiments, we found that the solvent mixture of ACN/DCM was more effective in extracting PAHs from SRM1944 samples than ACN and the mixture of ACN/MeOH. Therefore, we chose the mixture of ACN/DCM as the main extraction solvent and considered the proportion of DCM in the mixture as factor A, which can affect the QuEChERS extraction effect ranging from 0% to 50%. Factor B, named extraction salts, was a mixture of the three most common used salts ($MgSO_4$, Na_2SO_4, and NaOAc) and NaCl. The quality ratio of extracting salt and NaCl (w/w) in previous studies were inconsistent in either 4:1, 4:3, or even just NaCl [37], [51]–[55], thus we chose the

reagent ratio of 1:1 to ensure that we can obtain good experimental results. Factor C named clean-up reagents consisted of C18, PSA, and Florisil. Factor A is a numeric factor that can be comprise a value within the interval of 0 to 0.5. Factors B and C are categorical factors that can only correspond to the three types of substances. We used a response surface design method, named I-optimal (custom) design to design the QuEChERS extraction experiments. The coded values of these three factors are listed in **Table 2.1**.

Table 2.1 Codes of QuEChERS extraction parameters for optimal (custom) design

Factor	Types	-1	0	1
Percentage of DCM in extraction solvents (v/v) (A)	numeric		0 to 50%	
Salt (1:1, w/w) (B)	categoric	$MgSO_4$+NaCl	Na_2SO_4+NaCl	NaOAc+NaCl
Clean-up reagent (C)	categoric	PSA	C18	Florisil

2.2.3 Sample pre-treatment

For the traditional Soxhlet extraction of the SRM1944 sample, a modified Soxhlet apparatus (Büchi B-811, Switzerland) was used. A 50 mg sample was added to the glass extracting tube, and the solvent used was 120 ml DCM. The hot Soxhlet model was used for sample extraction. Extraction time was 3 h, followed by rinsing for 20 min. After extraction, the solvent was added to 200 μl of DMSO and reduced to 1 ml using rotary evaporation. The concentrated solution was dried with pure nitrogen gas (at room temperature), redissolved with 800 μl of ACN to 1ml, and filtered through a 0.22 μm membrane (PTFE, Hawach Scientific, Japan) for HPLC analysis. The detailed procedure has been reported in a previous study [12].

For QuEChERS extraction, 100 mg SRM1944 sample was placed in a centrifuge tube, and 100 mg of extracting salts was added with 2 ml of the extraction solvent. Next, ultrasonic extraction at 40 kHz for 20 min was performed, followed by centrifugation for 5 min at 3500 rpm. The supernatant was transferred to another centrifuge tube containing 40 mg of clean-up reagent and 80 mg of Na_2SO_4. After shaking for 5min,

followed by centrifugation for 5 min at 4500 rpm, 800 µl of supernatant was collected and filtered using a 0.22 µm membrane for HPLC analysis.

2.2.4 PAHs analysis

The HPLC system used for PAHs determination included an SCL-10Avp system controller, a DGU-12A degasser, two LC-10ATvp pumps, an SIL-10ADvp auto-injector, a CTO-10ASvp column oven, and an RF-10AXL fluorescence detector (FLD), which were all produced by Shimadzu Co. (Tokyo, Japan). The separation column used in this study was SPELCOSIL LC-PAHs (ODS column, 3.0 mm × 250 mm × 5 µm, Spelco, Co., Bellefonte, USA). The column oven temperature was 35 ℃, and the sample injection volume was 20 µl. The mobile phase was the mixture of ACN and water with the following gradient elution program: 65% ACN (v/v) at the beginning, 5 min hold then increased to 86% ACN linearly in 14 min, followed by a linear increased to 90% ACN in 12 min, 4 min linear gradient to 100% ACN and held for 2 min. The flow rate was 0.6 ml/min. The PAHs detection conditions (excitation and emission wavelength, Ex/Em) were adjusted according to the following time program: 270 nm/340 nm at the beginning, 254/370 nm at 8 min, 260/420 nm at 10 min, 254/390 nm at 13.4 min, 260/420 nm at 21.8 min, and 293/498 nm at 34.3 min.

The PAHs contaminants extracted from the SRM1944 sample were identified by comparison of retention times with those of standard compounds detected using the HPLC/FLD system (**Fig. 2.1**). Nap was not detected by HPLC/FLD due to its instability, whereas Acy was inactive under fluorescence irradiation [64], [65]. Therefore, the quantification of the 14 PAHs was based on constructing six-point calibration curves by diluting the 200 µg/ml PAHs standard solution in ACN into six concentration standard solutions which were 0.01, 0.05, 0.1, 0.5, 1, and 2 µg/ml. The calibration curves were highly linear (R^2>0.996). The limit of detection (LOD) and limit of quantification (LOQ) were calculated based on the parameters of the contaminant standard curves according to **Eq. 2.1** and **Eq. 2.2**, respectively.

$$LOD = (3.3 \cdot s)/b \tag{2.1}$$

$$LOQ = (10 \cdot s)/b \tag{2.2}$$

where s means the intercept's standard deviation (SD), and b means the calibration curve slope [66]. The LOD of the 14 PAHs were in the range of 1.9-27.2 ng/ml, and the LOQ ranged from 5.8-82.6 ng/ml (**Table 2.2**).

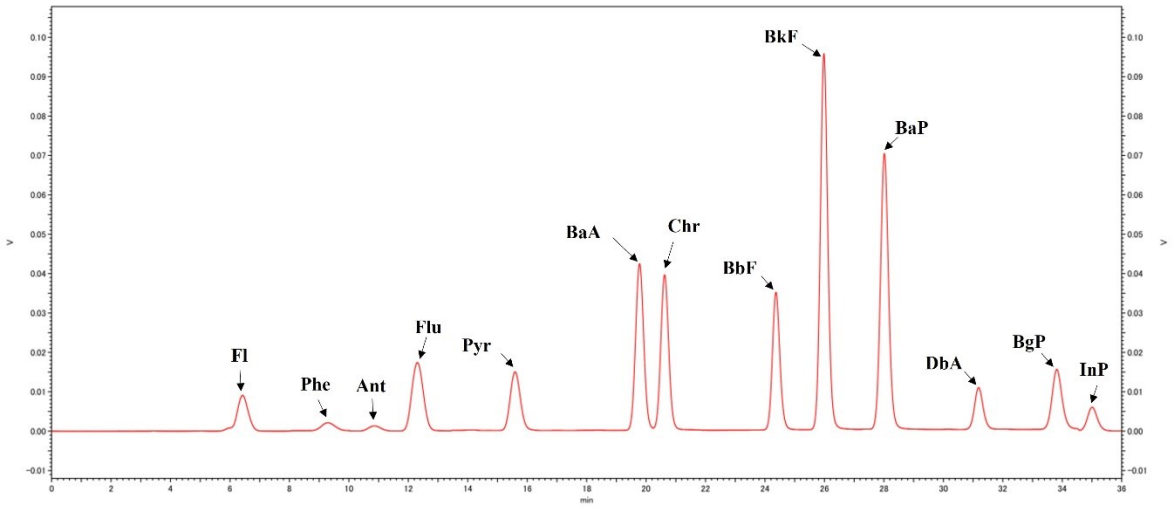


Fig. 2.1 PAHs chromatogram of standard solution

Table 2.2 Regression equations and correlation coefficients of calibration curves as well as LODs and LOQs (ng/ml) of 14 PAHs

Compounds	Regression equation	R^2	LOD	LOQ
Acenaphthene, Ace	y=21610.95x+657.74	0.9988	27	83
Fluorene, Fl	y=297332.81x+7709.20	0.9986	2	6
Phenanthrene, Phe	y=93348.61x+2299.05	0.9993	15	47
Anthracene, Ant	y=45552.73x+1734.24	0.9986	23	70
Fluoranthene, Flu	y=455262.59x+22374.71	0.9966	2	6
Pyrene, Pyr	y=506859.37x+9819.51	0.9994	2	7
Benz[a]anthracene, BaA	y=1133410.27x+30431.12	0.9989	4	12
Chrysene, Chr	y=1079093.39x+24856.47	0.9991	3	10
Benzo[b]fluoranthene, BbF	y=829978.28x+23960.87	0.9994	4	13
Benzo[k]fluoranthene, BkF	y=2296087.82x+64305.21	0.9988	5	14
Benzo[a]pyrene, BaP	y=1733896.38x+24187.98	0.9997	4	12
Dibenz[a,h]anthracene, DbA	y=344481.02x+762.13	0.9998	8	24
Benzo[g,h,i]perylene, BgP	y=510468.34x+20318.76	0.9997	3	10
Indeno[1,2,3-cd]pyrene, InP	y=112058.15x+5793.81	0.9981	11	36

2.2.5 Environmental powder aerosol sample

The actual environmental powder aerosol sample that a diameter smaller than 2.5μm was collected at Xi'an Jiaotong University (XJTU), China named CHN-PM2.5-23 using a large cyclone powder particle sampler. XJTU located in Xi'an, Shaanxi Province, which located in the Guanzhong Plain and is an important manufacturing and energy base in China. The sampling point (34°14'N, 108°59'E) is sited on the 6th floor of a teaching building (about 20m from the ground) on the Xingqin campus of XJTU, while near to the Xingqin roads and South Second Ring Road, where have heavy traffic flow (**Fig. 2.2**). The sampling period was from 1/4 to 1/28/2021, collected total powder aerosol particle sample was 3820 mg, sealed in a brown glass bottle and stored at 4 ℃

until analysis. The detail of the cyclone sampler refers to our previous studies [29], [67].

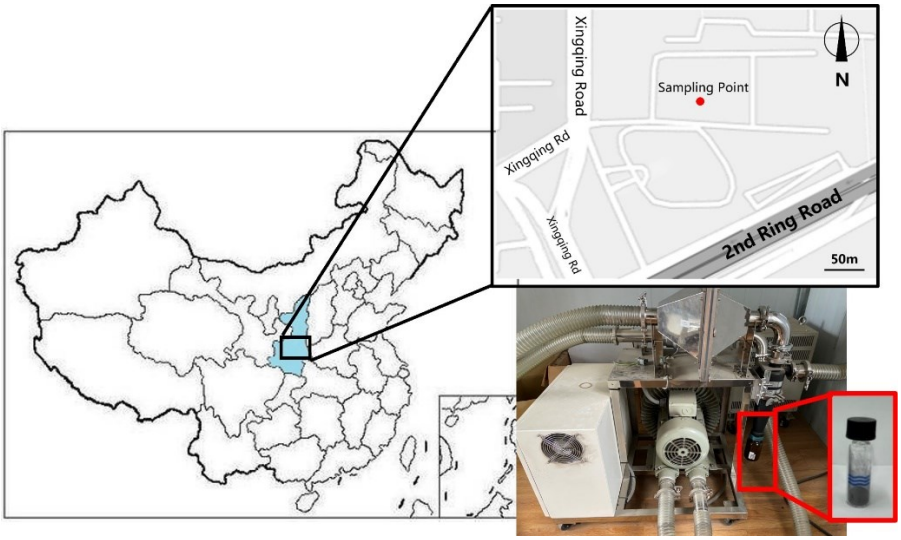


Fig. 2.2 Sampling site of actual aerosol particle and picture of the cyclone and sample

2.2.6 Statistical analysis

The extraction effect of each QuEChERS parameters combination experiment was determined using the recoveries of the 14 PAHs. The recoveries were calculated by the ratio of the contaminant concentration extracted using QuEChERS and Soxhlet extraction, which could avoid the influence of the matrix effect. When the recovery rate is zero, it suggests that the extraction conditions used for contaminant extraction did not work effectively. Conversely, a recovery rate of one indicates that the contaminant was fully extracted from the sample matrix, indicating optimal extraction efficiency. In actual research, a recovery rate between 70% and 130% indicates that the substance has a good recovery effect under the corresponding method [68]. To evaluate the effectiveness of each QuEChERS parameter combination experiment, we used the desirability function (**Eq. 2.3**) to convert the recoveries of all PAHs in each extraction combination experiment to values between zero and one, where d_i means the individual desirability for each PAH, and y means the recovery rate.

$$d_i = \begin{cases} \dfrac{y}{0.7}, & if\ y < 0.7 \\ 1, if\ 0.7 < y < 1.3 \\ \dfrac{3.0 - y}{3.0 - 1.3}, if\ y > 1.3 \end{cases} \quad (2.3)$$

To simplify the complexity of experimental design model prediction, we converted the individual desirability of each PAH (d_i) to the overall desirability (OD) as the response value for each group experiment using **Eq. 2.4**, where k is the number of individual desirability [69].

$$OD = \sqrt[k]{d_1 \cdot d_2 \cdots d_k} \quad (2.4)$$

The detecting results for all samples are reported as the mean values of triplicate measurements (n=3). Design Expert software (version 12) was used for the experimental design, I-optimal design result analysis including analysis of variance (ANOVA), lack of fit, determination coefficient (R^2), and experimental parameters optimization. The recovery rate and desirability function were calculated using Origin software (version OriginPro 2018C).

2.3 Results and discussion

2.3.1 I-optimal design results

The parameter combinations for each QuEChERS extraction experiment of the I-optimal (custom) design with the overall desirability (OD) are listed in **Table 2.3**. The experimental design included two lack-of-fit groups (Runs 13 and 17) which were used to make the design more robust to terms not in the design model, and two replication groups (Runs 4 and 20) which were used to support the optimality. We used the "categoric balance" strategy to force that all three codes (-1, 0, 1) in each categoric factor were present in equal amounts. Not following this method could result in a design with more codes than another in one categoric factor, which could potentially influence the model prediction result. The OD value was calculated using the recoveries of 11 PAHs following **Eq. 2.3** and **Eq. 2.4**, with the data lacking Ace, Fl, and Flt because of

the Soxhlet extraction evaporation loss and their low actual concentration in the SRM1944 sample.

The fitting results of several models showed that the 2-factor interaction (2FI) model had the best performance. The ANOVA and lack-of-fit results for the 2FI model are presented in **Table 2.4**. The model was significant (p-value=0.022<0.05), with a not significant lack of fit (p-value = 0.248>0.1). The results demonstrated good model performance for fitting and predicting the response values, as well as a high correlation coefficient of R^2=0.92 between the prediction values and actual responses. The model F-value of 5.64 implies that there is only a 2.17% chance that an F-value this high could occur due to noise, and the lack of fit F-value of 2.38 implies that the lack of fit is not significant relative to the pure error. A non-significant lack of fit is favorable, indicating that there is only a 24.75% chance that a lack of fit F-value this large could occur due to noise. The signal-to-noise ratio (S/N=6.601) greater than 4 indicated that this model had adequate discrimination.

Table 2.3 Experimental conditions for the optimal design performance of the extraction solvent, salt, and clean-up reagent optimization and the overall desirability (OD)

Run	Type	Factor A	Factor B	Factor C	OD
1	Model	0	1	-1	0.941
2	Model	12.5%	-1	0	0.896
3	Model	0	-1	1	0.954
4	Replicate	25%	1	-1	0.899
5	Model	12.5%	1	0	0.907
6	Model	12.5%	0	-1	1.000
7	Model	37.5%	0	0	0.951
8	Model	25%	-1	-1	0.972
9	Model	25%	1	-1	0.899
10	Model	25%	-1	0	0.948
11	Model	0	0	0	0.983
12	Model	33.33%	0	1	0.928
13	Lack of Fit	0	-1	1	0.992
14	Model	12.5%	1	1	0.970
15	Model	37.5%	-1	1	0.886
16	Model	37.5%	1	0	0.891
17	Lack of Fit	0	0	1	0.992
18	Model	50%	1	1	0.908
19	Model	50%	0	-1	0.890
20	Replicate	12.5%	0	-1	1.000

Table 2.4 Analysis of variance (ANOVA) analysis for the 2-factor interaction (2Fl) model

Source	Sum of Squares	df	Mean Square	F-value	p-value	
Model	0.0297	13	0.0023	5.64	0.022	significant
A-percentage of DCM	0.0111	1	0.0111	27.42	0.002	significant
B-salt	0.0080	2	0.0040	9.85	0.013	significant
C-clean-up reagent	0.0008	2	0.0004	0.98	0.430	
AB	0.0009	2	0.0005	1.16	0.376	
AC	0.0058	2	0.0029	7.20	0.025	significant
BC	0.0060	4	0.0015	3.70	0.075	
Residual	0.0024	6	0.0004			
Lack of Fit	0.0017	3	0.0006	2.38	0.248	not significant
Pure Error	0.0007	3	0.0002			
Cor Total	0.0321	19				

Based on the *p*-value of each single factor, the percentage of DCM in the extraction solvents mixture (factor A, $p=0.002<0.05$) and salts (factor B, $p=0.013<0.05$) were influential factors that showed a significant positive effect on the response value (OD), with no significant effect of factor C ($p=0.430>0.1$). However, in addition to the influence of the single factor, the 2FI model also accounted for the influence of the interaction of the two factors on the response results. **Fig. 2.3** - **Fig. 2.5** shows the interaction plots of the two factors. The interaction plot displays the levels of one variable on the x-axis and has a separate line to present each level of another variable (lines with different colors) under the confirmed third variable, which provides additional information on the second-order interaction between two factors. The dashed line indicates the 95% confidence interval (95% CI) of response value at the

corresponding factor combination.

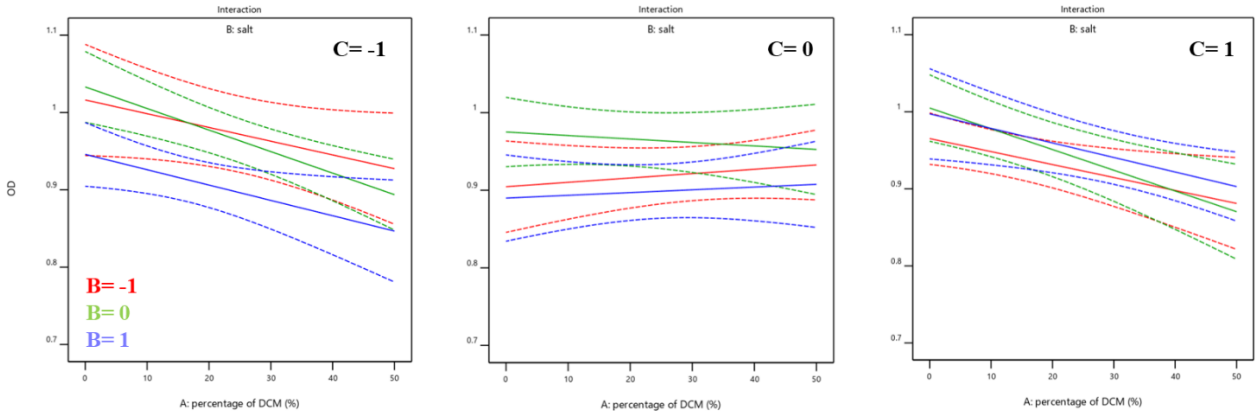


Fig. 2.3 Design expert interaction plot for factors A and B

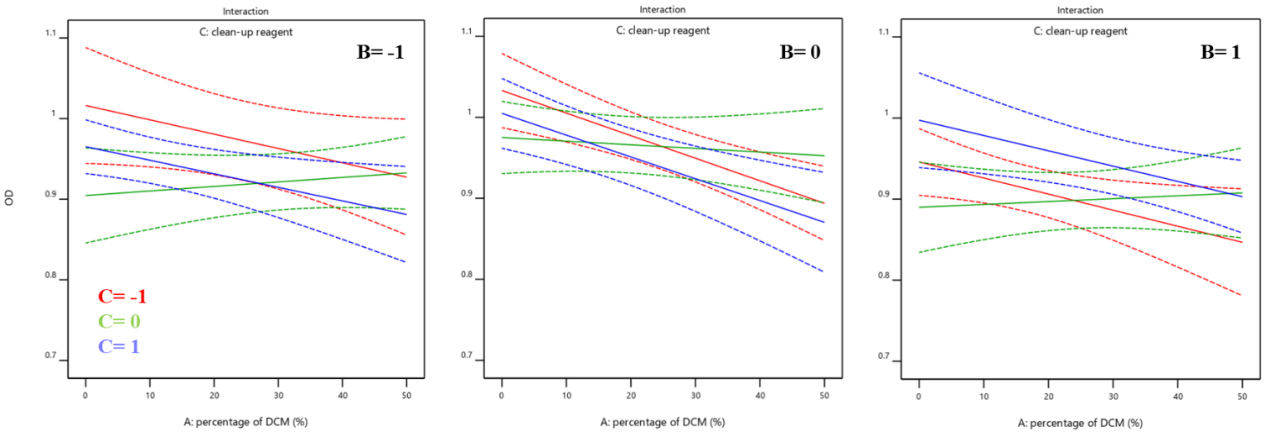


Fig. 2.4 Design expert interaction plot for factors A and C

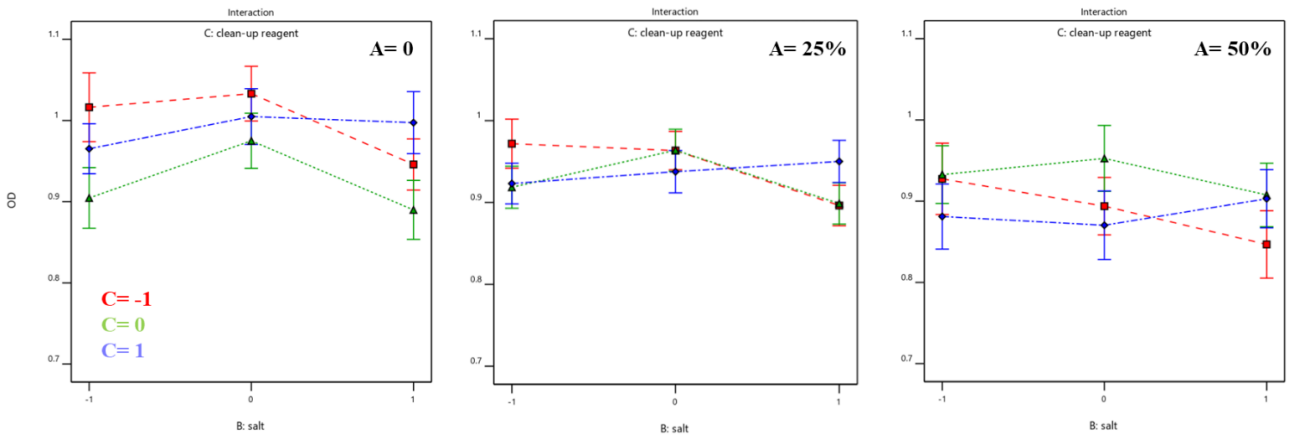


Fig. 2.5 Design expert interaction plot for factors B and C

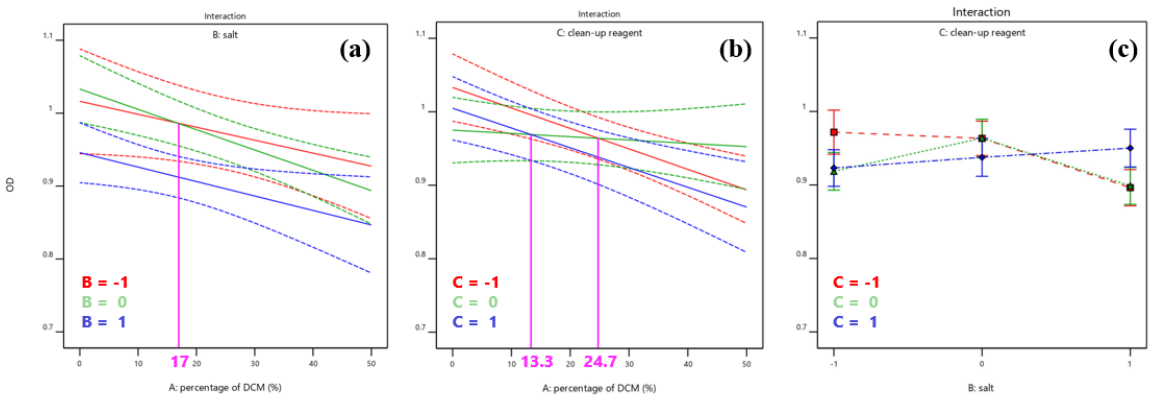


Fig. 2.6 Design expert interaction plot for factors (a) AB (C=-1), (b) AC (B=0), and (c) BC (A=25%)

Using the interaction of the factors A and B as an example (**Fig. 2.6(a)**), we concluded that the use of $MgSO_4$ or Na_2SO_4 as the extracting salt had a predominant effect on the response values, provided PSA was used as the clean-up reagent (C=-1). When the DCM percentage was less than 17% (factor A on x-axis < 17%), using Na_2SO_4/NaCl as the extracting salts (B=0) had a better extraction effect than that using $MgSO_4$/NaCl (B=-1), as indicated by the green line being above the red line in **Fig. 2.6(a)**, whereas the opposite was true when A>17%. In previous studies, ACN and DCM were used as single reagents, or mixed with other solvents with similar polarities, such as ACN/water and DCM/hexane, for PAHs extraction from the sample matrix [70]–[74]. However, some studies also found that the mixture of ACN and DCM, two solvents with a large difference in polarity, also has a good extraction effect on PAHs [75]–[77]. This phenomenon may be because the internal cavity structures inside PM2.5 make pollutants, such as PAHs, highly likely to exist in these cavities in addition to being adsorbed on the surface of the PM. The water contained in particles creates a "liquid seal" in these cavities, which maintains a relatively stable microenvironment. DCM is a non-polar solvent that matches the characteristics of PAHs, but it is insoluble in water; therefore, it can only extract PAHs from the particle surface. However, ACN is miscible with water, and its surface tension is lower than that of water, making it easier to penetrate these cavities and effectively extract the PAHs adsorbed on the inner

surface. This phenomenon can also explain why an increase in the proportion of DCM in the mixed solvent result in a significant decrease in the OD value because the water-insoluble DCM is unable to extract the PAHs adsorbed on the inner surface of the water bubbles. The combination of $MgSO_4$ and NaCl was the most commonly used extraction salt combination in the QuEChERS extraction method for different types of contaminants because of the best salting-out effect of $MgSO_4$ of ACN while NaCl can increase the selectivity through controlling the polarity of the extraction solvents [63]. When the concentration of ACN in the extraction solvent was high, the salting-out effect of Na_2SO_4 and $MgSO_4$ in ACN was not significantly different. However, when the concentration of DCM in the extraction solvent increased, the more competitive salting-out effect of $MgSO_4$ caused more PAHs to be extracted into the ACN phase, thus increasing the extraction efficiency. This interpretation contrasts with that of Zhou et al. [56] who argued that the combination of Na_2SO_4 and NaCl gives better extraction efficiency than $MgSO_4$+NaCl because of the complexing interactions that occurred between the target veterinary drugs and Mg^{2+} (from $MgSO_4$) which hindered the extraction procedure. However, this complexing reaction between PAHs and metallic ions has never been reported before. The worst results were obtained when NaOAc/NaCl were used as the extracting salts (the blue line was always lower than the other two lines), probably because NaOAc, a weak acid salt, is difficult to completely hydrolyze in the solution. This property results in a low ionic strength in the extracting solution which influences the co-extractive interferences and decreases the transfer of PAHs to the extractant.

Fig. 2.6(b) shows a clear interaction effect between the extraction solvents and clean-up reagents (factors A and C) on QuEChERS extraction efficiency when using Na_2SO_4/NaCl as salts (B=0). The significant result of the AC model term in the ANOVA also confirmed this phenomenon (p<0.05). The effectiveness of C18 in purifying the sample remained constant, while the efficiency of PSA and Florisil decreased as the concentration of DCM in the extraction solution increased. When the proportion of

DCM in the solvent surpassed 13.3%, C18 became the second most influential sorbent, replacing Florisil in affecting the extraction response. Further increases in DCM concentration to 24.7% caused the C18 sorbent to surpass PSA as the most effective substance in achieving the optimal extraction result. The complex interaction between the factors A and C may be due to the concentration increasing of DCM in the ACN/DCM mixed solution, which changes the polarity of the extraction solvent and causes more organic impurities to be extracted from the sample matrix. The dominance of different clean-up reagents under different DCM proportions is consistent with this result. The fact that PSA showed a better cleaning effect under low-concentration DCM is consistent with the findings of Li et al. [60] who used PSA as the clean-up reagent for 16 PAHs extracted from vegetables using the QuEChERS-based extraction method but contrary to that of Albinet et al. [46] who used Florisil as the cleaner for PAHs extraction from filter-particle samples. This result indicates that there is no single clean-up reagent that is suitable for all cases. The contaminants adsorption types of the three absorbents overlap, and the choice of clean-up sorbents can be affected by different types of sample matrices and target extractants, as well as variations in the proportion of extractants in the same cluster experiments.

Factors B and C are categoric types, thus the interaction plots of B and C are specific points instead of a continuous curve when factor A comprises a different value. **Fig. 2.6(c)** shows that the clean-up reagent with the best response value at different extraction salt levels was different when factor A was at 25%. Selecting PSA as the clean-up reagent resulted in the maximum response value when using $MgSO_4$/NaCl as the extracting salt (point (-1, -1)). On the contrary, the best response was obtained with Florisil when NaOAc was used as the extracting salt (point (1, 1)). The extraction effect was the same with PSA and C18 as the sorbent when Na_2SO_4/NaCl were used (point (0, -1) and (0, 1)). The purpose of adding extraction salt to the organic extraction solvent was to transfer the extract from the aqueous and sample matrix to the organic layer through the salting-out effect to increase the extraction efficiency, and the clean-up

reagent was used to remove impurities in the supernatant that were centrifuged from first-step extraction. The interaction of these two factors implies that the befitting combination of extraction salts and absorbs can increase the extraction and removal of specific impurities from the sample matrix. However, because several types of clean-up reagents can be used in overlapping application areas, the choice of absorbent is not unique. As a result, the term BC may not be not significant enough (p=0.075).

2.3.2 Extraction parameters optimization

Based on the experimental data obtained using the I-optimal design method, the 2FI model can explain the mathematical relationship between the three main parameters of QuEChERS and the extraction effect of PAHs. This result allows us to use the model to optimize the extraction parameters combination to obtain the best response values. Prior to optimization, however, it is imperative to establish the constraints associated with the parameters. During the sample pre-treatment step in research that uses DCM as a PAHs extraction solvent and water as the mobile phase of the HPLC detection system, DCM is often removed by nitrogen blowing then the extraction solvent is converted to other organic solvents, such as ACN or MeOH, which are miscible with water [64], [78], [79]. As shown in **Fig. 2.7** that the separation of PAHs characteristic peaks and impurity peaks becomes less effective as the DCM percentage increasing. This phenomenon is likely because the presence of DCM affects the elution and peak performance of contaminants on the HPLC column because it is immiscible with water. To reduce the influence of the extracted solvent components on the HPLC result, we set the range for factor A (the percentage of DCM in extraction solvents) to be 0%-15%. In addition, we set the range of values for the response results (OD) to be 0.99-1.00. A high OD value indicates that a higher number of PAHs contaminants have a recovery rate within the optimal range of 70% to 130%, which indicates a better extraction effect. The optimization results of the QuEChERS extraction parameters under the above boundary conditions are shown in **Fig. 2.8**.

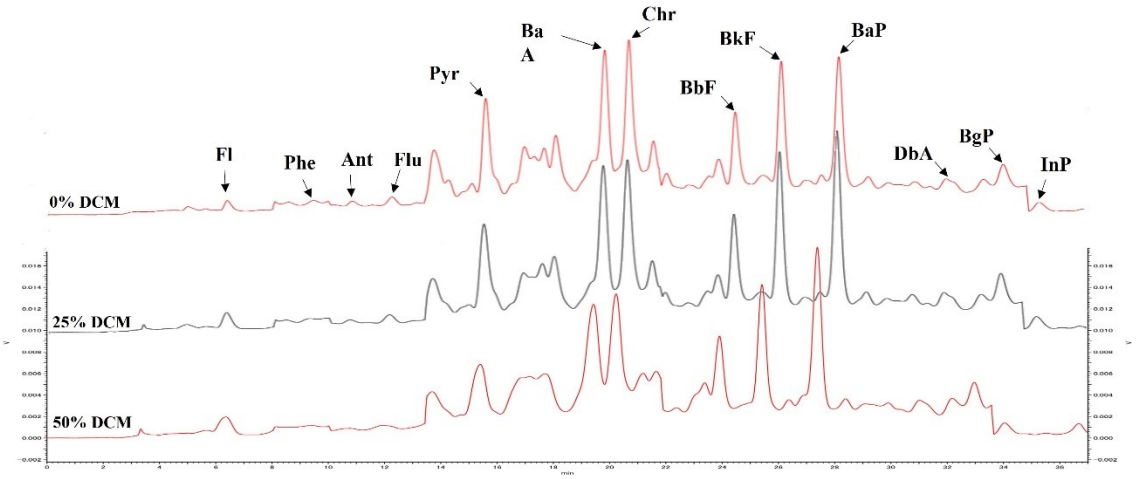


Fig. 2.7 Chromatograms comparison between different DCM percentage in mixture extraction solvents (arbitrary scale)

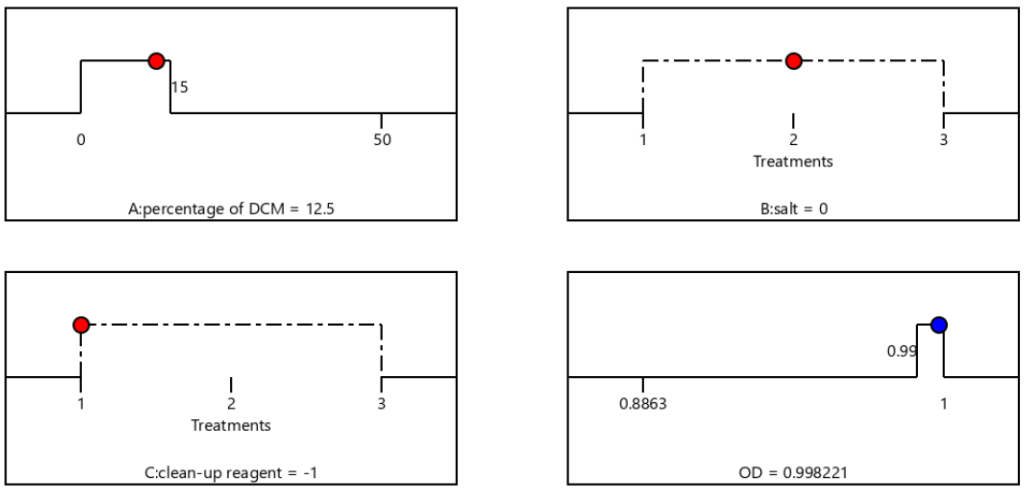


Fig. 2.8 QuEChERS parameters optimization result using I-optimal design and 2FI model

The prediction results of the I-optimal design and 2FI model indicated that the best response value, OD=0.998 (95% CI: 0.965-1.032), was obtained when the DCM percentage in the extraction solvents was 12.5% (A=12.5), Na_2SO_4+NaCl was used as the extracting salts (B=0), and PSA was used as the clean-up reagent (C=-1). This parameters combination corresponds to experiment Runs 6 and 20, whereas, the better response values of these two experiments (OD=1.000) also confirm the accuracy of the

2FI model prediction. The detailed PAHs recovery rates of Runs 6 and 20 are listed in **Table 2.5**.

Table 2.5 PAHs recoveries rate and OD values of Run 6 and Run 20

Compounds	Run 6		Run 20	
	recovery	d_i	recovery	d_i
Phe	0.79	1	0.76	1
Ant	0.91	1	0.81	1
Pry	1.18	1	1.22	1
BaA	1.14	1	1.15	1
Chr	1.04	1	1.17	1
BbF	0.87	1	0.96	1
BkF	0.85	1	0.90	1
BaP	0.91	1	0.95	1
DbA	0.80	1	0.82	1
BgP	1.04	1	1.06	1
InP	0.93	1	0.96	1
OD		1.000		1.000

A DCM concentration of 12.5% (250 μl of 2 ml) is relatively low, but the immiscibility of DCM and water may still affect the elution of contaminants on the surface of the column packing at the microscopic level, resulting in the chromatogram performance. Therefore, we designed an experiment to test the influence of DCM on the optimization conditions for the contaminant chromatogram results. The solvent extracted from one SRM1944 sample using the optimal conditions was divided into two equal-volume samples (0.8 ml of each). Sample 1, named “original”, was filtered through a 0.22 μm membrane and directly injected for HPLC detection. Sample 2 was added to 200 μl of DMSO and dried with pure N_2 (at room temperature) to remove the DCM in the solution then redissolved with ACN to 1 ml, then filtered by 0.22 μm

membrane for HPLC analysis and named "N_2 dry". A comparison of the PAHs concentrations between the two samples is shown in **Fig. 2.9**.

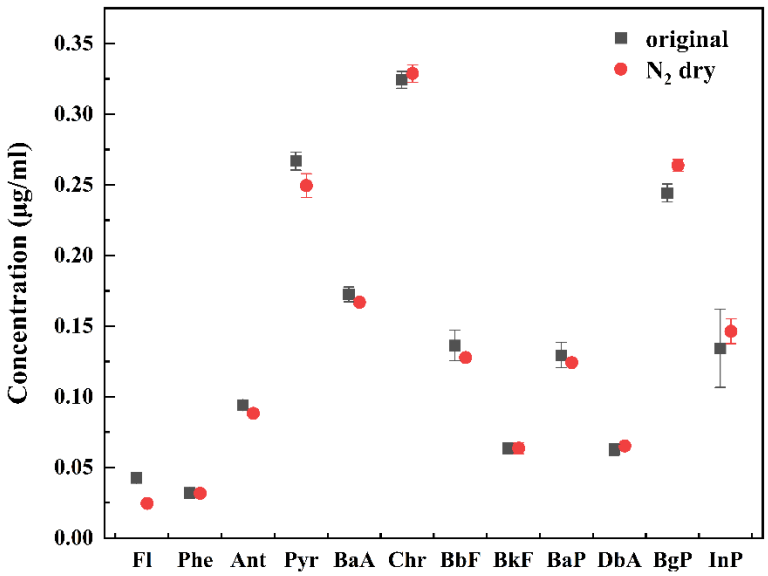


Fig. 2.9 PAHs concentration comparison between the original detecting sample and N_2 dry sample

Fig. 2.9 indicates that the contaminant concentrations are the same in the two samples with or without DCM. This result suggests that the immiscibility of 12.5% DCM under optimal extraction conditions with the mobile phase in the HPLC system did not affect the PAHs detection results. Conversely, the increased use of the N_2 purge procedure to remove DCM from the testing sample would result in additional losses of volatile components (low concentration of Fl and Pyr in the "N_2 dry" sample than "original" sample). Moreover, multiple transfers and dilutions of the sample could cause calculation errors in the contaminant concentrations (as evidenced by the concentration difference of BgP and InP in the two samples). Therefore, the QuEChERS method with optimized conditions can reduce experimental operation and prevent unnecessary experimental errors while ensuring good extraction results.

Regarding the good extraction performance of the optimized QuEChERS conditions for PAHs extraction from powder samples, we need determine whether if it is applicable to all PAHs extraction that were not tested in the above research. To assess this condition,

we utilized two standard solutions (SSs) with the concentration of 0.5 and 1.0 μg/ml to evaluate the extraction effect of the optimized QuEChERS conditions for all 14 PAHs. The experimental parameters are outlined below:

The volume of a standard solution: 1ml

Extraction solvents: 2 ml ACN/DCM (7:1, v/v)

Salts: 100 mg Na_2SO_4/NaCl (1:1, w/w)

Clean-up reagents: 40 mg PSA + 80 mg Na_2SO_4

The recoveries of the 14 PAHs from the two standard solutions are presented in **Fig. 2.10**. The detected concentration of the contaminant in the analyzed sample was found to be one-third of the original concentration, obtained by using a 2:1 ratio of extraction solvents to standard solution. Therefore, the absence of recovery data for Ace at a concentration of 0.5 μg/ml was attributed to the Ace concentration falling below the limit of quantification (LOQ) for this pollutant in the HPLC system.

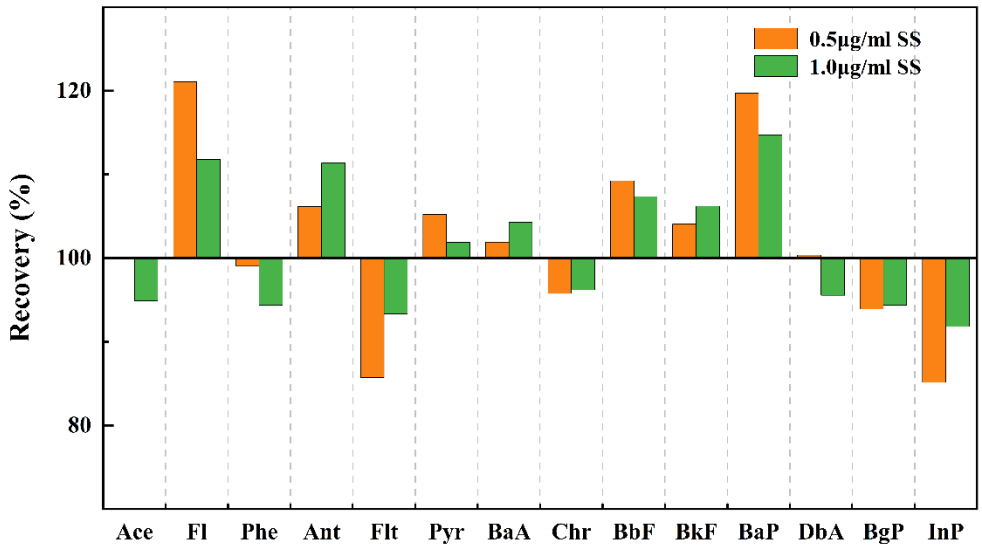


Fig. 2.10 14 PAHs recoveries in two standard solutions extracted by optimal QuEChERS parameters combination

The recoveries of 13 PAHs at a concentration of 0.5 μg/ml SS were in the range of 85.1% to 121.1% (102.1% on average), whereas 14 PAHs recoveries of 1.0 μg/ml SS

were in the range of 93.4% to 114.7% (101.3% on average). The Soxhlet extraction of SRM1944 resulted in the loss of Ace and Fl due to evaporation, rendering it impossible to evaluate the extraction efficacy and recovery efficiency of QuEChERS for these two target contaminants in SRM1944 sample. However, good extraction results were obtained for these two contaminants in the SS testing, with a recovery of 94.9% for Ace in 1.0 μg/ml SS, and recoveries of 121.1% and 111.8% for Fl in 0.5 and 1.0 μg/ml SS, respectively. In comparison to the recovery of Flt in SRM1944, which could not be calculated because its concentration was lower than the LOD of HPLC system, the recovery reached 85.7% and 93.4% in 0.5 and 1.0 μg/ml SS, respectively. These results demonstrate that the optimal extraction conditions have a good extraction effect for all 14 PAHs.

2.3.3 Actual sample extraction

We tested the application of the optimized QuEChERS method for PAHs extraction in an actual environmental aerosol sample named CHN-PM2.5-23. This sample was collected by large cyclone sampler sited in Xi'an, China. We weighed 30 mg of the sample and used the Soxhlet method to extract PAHs in it. The use of excess sample was to ensure that the concentration of PAHs in the extract is sufficient to be detected. For comparison, we weighed 10 mg of the sample and used the optimized QuEChERS method for PAHs extraction. The two extraction procedures were the same as those described in Section 2.3. We also reduced the amounts of reagents required for QuEChERS extraction owing to the lower sample usage. The detailed QuEChERS reagents usage is listed below. **Fig. 2.11** shows the PAHs concentration obtained from the two methods and their recoveries.

CHN-PM2.5-23 sample: 10 mg

Extraction solvents: 0.4 ml ACN/DCM (7:1, v/v)

Salts: 20 mg Na_2SO_4/NaCl (1:1, w/w)

Clean-up reagents: 8 mg PSA + 16 mg Na_2SO_4

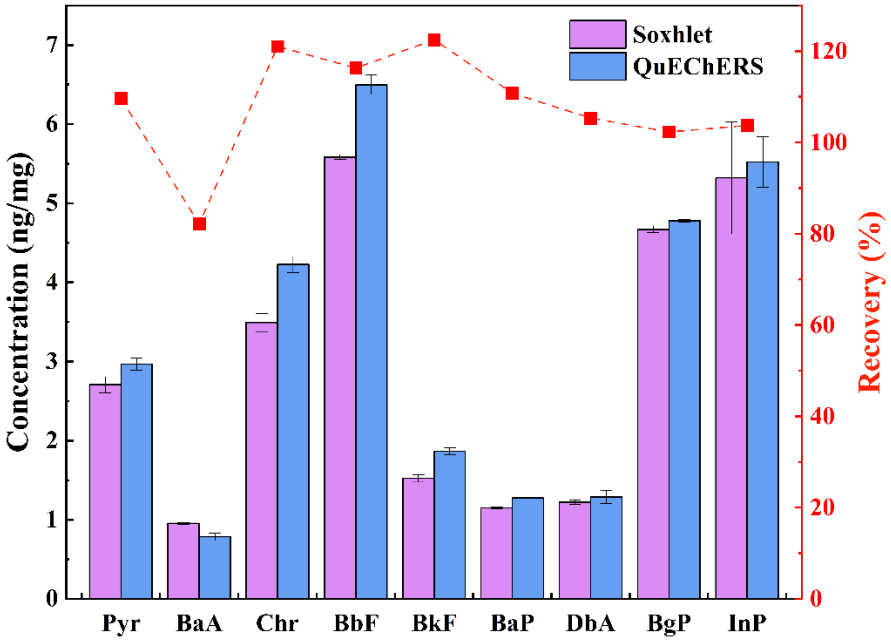


Fig. 2.11 PAHs concentration comparison between the two extraction methods and recoveries of CHN-PM2.5-23 sample (n=3)

Fig. 2.11 shows that the optimized QuEChERS method had comparable extraction efficiency to the traditional Soxhlet method. The PAHs concentration obtained by the two methods were similar, and the PAHs recoveries were in the range of 80% to 120% (108% on average). The optimized QuEChERS reagent dosage can be adjusted according to the amount of sample to be treated while maintaining the extraction effect, ensuring reliable experimental results while minimizing the use of toxic reagents. **Table 2.6** compares the solvent volumes, time consumption, and cost of PAHs extraction (per mg sample) from atmospheric aerosol particle using the QuEChERS and Soxhlet methods. QuEChERS can significantly reduce the use of extraction solvent, especially the volume of DCM which is a potentially hazardous chemical. Without considering the detection speed of the HPLC system, the optimized QuEChERS can process 24-27 samples per day in sequence compared with the conventional methods (the extraction rate of QuEChERS is nine times faster than that of Soxhlet). The estimated extraction cost (per mg sample) using the optimized QuEChERS is about 0.4 JPY (Japanese Yen, including the cost of solvent and electricity), compared with approximately 18.7 JPY

per mg sample using Soxhlet and more using other extraction methods.

Table 2.6 Comparison of solvent volume, time consumption, and cost of PAHs extraction using two methods

Sample mass	Extraction method	Solvent (volume)	Extracting	Concentrating and cleaning-up	Cost (per mg sample)
10mg	QuEChERS	ACN/DCM (7:1, v/v) (0.4ml)	20min	5min	0.4 JPY
30mg	Soxhlet	DCM (120ml)	200min	30min	18.7JPY

2.4 Summary

This study was undertaken to design interaction experiments of three main factors of the QuEChERS extraction method using the response surface method and evaluate the application of optimal extraction combination for cyclone-collected powder aerosol samples PAHs extraction results. The method presented here is based on ultrasonic extraction, and uses the I-optimal design method to investigate the interaction and contribution of the three main factors (extraction solvent, salt, and clean-up reagent) in the QuEChERS method for the extraction of PAHs from the standard sample SRM1944. Subsequently, the 2FI model was used to calculate the optimal combination of extraction parameters, combining the experimental results and boundary conditions. The optimal combination was determined to be as follows:

- Extraction solvents: ACN/DCM (7:1, v/v)
- Extraction salts: Na_2SO_4/NaCl (1:1, w/w)
- Clean-up reagents: PSA

This combination had good PAHs recovery rates of 76%-118% and 85%-121% for the standard material and standard solutions, respectively. The results of applying the optimal QuEChERS method to actual aerosol samples indicated that this method has a good extraction efficiency as the traditional Soxhlet method while adjusting the

reagents usage flexibility following the mass of sample. The developed method can significantly reduce the use of toxic organic extraction solvents and costs while improving the experimental efficiency for particle-bound PAHs extraction combined with the powder aerosol sample collected by the cyclone. The combination of "powder aerosol particle collection and modified QuEChERS extraction" is an excellent alternative to the particle-bound contaminants collection and extraction most common reported in the literature. In future study, we will continue to optimize the amount of QuEChERS reagents and investigate the pollution characteristics of powder particle-bound PAHs, including their concentrations, trends, and correlations with other contaminants.

2.5 Reference

[1] W. Jing, K. Nakano, Z. Shen, and T. Okuda, “Optimization of the QuEChERS extraction method to determine Polycyclic Aromatic Hydrocarbons (PAHs) in powder aerosol particles collected by cyclone,” *Environ. Technol. Innov.*, vol. 31, p. 103141, Aug. 2023, doi: 10.1016/j.eti.2023.103141.

[2] U. M. Sofowote *et al.*, “Assessing the long-range transport of PAH to a sub-Arctic site using positive matrix factorization and potential source contribution function,” *Atmos. Environ.*, vol. 45, no. 4, pp. 967–976, Feb. 2011, doi: 10.1016/j.atmosenv.2010.11.005.

[3] Y. Lin, X. Qiu, Y. Ma, J. Ma, M. Zheng, and M. Shao, “Concentrations and spatial distribution of polycyclic aromatic hydrocarbons (PAHs) and nitrated PAHs (NPAHs) in the atmosphere of North China, and the transformation from PAHs to NPAHs,” *Environ. Pollut.*, vol. 196, pp. 164–170, Jan. 2015, doi: 10.1016/j.envpol.2014.10.005.

[4] M. Gope, R. E. Masto, J. George, and S. Balachandran, “Exposure and cancer risk assessment of polycyclic aromatic hydrocarbons (PAHs) in the street dust of Asansol city, India,” *Sustain. Cities Soc.*, vol. 38, pp. 616–626, Apr. 2018, doi: 10.1016/j.scs.2018.01.006.

[5] E. Kalisa *et al.*, “Pollution characteristics and risk assessment of ambient PM2.5-bound PAHs and NPAHs in typical Japanese and New Zealand cities and rural sites,” *Atmospheric Pollut. Res.*, vol. 10, no. 5, pp. 1396–1403, Sep. 2019, doi: 10.1016/j.apr.2019.03.009.

[6] J. Zhao *et al.*, “Characterization of PM2.5-bound polycyclic aromatic hydrocarbons and their derivatives (nitro-and oxy-PAHs) emissions from two ship engines under different operating conditions,” *Chemosphere*, vol. 225, pp. 43–52,

Jun. 2019, doi: 10.1016/j.chemosphere.2019.03.022.
[7] P. Sims and P. L. Grover, “Epoxides in Polycyclic Aromatic Hydrocarbon Metabolism and Carcinogenesis,” in *Advances in Cancer Research*, vol. 20, Elsevier, 1974, pp. 165–274. doi: 10.1016/S0065-230X(08)60111-6.
[8] M. Hall and P. L. Grover, “Polycyclic Aromatic Hydrocarbons: Metabolism, Activation and Tumour Initiation,” in *Chemical Carcinogenesis and Mutagenesis I*, vol. 94 / 1, C. S. Cooper and P. L. Grover, Eds., in Handbook of Experimental Pharmacology, vol. 94 / 1. , Berlin, Heidelberg: Springer Berlin Heidelberg, 1990, pp. 327–372. doi: 10.1007/978-3-642-74775-5_9.
[9] H. Valli, “Cancer risk assessment, indicators, and guidelines for polycyclic aromatic hydrocarbons in the ambient air.,” *Environ. Health Perspect.*, vol. 110, p. 38, 2002.
[10] S. B. Hawthorne, C. B. Grabanski, E. Martin, and D. J. Miller, “Comparisons of Soxhlet extraction, pressurized liquid extraction, supercritical fluid extraction and subcritical water extraction for environmental solids: recovery, selectivity and effects on sample matrix,” *J. Chromatogr. A*, vol. 892, no. 1–2, pp. 421–433, Sep. 2000, doi: 10.1016/S0021-9673(00)00091-1.
[11] T. Okuda *et al.*, “Polycyclic aromatic hydrocarbons (PAHs) in the aerosol in Beijing, China, measured by aminopropylsilane chemically-bonded stationary-phase column chromatography and HPLC/fluorescence detection,” *Chemosphere*, vol. 65, no. 3, pp. 427–435, Oct. 2006, doi: 10.1016/j.chemosphere.2006.01.064.
[12] T. Okuda, K. Okamoto, S. Tanaka, Z. Shen, Y. Han, and Z. Huo, “Measurement and source identification of polycyclic aromatic hydrocarbons (PAHs) in the aerosol in Xi’an, China, by using automated column chromatography and applying positive matrix factorization (PMF),” *Sci. Total Environ.*, vol. 408, no. 8, pp. 1909–1914, Mar. 2010, doi: 10.1016/j.scitotenv.2010.01.040.
[13] C.-T. Pham *et al.*, “Emission Characteristics of Polycyclic Aromatic Hydrocarbons and Nitro-Polycyclic Aromatic Hydrocarbons from Open Burning of Rice Straw in the North of Vietnam,” *Int. J. Environ. Res. Public. Health*, vol. 16, no. 13, p. 2343, Jul. 2019, doi: 10.3390/ijerph16132343.
[14] Y. Liu, X. Li, W. Wang, B. Yin, Y. Gao, and X. Yang, “Chemical Characteristics of Atmospheric PM10 and PM2.5 at a Rural Site of Lijiang City, China,” *Int. J. Environ. Res. Public. Health*, vol. 17, no. 24, p. 9553, Dec. 2020, doi: 10.3390/ijerph17249553.
[15] T. Zhao *et al.*, “PM2.5-bound polycyclic aromatic hydrocarbons (PAHs) and nitrated-PAHs (NPAHs) emitted by gasoline vehicles: Characterization and health risk assessment,” *Sci. Total Environ.*, vol. 727, p. 138631, Jul. 2020, doi: 10.1016/j.scitotenv.2020.138631.
[16] L. Chen, W. Liu, S. Tao, and W. Liu, “Spatiotemporal variations and source identification of atmospheric nitrated and oxygenated polycyclic aromatic hydrocarbons in the coastal cities of the Bohai and Yellow Seas in northern China,” *Chemosphere*, vol. 279, p. 130565, Sep. 2021, doi:

10.1016/j.chemosphere.2021.130565.
[17] Y. Hong *et al.*, "Air pollution increases human health risks of PM2.5-bound PAHs and nitro-PAHs in the Yangtze River Delta, China," *Sci. Total Environ.*, vol. 770, p. 145402, May 2021, doi: 10.1016/j.scitotenv.2021.145402.
[18] C. Wei *et al.*, "Polycyclic aromatic compounds (PAHs, oxygenated PAHs, nitrated PAHs, and azaarenes) in air from four climate zones of China: Occurrence, gas/particle partitioning, and health risks," *Sci. Total Environ.*, vol. 786, p. 147234, Sep. 2021, doi: 10.1016/j.scitotenv.2021.147234.
[19] M. Moradi *et al.*, "Assessment of Alkylated and Unsubstituted Polycyclic Aromatic Hydrocarbons in Air in Urban and Semi-Urban Areas in Toronto, Canada," *Environ. Sci. Technol.*, p. acs.est.1c04299, Feb. 2022, doi: 10.1021/acs.est.1c04299.
[20] W. Xing *et al.*, "Variations in traffic-related polycyclic aromatic hydrocarbons in PM2.5 in Kanazawa, Japan, after the implementation of a new vehicle emission regulation," *J. Environ. Sci.*, vol. 121, pp. 38–47, Nov. 2022, doi: 10.1016/j.jes.2021.08.046.
[21] K. Kristensen, M. Bilde, P. P. Aalto, T. Petäjä, and M. Glasius, "Denuder/filter sampling of organic acids and organosulfates at urban and boreal forest sites: Gas/particle distribution and possible sampling artifacts," *Atmos. Environ.*, vol. 130, pp. 36–53, Apr. 2016, doi: 10.1016/j.atmosenv.2015.10.046.
[22] M. Brüggemann *et al.*, "Organosulfates in Ambient Aerosol: State of Knowledge and Future Research Directions on Formation, Abundance, Fate, and Importance," *Environ. Sci. Technol.*, vol. 54, no. 7, pp. 3767–3782, Apr. 2020, doi: 10.1021/acs.est.9b06751.
[23] A. Bhardwaj and R. Sunder Raman, "Evaluation of organic aerosol filter sampling artefacts and implications to gravimetric PM2.5 mass at a COALESCE network site - Bhopal, India," *J. Environ. Manage.*, vol. 319, p. 115749, Oct. 2022, doi: 10.1016/j.jenvman.2022.115749.
[24] L. Melymuk *et al.*, "Uncertainties in monitoring of SVOCs in air caused by within-sampler degradation during active and passive air sampling," *Atmos. Environ.*, vol. 167, pp. 553–565, Oct. 2017, doi: 10.1016/j.atmosenv.2017.08.038.
[25] C. Balducci *et al.*, "Volatilization and oxidative artifacts of PM bound PAHs collected at low volume sampling (1): Laboratory and field evaluation," *Chemosphere*, vol. 200, pp. 106–115, Jun. 2018, doi: 10.1016/j.chemosphere.2018.02.090.
[26] J. Lintelmann, K. Fischer, E. Karg, and A. Schröppel, "Determination of selected polycyclic aromatic hydrocarbons and oxygenated polycyclic aromatic hydrocarbons in aerosol samples by high-performance liquid chromatography and liquid chromatography-tandem mass spectrometry," *Anal. Bioanal. Chem.*, vol. 381, no. 2, pp. 508–519, Jan. 2005, doi: 10.1007/s00216-004-2883-8.
[27] L. S. Van Winkle *et al.*, "Biological Dose Response to PM2.5: Effect of Particle Extraction Method on Platelet and Lung Responses," *Toxicol. Sci.*, vol. 143, no. 2,

pp. 349–359, Feb. 2015, doi: 10.1093/toxsci/kfu230.
[28] C. Roper, L. S. Delgado, D. Barrett, S. L. Massey Simonich, and R. L. Tanguay, “PM2.5 Filter Extraction Methods: Implications for Chemical and Toxicological Analyses,” *Environ. Sci. Technol.*, vol. 53, no. 1, pp. 434–442, Jan. 2019, doi: 10.1021/acs.est.8b04308.
[29] T. Okuda, R. Isobe, Y. Nagai, S. Okahisa, K. Funato, and K. Inoue, “Development of a High-Volume PM2.5 Particle Sampler Using Impactor and Cyclone Techniques,” *Aerosol Air Qual. Res.*, vol. 15, no. 3, pp. 759–767, 2015, doi: 10.4209/aaqr.2014.09.0194.
[30] N. Ishihara *et al.*, “Involvement of polycyclic aromatic hydrocarbons and endotoxin in macrophage expression of interleukin-33 induced by exposure to particulate matter,” *J. Toxicol. Sci.*, vol. 47, no. 5, pp. 201–210, 2022, doi: 10.2131/jts.47.201.
[31] W. Jing *et al.*, “Characterization of Elemental Composition and Valence State of Cyclone-collected Aerosol Particles Using EDXRF and XAFS at Three Sites in Japan,” *Asian J. Atmospheric Environ.*, vol. 16, no. 2, pp. 40–58, Jun. 2022, doi: 10.5572/ajae.2021.137.
[32] A. Honda, T. Okuda, M. Nagao, N. Miyasaka, M. Tanaka, and H. Takano, “PM2.5 collected using cyclonic separation causes stronger biological responses than that collected using a conventional filtration method,” *Environ. Res.*, vol. 198, p. 110490, Jul. 2021, doi: 10.1016/j.envres.2020.110490.
[33] S. Bang Ye, Y. Huang, and D.-Y. Lin, “QuEChERS sample pre-processing with UPLC-MS/MS: A method for detecting 19 quinolone-based veterinary drugs in goat’s milk,” *Food Chem.*, vol. 373, no. Pt B, p. 131466, Mar. 2022, doi: 10.1016/j.foodchem.2021.131466.
[34] H. Harmoko, R. E. Kartasasmita, H. Munawar, A. Rakhmawati, and B. Budiawan, “Determination of histamine in different compositions of commercially canned fish in Indonesia by modified QuEChERS and LC-MS/MS,” *J. Food Compos. Anal.*, vol. 105, p. 104256, Jan. 2022, doi: 10.1016/j.jfca.2021.104256.
[35] M. Zhuang *et al.*, “Method Development and Validation of Seven Pyrethroid Insecticides in Tea and Vegetable by Modified QuEChERS and HPLC-MS/MS,” *Bull. Environ. Contam. Toxicol.*, vol. 108, no. 4, pp. 768–778, Apr. 2022, doi: 10.1007/s00128-021-03442-x.
[36] M. Anastassiades, S. J. Lehotay, D. Štajnbaher, and F. J. Schenck, “Fast and Easy Multiresidue Method Employing Acetonitrile Extraction/Partitioning and ‘Dispersive Solid-Phase Extraction’ for the Determination of Pesticide Residues in Produce,” *J. AOAC Int.*, vol. 86, no. 2, pp. 412–431, Mar. 2003, doi: 10.1093/jaoac/86.2.412.
[37] E. H. da Costa Morais, C. H. Collins, and I. C. S. F. Jardim, “Pesticide determination in sweet peppers using QuEChERS and LC–MS/MS,” *Food Chem.*, vol. 249, pp. 77–83, May 2018, doi: 10.1016/j.foodchem.2017.12.092.
[38] T. Daimon and K. Takahashi, “Usefulness of Dilution for Rapid Simultaneous

Determination of Residual Pesticides in Edamame (Immature Soybeans) by LC-MS/MS," *Food Hyg. Saf. Sci. Shokuhin Eiseigaku Zasshi*, vol. 62, no. 4, pp. 133–137, Aug. 2021, doi: 10.3358/shokueishi.62.133.

[39] A. Wilkowska and M. Biziuk, "Determination of pesticide residues in food matrices using the QuEChERS methodology," *Food Chem.*, vol. 125, no. 3, pp. 803–812, Apr. 2011, doi: 10.1016/j.foodchem.2010.09.094.

[40] F. Ben Salem, O. Ben Said, R. Duran, and M. Monperrus, "Validation of an Adapted QuEChERS Method for the Simultaneous Analysis of Polycyclic Aromatic Hydrocarbons, Polychlorinated Biphenyls and Organochlorine Pesticides in Sediment by Gas Chromatography–Mass Spectrometry," *Bull. Environ. Contam. Toxicol.*, vol. 96, no. 5, pp. 678–684, May 2016, doi: 10.1007/s00128-016-1770-2.

[41] A. Kaium *et al.*, "Validation of QuEChERS-based UPLC-MS/MS method for determination of quinoid niclosamide (LDS) residue in water, soil and rice samples," *Int. J. Environ. Anal. Chem.*, vol. 98, no. 7, pp. 644–654, May 2018, doi: 10.1080/03067319.2018.1487062.

[42] A. F. Marzoq Hadi., A.-S. Mohamed S., and E.-S. Mohamed Hamza, "Impact of Forest Combustion on Soil Contamination by PAHs Using QuEChERS and GC-MS/MSTQD," *Int. Res. J. Pure Appl. Chem.*, pp. 1–13, Apr. 2019, doi: 10.9734/irjpac/2019/v18i330090.

[43] Q. Liu *et al.*, "[Hmim]PF6 enhanced the extraction of polycyclic aromatic hydrocarbons from soil with the QuEChERS method," *Arab. J. Chem.*, vol. 13, no. 2, pp. 4102–4110, Feb. 2020, doi: 10.1016/j.arabjc.2019.06.009.

[44] A. Acosta-Dacal *et al.*, "Validation of a Method Scope Extension for the Analysis of POPs in Soil and Verification in Organic and Conventional Farms of the Canary Islands," *Toxics*, vol. 9, no. 5, p. 101, May 2021, doi: 10.3390/toxics9050101.

[45] J. Park *et al.*, "Determination of pharmaceuticals in solid samples in municipal wastewater treatment plants by online SPE LC–MS/MS using QuEChERS extraction," *Environ. Monit. Assess.*, vol. 193, no. 5, p. 279, May 2021, doi: 10.1007/s10661-021-09069-z.

[46] A. Albinet, S. Tomaz, and F. Lestremau, "A really quick easy cheap effective rugged and safe (QuEChERS) extraction procedure for the analysis of particle-bound PAHs in ambient air and emission samples," *Sci. Total Environ.*, vol. 450–451, pp. 31–38, Apr. 2013, doi: 10.1016/j.scitotenv.2013.01.068.

[47] A. Albinet, F. Nalin, S. Tomaz, J. Beaumont, and F. Lestremau, "A simple QuEChERS-like extraction approach for molecular chemical characterization of organic aerosols: application to nitrated and oxygenated PAH derivatives (NPAH and OPAH) quantified by GC–NICIMS," *Anal. Bioanal. Chem.*, vol. 406, no. 13, pp. 3131–3148, May 2014, doi: 10.1007/s00216-014-7760-5.

[48] A. Hiba, A. Carine, A. R. Haifa, L. Ryszard, and J. Farouk, "Monitoring of twenty-two sulfonamides in edible tissues: Investigation of new metabolites and their potential toxicity," *Food Chem.*, vol. 192, pp. 212–227, Feb. 2016, doi:

10.1016/j.foodchem.2015.06.093.
[49] Y. Ruiz-García, C. L. Silva, E. Gómez-Plaza, and J. S. Câmara, "A Powerful Analytical Strategy Based on QuEChERS-Dispersive Solid-Phase Extraction Combined with Ultrahigh Pressure Liquid Chromatography for Evaluating the Effect of Elicitors on Biosynthesis of trans-Resveratrol in Grapes," *Food Anal. Methods*, vol. 9, no. 3, pp. 670–679, Mar. 2016, doi: 10.1007/s12161-015-0227-2.
[50] M. F. Abdel-Ghany, L. A. Hussein, and N. F. El Azab, "Multiresidue Analysis of Five Neonicotinoid Insecticides and Their Primary Metabolite in Cucumbers and Soil Using High-Performance Liquid Chromatography with Diode-Array Detection," *J. AOAC Int.*, vol. 100, no. 1, pp. 176–188, Jan. 2017, doi: 10.5740/jaoacint.16-0162.
[51] Z. Cheng *et al.*, "Atmospheric pressure gas chromatography quadrupole-time-of-flight mass spectrometry for simultaneous determination of fifteen organochlorine pesticides in soil and water," *J. Chromatogr. A*, vol. 1435, pp. 115–124, Feb. 2016, doi: 10.1016/j.chroma.2016.01.025.
[52] W. Mei, Q. Li, H. Fang, H. Geng, and X. Chen, "Determination of six amide herbicide residues in soil by QuEChERS-gas chromatography-mass spectrometry," *Chin. J. Chromatogr.*, vol. 35, no. 12, p. 1317, 2017, doi: 10.3724/SP.J.1123.2017.09003.
[53] Z. Xu *et al.*, "Field investigations of dissipations and residues of cyazofamid in soil and tomato: risk assessment of human exposure to cyazofamid via tomato intake," *Environ. Sci. Pollut. Res.*, vol. 24, no. 4, pp. 3483–3492, Feb. 2017, doi: 10.1007/s11356-016-8106-y.
[54] R. Mondal, A. Mukherjee, S. Biswas, and R. K. Kole, "GC-MS/MS determination and ecological risk assessment of pesticides in aquatic system: A case study in Hooghly River basin in West Bengal, India," *Chemosphere*, vol. 206, pp. 217–230, Sep. 2018, doi: 10.1016/j.chemosphere.2018.04.168.
[55] C. I. Nannou, V. I. Boti, and T. A. Albanis, "Trace analysis of pesticide residues in sediments using liquid chromatography–high-resolution Orbitrap mass spectrometry," *Anal. Bioanal. Chem.*, vol. 410, no. 7, pp. 1977–1989, Mar. 2018, doi: 10.1007/s00216-018-0864-6.
[56] J. Zhou *et al.*, "Optimization for quick, easy, cheap, effective, rugged and safe extraction of mycotoxins and veterinary drugs by response surface methodology for application to egg and milk," *J. Chromatogr. A*, vol. 1532, pp. 20–29, Jan. 2018, doi: 10.1016/j.chroma.2017.11.050.
[57] L. Chen *et al.*, "Determination of thiamethoxam and its metabolite clothianidin residue and dissipation in cowpea by QuEChERS combining with ultrahigh-performance liquid chromatography–tandem mass spectrometry," *Environ. Sci. Pollut. Res.*, vol. 28, no. 7, pp. 8844–8852, Feb. 2021, doi: 10.1007/s11356-020-11164-6.
[58] A. L. Ahmad, C. Y. Chan, S. R. Abd Shukor, and M. D. Mashitah, "Adsorption kinetics and thermodynamics of β-carotene on silica-based adsorbent," *Chem. Eng.*

J., vol. 148, no. 2–3, pp. 378–384, May 2009, doi: 10.1016/j.cej.2008.09.011.

[59] L. da C. Cabrera, S. S. Caldas, O. D. Prestes, E. G. Primel, and R. Zanella, "Evaluation of alternative sorbents for dispersive solid-phase extraction clean-up in the QuEChERS method for the determination of pesticide residues in rice by liquid chromatography with tandem mass spectrometry: Sample Preparation," *J. Sep. Sci.*, vol. 39, no. 10, pp. 1945–1954, May 2016, doi: 10.1002/jssc.201501204.

[60] H. Li, D. Zhu, X. Lu, H. Du, S. Guan, and Z. Chen, "Determination and risk assessment of sixteen polycyclic aromatic hydrocarbons in vegetables," *J. Environ. Sci. Health Part A*, vol. 53, no. 2, pp. 116–123, Jan. 2018, doi: 10.1080/10934529.2017.1377573.

[61] A. S. Kachhawaha, P. M. Nagarnaik, M. Jadhav, A. Pudale, P. K. Labhasetwar, and K. Banerjee, "Optimization of a Modified QuEChERS Method for Multiresidue Analysis of Pharmaceuticals and Personal Care Products in Sewage and Surface Water by LC-MS/MS," *J. AOAC Int.*, vol. 100, no. 3, pp. 592–597, May 2017, doi: 10.5740/jaoacint.17-0060.

[62] P. Kaczyński and B. Łozowicka, "One-Step QuEChERS-Based Approach to Extraction and Cleanup in Multiresidue Analysis of Sulfonylurea Herbicides in Cereals by Liquid Chromatography–Tandem Mass Spectrometry," *Food Anal. Methods*, vol. 10, no. 1, pp. 147–160, Jan. 2017, doi: 10.1007/s12161-016-0564-9.

[63] R. Perestrelo *et al.*, "QuEChERS - Fundamentals, relevant improvements, applications and future trends," *Anal. Chim. Acta*, vol. 1070, pp. 1–28, Sep. 2019, doi: 10.1016/j.aca.2019.02.036.

[64] B. Fang *et al.*, "PM2.5-Bound Polycyclic Aromatic Hydrocarbons: Sources and Health Risk during Non-Heating and Heating Periods (Tangshan, China)," *Int. J. Environ. Res. Public. Health*, vol. 17, no. 2, p. 483, Jan. 2020, doi: 10.3390/ijerph17020483.

[65] X. Guo, W. Zhang, J. Gu, F. Chen, and Q. Yang, "The determination of the level, source, and risk of polycyclic aromatic hydrocarbon content in traditional Chinese medicines using a QuEChERS based extraction and HPLC-UV-FLD analysis," *J. Liq. Chromatogr. Relat. Technol.*, vol. 44, no. 3–4, pp. 210–219, Feb. 2021, doi: 10.1080/10826076.2021.1883649.

[66] P. Świt, J. Orzeł, and S. Maślanka, "Monitoring of PAHs in simulated natural and artificial fires by HPLC-DAD-FLD with the application of Multi-Component Integrated calibration method to improve quality of analytical results," *Measurement*, vol. 196, p. 111242, Jun. 2022, doi: 10.1016/j.measurement.2022.111242.

[67] T. Okuda *et al.*, "Development of a High-Volume Simultaneous Sampler for Fine and Coarse Particles using Virtual Impactor and Cyclone Techniques," *Asian J. Atmospheric Environ.*, vol. 12, no. 1, pp. 78–86, Mar. 2018, doi: 10.5572/ajae.2018.12.1.078.

[68] C. Scaramboni *et al.*, "Optimization of a Low Volume Extraction Method to

Determine Polycyclic Aromatic Hydrocarbons in Aerosol Samples," *Front. Environ. Sci.*, vol. 9, p. 742251, Nov. 2021, doi: 10.3389/fenvs.2021.742251.

[69] M. C. Bruzzoniti *et al.*, "Optimization and Validation of a Method Based on QuEChERS Extraction and Gas Chromatographic-Mass Spectrometric Analysis for the Determination of Polycyclic Aromatic Hydrocarbons and Polychlorinated Biphenyls in Olive Fruits Irrigated with Treated Wastewaters," *Separations*, vol. 9, no. 3, p. 82, Mar. 2022, doi: 10.3390/separations9030082.

[70] M. Urban and C. Lesueur, "Comparing d-SPE Sorbents of the QuEChERS Extraction Method and EMR-Lipid for the Determination of Polycyclic Aromatic Hydrocarbons (PAH4) in Food of Animal and Plant Origin," *Food Anal. Methods*, vol. 10, no. 7, pp. 2111–2124, Jul. 2017, doi: 10.1007/s12161-016-0750-9.

[71] H. Al-Thaiban, N. Al-Tamimi, and M. Helaleh, "Development of QuEChERS Method for the Determination of Polycyclic Aromatic Hydrocarbons in Smoked Meat Products Using GC-MS from Qatar," *J. Anal. Methods Chem.*, vol. 2018, pp. 1–11, Jul. 2018, doi: 10.1155/2018/9206237.

[72] D. Wang, J. Ma, H. Li, and X. Zhang, "Concentration and Potential Ecological Risk of PAHs in Different Layers of Soil in the Petroleum-Contaminated Areas of the Loess Plateau, China," *Int. J. Environ. Res. Public. Health*, vol. 15, no. 8, p. 1785, Aug. 2018, doi: 10.3390/ijerph15081785.

[73] G. Gbeddy, A. Goonetilleke, G. A. Ayoko, and P. Egodawatta, "Application of multivariate data techniques in photochemical study of polycyclic aromatic hydrocarbons (PAHs) and transformed PAH products in road dust," *Ecotoxicol. Environ. Saf.*, vol. 196, p. 110478, Jun. 2020, doi: 10.1016/j.ecoenv.2020.110478.

[74] E. T. M. Erawaty Silalahi, S. Anita, and H. Y. Teruna, "Comparison of Extraction Techniques for the Determination of Polycyclic Aromatic Hydrocarbons (PAHs) in Soil," *J. Phys. Conf. Ser.*, vol. 1819, no. 1, p. 012061, Mar. 2021, doi: 10.1088/1742-6596/1819/1/012061.

[75] X. Liu, S. Zhou, Q. Zhu, Y. Ye, and H. Chen, "Ultra Preconcentration of Polycyclic Aromatic Hydrocarbons in Smoked Bacon by a Combination of SPE and DLLME," *J. Chromatogr. Sci.*, vol. 52, no. 8, pp. 932–937, Sep. 2014, doi: 10.1093/chromsci/bmt119.

[76] A. G. Santos, A. C. D. Regis, G. O. da Rocha, M. de A. Bezerra, R. M. de Jesus, and J. B. de Andrade., "A simple, comprehensive, and miniaturized solvent extraction method for determination of particulate-phase polycyclic aromatic compounds in air," *J. Chromatogr. A*, vol. 1435, pp. 6–17, Feb. 2016, doi: 10.1016/j.chroma.2016.01.018.

[77] L. O. Santos, A. G. Santos, and J. B. de Andrade, "Methodology to examine polycyclic aromatic hydrocarbons (PAHs) nitrated PAHs and oxygenated PAHs in sediments of the Paraguaçu River (Bahia, Brazil)," *Mar. Pollut. Bull.*, vol. 136, pp. 248–256, Nov. 2018, doi: 10.1016/j.marpolbul.2018.09.022.

[78] Y. A. Zavgorodnyaya, A. L. Chikidova, M. V. Biryukov, and V. V. Demin, "Polycyclic aromatic hydrocarbons in atmospheric particulate depositions and

urban soils of Moscow, Russia," *J. Soils Sediments*, vol. 19, no. 8, pp. 3155–3165, Aug. 2019, doi: 10.1007/s11368-018-2067-3.

[79] S. Feng *et al.*, "Polycyclic and nitro-polycyclic aromatic hydrocarbon pollution characteristics and carcinogenic risk assessment of indoor kitchen air during cooking periods in rural households in North China," *Environ. Sci. Pollut. Res.*, vol. 28, no. 9, pp. 11498–11508, Mar. 2021, doi: 10.1007/s11356-020-11316-8.

Chapter 3: Pollution Characteristics, Sources, and Risk Assessment of Powder $PM_{2.5}$-bound Polycyclic Aromatic Hydrocarbons (PAHs) Collected at Yokohama, Japan between Pre- and Post-COVID-19

This study aims to investigate the PM-bound PAHs pollution characteristics, environmental existence influence factors, and human exposure risk in Yokohama, Japan under the influence of global coronavirus disease (COVID-19) outbreaking. The PAHs were extracted in 30 cyclone-collected aerosol samples from 2018 to 2023 in Yokohama using the QuEChERS method, analyzed its concentration trend, interaction with meteorological and chemical factors, and assessed the human health risk based on various exposure routes.

3.1 Introduction

The novel coronavirus disease (COVID-19) has become the most critical global health challenge in recent history. COVID-19 disease caused by Severe Acute Respiratory Syndrome Coronavirus (SARS-CoV-2) and its variants has exceeded 695,750,000 cases, with more than 6,919,476 deaths (26 September, 2023) in 231 countries [1]. Until 26 September, 2023 Japan reported 33,803,572 COVID-19 cases, and 74,694 deaths representing 595 deaths per one million population [1].

According to the daily confirmed COVID-19 positive cases number, eight waves of coronavirus infections have been observed throughout Japan since the announcement of the first confirmed case of COVID-19 on 16 January, 2020, and as of 8 May 2023, when the Japanese government officially downgraded the coronavirus infection to a category 5 infection [2]. However, the number of deaths as a percentage of the population in Japan is one of the lowest among developed countries, with only 17% of the number of deaths per million population as in the United States and the United Kingdom [1]. Besides the factors including a milder strain of the virus, cultural habits

such as bowing etiquette and wearing face masks, hand washing with sanitizing equipment, a protective genetic trait, and a relative immunity conferred by the mandatory BCG tuberculosis vaccine, the strong government response also played an important role [3].

Japan's adopted policy for COVID-19 was to contain the infection outbreak, maintain the medical system, and focus on the prevention of large-scale disease clusters and a decrease in outbreaks and deaths. Therefore, the Japanese government originated the Three C's policy in 2020 in combating the COVID-19 pandemic which warns people to avoid three factors that contribute to clusters of infection: Closed spaces with poor ventilation; Crowded places with many people nearby; and Close-contact settings such as close-range conversations [4]. Besides, the government also issued several States of Emergency (SoEs) to limit the spread of COVID-19, including asking residents to avoid unnecessary outings, restricting the use of schools, stadiums, and other social venues, or requesting temporary closures [5].

In addition to Japan, China, France, Spain, Germany, Italy and other countries have also introduced strict social control measures to curb the rapid spread of COVID-19 [6]–[10]. These prevention and control strategies have significantly reduced the rate of spread and prevalence of the epidemic by restricting social activities, effectively slowing the overall disease progression trend. In addition, these measures have sharply reduced socio-economic activities including reductions in fossil fuel use, industry productions, and traffic volumes, and have made an unanticipated contribution to reducing regional air pollution. Studies in several countries have observed significant improvements in regional air quality during outbreak control periods [11]–[15].

In addition to conventional pollutants such as $PM_{2.5}$, PM_{10}, NO_x, and O_3, the concentrations of polycyclic aromatic hydrocarbons (PAHs), which are closely related to anthropogenic activities such as fossil fuel combustion, transportation emissions, and industrial production, also showed significant reductions [16]–[19]. PAHs are a class of toxic organic contaminants in the atmosphere, they can enter the body and induce cell

inflammation. Recent studies have shown that PAHs may contribute to coronavirus replication by affecting the expression of signaling pathways in cells that lead to oxidative stress and cellular autophagy, and that exposure to PAHs exacerbates the disease by enhancing inflammation during viral infections [20], [21]. Thus, it is important to investigate and analyze the atmospheric behavior of these contaminants. In this study, we analyzed the concentration trends of fourteen PAHs in 30 powder $PM_{2.5}$ samples collected using cyclone continuously during 2018-2023, the correlation of PAHs concentrations with the COVID-19 epidemic, meteorological conditions, and other environmental factors, as well as their contributing sources and human health exposure risks before and after the outbreaking. To the best of the author's knowledge, no studies have been conducted on the trend of atmospheric PM-bound PAHs concentration before and after the COVID-19 epidemic in Japan. Understanding the changing characteristics of air PAHs pollution status brought about by epidemic prevention and control policies can better help governments formulate regional air pollution control policies.

3.2 Materials and methods

3.2.1 Sample collection

Powder form particulate matter samples were collected on the 6th floor of the No. 25 building (35.55°N, 139.65°E) at the Yagami Campus of Keio University, Japan. Keio university located in Kanagawa prefecture which is part of the Tokyo Metropolitan Area (**Fig. 3.1**). The powder sample collection method using cyclone was the same as in our previous studies. Briefly, aerosol particles entered the cyclone with the airflow, and the powder particles were subsequently separated from the air and collected in an attached brown bottle [22]–[24]. The detailed collecting schedule and information of total 30 samples from Apr. 2018 to Feb. 2023 was listed in Supplementary Information (**Table 3.1**).



Fig. 3.1 Location of the sampling site

3.2.2 Chemical analysis

The powder particle-bound PAHs were extracted using optimized QuEChERS method (**Chapter 2**). Briefly, a 5 mg sample was placed in one glass centrifuge tube with 8 mg extracting salts (Na_2SO_4/NaCl, 1:1, w/w) and 0.2 ml mixture extracting solvents (ACN/DCM, 7:1, v/v), shaking and ultrasonic extraction at 40 kHz for 20 min, followed by centrifugation for 5 min at 3500 rpm. The supernatant was transferred to another centrifuge tube, which had 4 mg PSA and 8 mg Na_2SO_4 as clean-up reagents, after shaking for 5 min then centrifuged for 5 min at 4500 rpm. Finally, the supernatant was collected and filtered using 0.22 μm membrane for PAHs concentration analysis.

Fourteen PAHs contaminants of acenaphthene (Ace), fluorene (Fl), phenanthrene (Phe), anthracene (Ant), fluoranthene (Flt), pyrene (Pyr), benz[*a*]anthracene (BaA), chrysene (Chr), benzo[*b*]fluo-ranthene(BbF), benzo[*k*]fluoranthene (BkF), benzo[*a*]pyrene (BaP), dibenz[*a,h*]anthracene (DbA), benzo[*g,h,i*]perylene (BgP), and indeno[*1,2,3-cd*]pyrene (InP) were detected using HPLC-FLD system (Shimadzu Co. Tokyo, Japan), the sample injection volume was 20 μl and each sample extraction solution was tested twice because of the limitation of solution volume then used the average value as the contaminants concentration. Details of the PAHs detection conditions by HPLC-FLD system was provided in **Section 2.2.4**.

Carbon components (organic carbon, OC/elemental carbon, EC) were analyzed using a thermal/optical carbon analyzer (Sunset Model 5L, US) based on the IMPROVE thermal/optical transmittance (TOT) method. 0.3 mg of powdered sample was used for measurement OC/EC, the sample was uniformly coated on a 1 cm^2 quartz membrane that had been pretreated to high-temperature heating, and then placed into the OC/EC analyzer to be calcinated at high temperatures according to the set program, and the optical signals were collected for the calculation of the values of the carbon fractions.

Table 3.1 PAHs concentration (ng/mg) in each cyclone sample and meteorological parameters during the sampling period

No.	sampling period	Ace	Fl	Phe	Flt	Pyr	BaA	Chr	BbF	BkF	BaP	DbA	BgP	InP	∑PAHs (ng/mg)	$PM_{2.5}$ (mg/m3)	AOD[a]	Rain (mm)[b]	Temp. (°C)	Humidity (%)	Weed speed (m/s)	Daily Insolation (MJ/m^2)[c]	O_3 (ppb)[d]	NO_2 (ppb)
Cyclone1	2018/4/24-5/14	2.29	0.41	0.86	0.19	0.48	0.30	1.22	2.07	0.62	0.34	- [e]	1.59	1.24	11.62	6.2	0.26	164.5	18.7	67.8	4.1	19.33	52.0	13.0
Cyclone2	2018/5/15-6/5	2.69	1.95	3.20	0.41	1.21	0.92	2.29	4.18	1.27	0.90	0.08	3.33	2.16	24.59	7.7	0.57	27.5	21.5	69.3	3.3	20.9	54	14
Cyclone3	2018/10/30-11/20	3.30	0.86	2.07	0.27	0.91	0.51	1.88	2.19	0.76	0.58	0.17	2.16	1.45	17.11	3.0	0.22	45.5	15.6	70.3	2.8	9.48	25.0	20.0
Cyclone4	2019/2/15-3/5	2.11	0.47	0.53	0.16	0.91	0.48	1.31	1.53	0.55	0.61	-	1.50	0.97	11.13	5.9	0.33	73	9.3	62.0	3.7	10.78	33.0	20.0
Cyclone5	2019/5/15-5/23	2.97	1.28	1.85	0.21	0.89	0.78	1.73	2.87	1.00	0.80	0.33	2.85	1.80	19.38	7.4	0.24	93	20.9	66.0	3.4	22.45	50.0	14.0
Cyclone7	2019/9/11-10/01	2.53	0.63	1.25	0.15	0.48	0.37	1.02	1.33	0.51	0.43	-	1.34	0.93	10.98	3.4	0.54	62	24.2	74.0	3.1	13.13	37.0	13.0
Cyclone8	2019/10/15-11/05	3.32	1.05	3.07	0.34	0.98	0.62	2.43	3.38	1.22	0.82	0.74	3.41	2.35	23.73	3.1	0.30	219.5	17.3	75.5	3.2	8.78	29	19
Cyclone9	2019/11/28-12/20	2.59	1.74	2.37	0.36	1.54	0.86	3.11	3.43	1.30	1.14	0.93	3.94	2.36	25.66	3.1	0.22	114	9.8	65.2	3.2	6.96	21	22
Cyclone10	2019/12/24-2020/1/14	9.90	1.20	2.40	0.35	1.92	0.97	3.45	3.29	1.26	1.23	0.96	3.83	2.30	33.05	3.7	0.22	35	8.1	61.3	3.3	8,48	23	19
Cyclone11	2020/1/22-2/12	3.02	0.72	1.67	0.19	1.89	0.84	2.39	2.46	0.94	1.00	0.45	2.89	1.73	20.18	5.4	0.26	76.5	7.4	55.0	4.0	10.6	28	16
Cyclone12	2020/4/2-6/2	1.18	0.82	1.02	0.18	0.62	0.36	1.18	1.74	0.49	0.43	-	1.32	0.82	10.17	7.1	0.41	342	16.5	68.3	3.8	17.87	44.0	11.0
Cyclone13	2020/6/4-7/6	0.34	0.63	1.39	0.14	0.43	0.28	0.85	1.35	0.47	0.35	-	1.16	0.74	8.13	4	0.58	335.5	23.7	81.0	3.9	15.27	39	11

Cyclone14	2020/7/8-8/12	0.78	0.52	1.44	0.22	0.49	0.29	0.90	1.48	0.52	0.54	0.13	1.92	1.11	10.34	4.7	0.46	283.5	25.5	84.3	3.5	13.17	29.0	10.0
Cyclone15	2020/8/17-9/16	1.74	0.59	1.47	0.24	0.43	0.26	0.74	1.01	0.36	0.30	-	1.06	0.71	8.92	6.6	0.25	111	28.0	79.0	3.3	16.4	28.0	8.0
Cyclone16	2020/9/18-/10/14	4.69	0.58	3.16	0.17	0.43	0.29	1.00	1.33	0.47	0.40	-	1.58	1.11	15.21	3.7	0.42	222	21.0	79.5	3.7	8.68	32.0	10.0
Cyclone17	2020/10/22-11/12	2.77	0.62	2.33	0.27	0.41	0.39	1.07	1.46	0.65	0.40	-	1.27	1.17	12.80	5.4	0.20	12.5	15.5	62.0	3.1	10.55	27.0	17.0
Cyclone18	2020/11/17-12/8	1.39	0.47	1.04	0.19	0.35	0.28	0.87	1.01	0.46	0.33	-	0.87	0.87	8.12	5.6	0.26	10	12.8	67.8	3.4	8.1	24.0	18.0
Cyclone19	2020/12/10-2021/1/6	3.33	1.59	2.58	0.33	2.14	1.09	2.78	2.75	1.09	1.29	0.58	3.33	1.76	24.67	4.6	0.17	8.5	7.9	52.6	2.8	9.24	22.0	24.0
Cyclone20	2021/1/8-2/4	3.26	0.71	2.33	0.20	1.19	0.52	1.56	1.55	0.59	0.64	-	1.80	0.93	15.27	5.1	0.21	53.5	6.5	55.5	3.6	9.62	26.0	20.0
Cyclone21	2021/2/8-3/9	1.40	0.88	1.16	0.30	0.99	0.47	1.54	1.79	0.65	0.66	0.15	2.01	1.11	13.12	13.6	0.25	114.5	9.6	52.0	4.0	14	33.0	15.0
Cyclone22	2021/3/10-4/14	1.19	0.77	1.26	0.15	0.54	0.31	1.22	1.51	0.51	0.34	-	1.56	1.04	10.41	12.0	0.33	251.5	14.2	61.4	3.7	16.34	41.0	12.0
Cyclone23	2021/4/19-6/18	0.82	0.52	0.91	0.17	0.37	0.27	1.05	1.33	0.41	0.29	-	1.02	0.75	7.92	10.9	0.50	98.5	18.2	66.7	3.9	17.36	47.0	12.0
Cyclone24	2021/6/30-9/6	0.93	0.75	1.09	0.16	0.37	0.28	0.79	1.03	0.33	0.31	-	0.84	0.63	7.52	7.8	0.23	700	26.2	81.6	3.2	15.14	33.0	10.0
Cyclone25	2021/9/8-11/25	1.22	0.63	1.61	0.23	0.44	0.30	1.15	1.50	0.47	0.38	-	1.47	1.09	10.50	6.1	0.24	317.5	21.2	76.3	3.3	11.33	32.0	13.0
Cyclone26	2021/11/29-2022/2/8	2.21	1.57	1.43	0.44	1.47	0.59	2.02	2.60	0.83	0.65	0.19	2.31	1.59	17.89	5.9	0.16	174.5	6.9	53.1	3.5	10.28	26.0	19.0
Cyclone27	2022/2/17-5/6	0.89	0.84	0.63	0.19	0.68	0.34	1.05	1.45	0.42	0.39	-	1.20	0.73	8.82	7.9	0.37	399	12.3	64.0	3.5	15.91	43.0	14.0
Cyclone28	2022/5/10-7/5	1.21	1.23	1.42	0.25	0.52	0.40	1.15	1.87	0.57	0.45	-	1.30	0.84	11.21	6.0	0.54	233.5	22.2	77.1	3.3	17.23	45.0	12.0
Cyclone29	2022/7/11-9/13	0.89	0.73	1.61	0.16	0.45	0.29	0.84	1.47	0.49	0.39	-	1.11	0.68	9.11	4.3	0.53	402	27.1	79.2	3.5	15.35	34.0	8.0

Cyclone30	2022/9/13-11/28	1.24	1.03	1.85	0.31	0.78	0.45	1.41	1.88	0.65	0.57	0.04	1.80	0.90	12.93	3.5	0.28	482.5	18.4	71.9	3.4	10.79	31.0	13.0
Cyclone31	2022/12/1-2023/2/20	1.15	1.32	1.49	0.41	1.10	0.36	2.04	2.72	0.86	0.39	0.28	2.04	1.24	15.41	5.0	0.19	119.5	7.6	55.4	3.5	9.84	27.0	18.0

[a], Aerosol optical depth (AOD) data was obtained from NASA Earth Observations [25]

[b], Meteorological parameters of precipitation (mm), temperature (℃), humidity (%), wind speed (m/s), and wind direction were obtained from Yokohama meteorological station [26]

[c], Historical solar radiation intensity data (average daily insolation, unit: MJ/m^2) was collected from Tokyo meteorological station [27]

[d], The air quality index (AQI) of gaseous pollutants (O_3 and NO_2) concentration was collected from Chidori Ota, Tokyo observation station [28]

[e], the concentration of DbA lower than the detection limitation of HPLC-FLD system.

3.2.3 Meteorological conditions

Meteorological parameters of precipitation (mm), temperature (℃), humidity (%), wind speed (m/s), and wind direction during the sampling period were obtained from Yokohama meteorological station [26]. Historical solar radiation intensity data (average daily insolation, unit: MJ/m^2) was collected from Tokyo meteorological station [27]. The air quality index (AQI) of gaseous pollutants (O_3 and NO_2) concentration was collected from Chidori Ota, Tokyo observation station [28], then we reverse calculated each pollutant concentration using the 'AQI Calculator' offered by Unites States Environmental Protection Agency [29].

Aerosol optical depth (AOD) data was obtained from NASA Earth Observations [25]. These observation data were provided by Terra/MODIS satellite. The straight-line distance between the observation point of the satellite data and the sampling point is only 700m, and the observation time that the satellite transited Japan was 9:00-11:30 AM (Japan Standard Time, JST). Every eight days satellite observation data was used to calculate the average AOD data during the sampling period.

3.2.4 Health risk assessments

The toxicity of benzo[a]pyrene is an international evaluation model used as a reference to measure the toxicity of other PAHs. Previous reports showed that toxicity equivalency (TEQ) and incremental lifetime cancer risk (ILCR) effectively determine the carcinogenic risk of PAHs [30]–[32]. The equation of TEQ is expressed as **Eq. 3.1** [33]:

$$TEQ = \sum C_i \times TEF_i \tag{3.1}$$

where TEQ is the total carcinogenic equivalent concentration of PAHs, ng/m^3; C_i represents the *i*th PAHs in PM2.5, ng/m^3; TEF_i represents the carcinogenic equivalent coefficient of the *i*th PAH (**Table 3.2**).

ILCR is accumulated due to inhalation, ingestion, and dermal exposure to atmospheric $PM_{2.5}$-bound PAHs, and are calculated by **Eq. 3.2 - Eq. 3.5**:

`

$$ILCR_{inhalation} = \frac{TEQs \times CSF_{inhal} \times \sqrt[3]{\frac{BW}{70}} \times IR_{inhal} \times ET \times EF \times ED}{BW \times AT} \times 10^{-6} \quad (3.2)$$

$$ILCR_{ingestion} = \frac{TEQs \times CSF_{inge} \times \sqrt[3]{\frac{BW}{70}} \times IR_{ing} \times EF \times ED}{BW \times AT} \times 10^{-6} \quad (3.3)$$

$$ILCR_{dermal} = \frac{TEQs \times CSF_{derm} \times \sqrt[3]{\frac{BW}{70}} \times SA \times AF \times ABS \times EF \times ED}{BW \times AT} \times 10^{-6} \quad (3.4)$$

$$Carcinogenic\ Risk = ILCR_{inhal} + ILCR_{ing} + ILCR_{dermal} \quad (3.5)$$

where, CSF is the cancer slope factor of BaP; BW is body weight; IR_{inhal} and IR_{ing} are the inhalation rate and ingestion rate, respectively; ET is the daily exposure time; EF is the exposure frequency; ED is the exposure duration; AT is the average life span; SA is the dermal surface exposure; AF is the dermal adherence factor; ABS is the dermal adsorption fraction [34]–[37], [30]. The parameter values used to calculate the cancer risk for children (1-16) and adults (17-70) were cited the Handbook of USEPA and other researches, and they were listed in **Table 3.2**. An ILCR value < 10^{-6} indicates a relatively low or negligible cancer risk, in the range of 10^{-6} to 10^{-4} acceptable cancer risk, and > 10^{-4} high cancer risk.

Table 3.2 Proposed toxicity equivalency factors (TEFs) for individual PAHs [33]

Compound	TEF
Dibenz[*a,h*]anthracene (DbA)	5
Benzo[*a*]pyrene (BaP)	1
Benz[*a*]anthracene (BaA)	0.1
Benzo[*b*]fluoranthene (BbF)	0.1
Benzo[*k*]fluoranthene (BkF)	0.1
Indeno[*1,2,3-cd*]pyrene (InP)	0.1
Anthracene (Ant)	0.01
Benzo[*g,h,i*]perylene (BgP)	0.01
Chrysene (Chr)	0.01
Acenaphthene (Ace)	0.001
Fluoranthene (Flt)	0.001
Fluorene (Fl)	0.001
Phenanthrene (Phe)	0.001
Pyrene (Pyr)	0.001

3.3 Results and discussion

3.3.1 Pollution trends of PAHs in PM from 2018 to 2023

The first confirmed case of COVID-19 in the Tokyo metropolitan area appeared on January 24, 2020, and then increased day by day, with the number of daily confirmed cases exceeding one hundred since April 4th [38]. Therefore, this research used April 1, 2020 as the time point for the outbreak of COVID-19 in Japan to facilitate the analysis in conjunction with the sampling time. **Fig. 3.2(a)** depicted the box-plot of 13 PAHs concentration contribution and the detailed PAHs contaminants information were listed in **Table 3.1**. Except for one anomaly point (Cyclone10 sample collected at 2019/12/24-2020/1/14) in the concentration of acenaphthene (Ace), the distribution of the concentrations of the other pollutants conformed to the normal distribution. However, there are two noteworthy observations. Firstly, the data points exhibit an eccentric distribution, which the contaminants concentration in some samples were larger than others. Secondly, the average concentration of dibenz[a,h]anthracene (DbA) was negative (negative value means DbA concentration in extract was lower than the detection limitation of HPLC system) (**Fig. 3.2(b)**). This is due to the inherently low concentrations of DbA in particulate matter samples and the fact that the concentration of DbA in majority of samples taken since 2020 has failed to reach the detection limit due to the significant improvement in air quality because of the social policies introduced after 2020 to limit the spread of COVID-19. This trend is clearly demonstrated by the variation of the average ∑PAHs concentrations in each sampling years (**Fig. 3.2(c)**). Obviously, the annual average of ∑PAHs concentrations showed an increasing trend from 2018 to 2019 (17.64 ng/mg in 2018 vs. 20.66 ng/mg in 2019), oppositely, there was a significant decrease in PAHs concentrations since the COVID-19 outbreak and decreased continually following the years (13.17 ng/mg, 11.80 ng/mg, and 11.49 ng/mg from 2020 to 2022). However, there was little change in the composition of PAHs before and after the COVID-19 outbreak (**Fig. 3.2(b)**), which consisted of the research results observed at other sampling sites in Japan [39], [40].

`

The trend of ∑PAHs concentration in each sample collected by cyclone during 2018-2023 is shown as blue and dots lines in **Fig. 3.2(d)**. The red curve illustrated the daily confirmed cases of COVID-19 in Tokyo metropolis until February 2023. The concentration of PAHs in PM presented a certain periodicity, the concentration is higher in winter and spring, and lower in summer and autumn. This seasonal variation is consistent with the existing studies [41], [30], [42]. Moreover, this seasonal characterization began to become complicated with the COVID-19 outbreak. Since the COVID-19 outbreak, the Japanese government quickly imposed a state of emergency (SoE) declaration in 47 prefectures. This policy, which requires people to minimize unnecessary outings, has strongly controlled the spread of the epidemic. At the same time, the reduction in travel and restrictions on public transportation services have also reduced the emission of PAHs at the source. However, with the lifting of the first SoE (May 6, 2020), anthropogenic activities began to resume and concentrations of PAHs began to rebound. In the subsequent years 2021 and 2022, high levels of PAHs contamination all occurred when the number of daily diagnoses is at a low or rising level. Especially, an anomalous high PAHs contamination event occurred in the summer of 2022 (11.21 ng/mg in the sample collected in 2022/5/10-7/5). However, high PAHs contamination events still observed in the fall and winter seasons, which may be attributed to the increase in PAHs emissions due to frequent anthropogenic activities caused by unfavorable virus transmission in cold seasons, as well as to the distribution pattern of PAHs that mentioned earlier. Since the Japanese government announced the full relaxation of border controls on October 11, 2022, atmospheric PAHs contamination has also begun to increase. Overall, it has not yet reached the levels seen before the outbreak. This confirms that economic activities in the post epidemic era have not yet recovered to their previous levels.

`

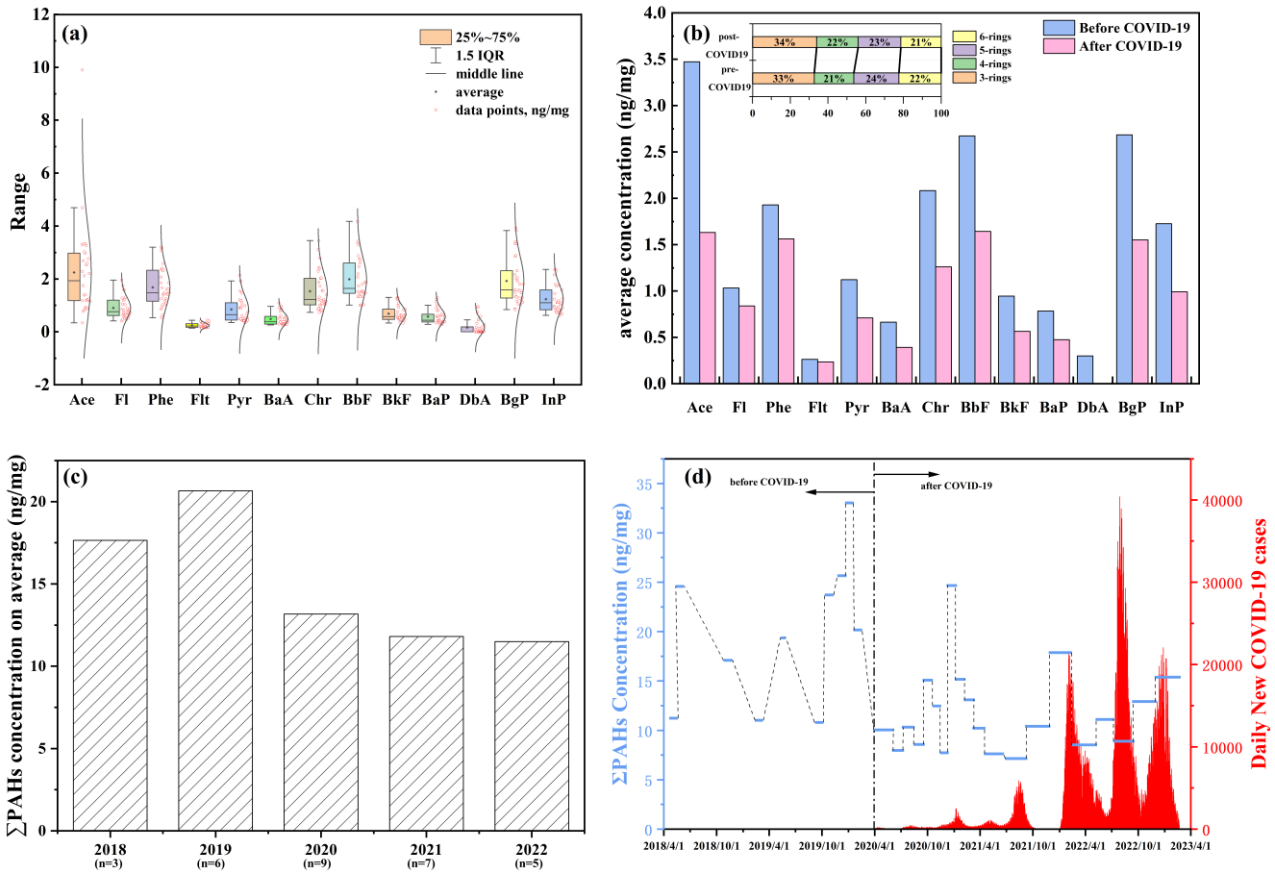


Fig. 3.2 Evolution of PAHs concentration in PM during 2018-2022, and daily confirmed cases in Tokyo metropolis after COVID-19 spreading in Japan

3.3.2 Meteorological conditions impact on PAHs contamination

Significant negative correlations were observed between PAHs concentrations and typical meteorological factors (precipitation, temperature, and humidity) in **Fig. 3.3**. In general, negative correlations between atmospheric pollutants including PAHs and precipitation/humidity because of the washout effect [43], [44]. The negative correlation between PAHs concentration and temperature is due to the gas/particle partitioning characteristics of the contaminant [45]. The vapor pressures of low-ring PAHs (4-ring PAHs and lower) are lower than those of high-ring (5 and 6-ring PAHs), the gas/particle partition of atmospheric low-ring PAHs increased with increasing temperature, resulting in the higher the temperature, the higher concentration of low-ring PAHs exist in gas phase.

Aerosol optical depth (AOD) is a measure of the dissipation of electromagnetic radiation at a specific wavelength (550 nm) due to the presence of particles such as pollutants, dust, and smoke in the atmosphere [46]–[48]. The average AOD value change in sampling periods increased during 2020 and 2022 by 7.7% and 22.5% respectively, while in 2021 decreased by 11.3% compared to the average value in 2019. Similar trend also has been reported by other studies [48]–[50]. AOD can be used to reflect the degree of turbidity and pollution in the air, but the result in **Fig. 3.3** shown the significant negative correlation between PAHs and AOD. Thus, this study also calculated the correlation between these two factors with the O_3 concentration. The high positive correlation between O_3 with AOD and solar irradiation (R^2=0.69, p<0.01; and R^2=0.89, p<0.01), and the negative correlation between O_3 and PAHs (R^2=-0.41, p<0.05) proved the point. The increasing AOD will enhance the scattering and absorption of solar radiation, which in turn reduces the solar flux at the ground level, and stronger solar irradiation drives photochemical reactions, resulting in the degradation of PAHs and producing more secondary aerosols revolving to increasing the atmospheric aerosol loading [51]–[53]. But it must to be noted that the AOD is not only related with atmospheric aerosol loading, but also affected by a variety of parameters, such as boundary layer height, humidity, hygroscopic growth factor, and variability in surface reflectance [54], [55]. In addition to the potential health hazards posed by PAHs and their degradation products, an increase in AOD leads to an increase in physiological equivalent temperature (PET) for urban residents, which can make people feel hotter and can raise the risk of heat stress in humans [56].

Fig. 3.4 listed the trend of ∑PAHs, $PM_{2.5}$, O_3, and NO_2 from 2019 to 2022. With the outbreak of COVID-19 and the government's rapid epidemic preparedness policy (such as SoE), concentrations of PAHs, O_3, and NO_2 declined significantly from 2019 to 2020 but increased to varying concentration of O_3 and NO_2 with the improvement of the epidemic compared to 2020. The significant positive correlation between $PM_{2.5}$-bound PAHs and NO_2 suggested PAHs originated from primary emission sources [57]. O_3 is a

`

typical photochemical reaction marker for secondary pollutant generation [58], and the positive link of O_3, AOD, and solar irradiation with OC also indicated the contribution of photo-oxidation process for PM-bound organic compounds. However, the concentration of PAHs showed a significant negative correlation with $PM_{2.5}$. On the one hand, this may result in the concentration of $PM_{2.5}$ being strongly influenced by the location of the source and the relative distance from the sampling point (R^2=0.42 between $PM_{2.5}$ and wind speed, p<0.05), which might only particulate matter originating from a specific direction contains PAHs. On the other hand, it is possible that the PM-bound PAHs were photo-oxidized/degraded to generate secondary organic aerosols. The weak link between PAHs and OC might be because the concentration of PM-bound PAHs is so low that has less contribution to OC, however, the significant correlation between PAHs/$PM_{2.5}$ and OC/$PM_{2.5}$ (R^2=0.42, p<0.05) verified our view.

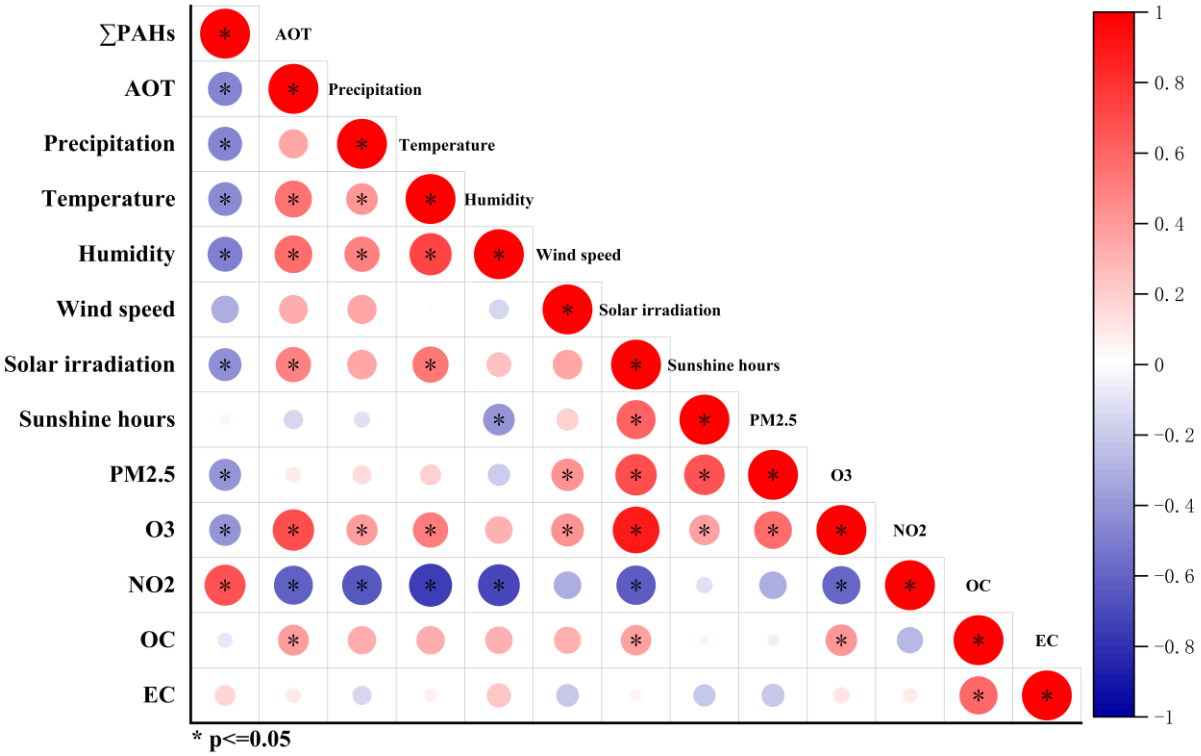


Fig. 3.3 Spearman correlation analysis between ∑PAHs with meteorological conditions, air pollutants, and OC/EC

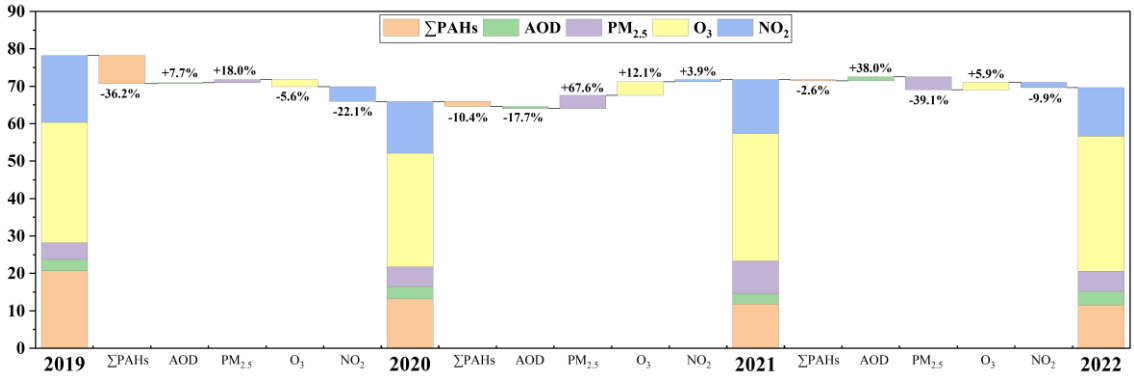


Fig. 3.4 The difference of ∑PAHs, AOD, $PM_{2.5}$, O_3, and NO_2 from 2019 to 2022 (arbitrary scale)

3.3.3 Source identification

Sources of PAHs were identified by diagnostic ratios, the typical diagnostic ratios of BaA/(BaA+Chr), InP/(InP+BgP), and Flt/(Flt+Pyr) were used to confirm the possible sources of PM-bound PAHs [37], [59], [60]. As shown in **Fig. 3.5**, the values of BaA/(BaA+Chr), InP/(InP+BgP), and Flt/(Flt+Pyr) in 30 cyclone samples were in the range of 0.2 to 0.35, 0.2 to 0.5, and lower than 0.4, respectively, implying that PM-bound PAHs were mainly from petroleum combustion. Besides, the average ratio of BaP/BgP was 0.3, which is lower than 0.6 means they might be from non-traffic emissions [42]. Comparing the characteristic ratios of pollutants before (red dots) and after (black dots) the COVID-19 pandemic shows no difference between the sources of PM-bound PAHs in the sampling area.

Besides, the principal component analysis (PCA) was also used to determine whether there was any impact of other emission sources during the sampling period. Three principal components (PCs), which can be explained up to 90% of the total variance, were highlighted for PM-bound PAHs emission sources identification in two sampling stages (**Table 3.3**). The PCA results showed that there is no difference in the contribution load of PAHs pollutants to the PC between the two sampling stages. PC1 alone can explain higher than 60% of the variance with a high loading of most of PAHs, which reflected the mix contribution of incomplete combustion of fossil fuel (coal,

petroleum, and natural gas). Fl, Phe, BbF, and DbA contributed the remain variance and named PC2 and PC3 that was attributed to be linked with the vehicle exhaust emission and coal burning [61]–[64]. This implies that the spread of COVID-19 and the corresponding epidemic prevention policies have not affected the region's stable source structure of PAHs. However, this conclusion is in contrast with the view of Kubo et al. [40] who pointed out that the decreasing behavior in PAHs concentrations in Nagasaki in recent years due to less PAHs origination from the limitation of economic activities in response to COVID-19 outbreaking by China government. This difference may be due to the geographic location of the two sampling sites, with Nagasaki being the closest Japanese city to mainland China, and therefore more significantly affected by the long-distance dispersion of pollutants from the East Asian continent.

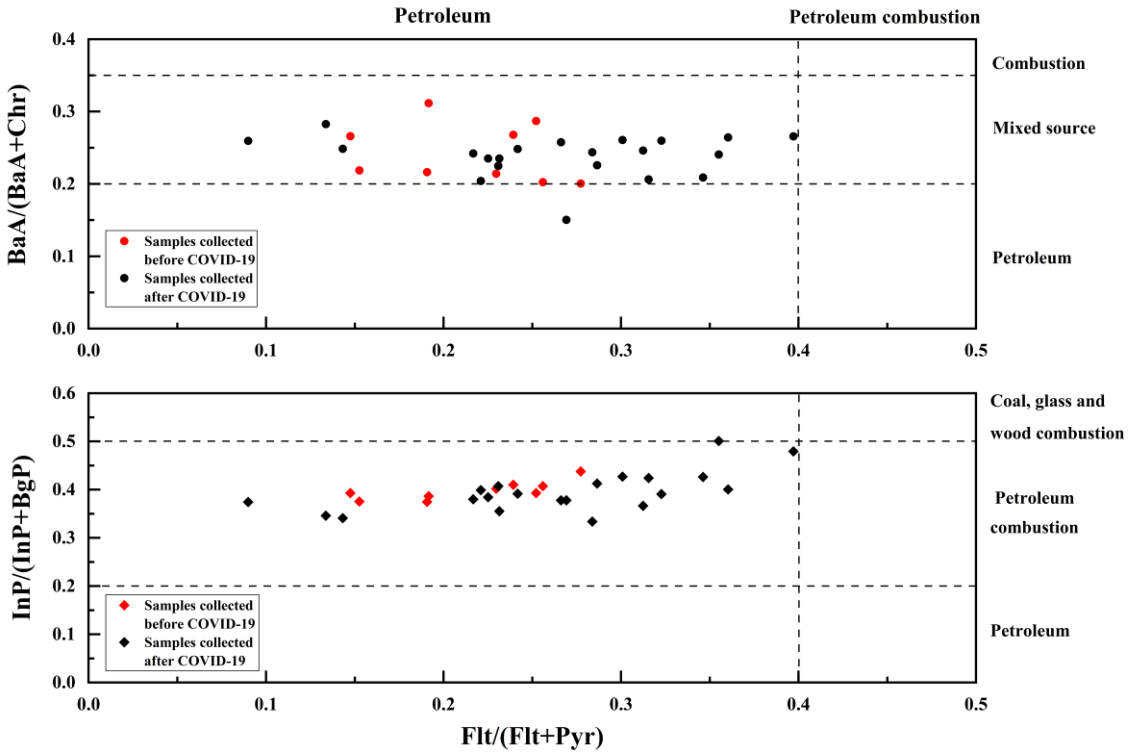


Fig. 3.5 Cross-plots of PAHs diagnostic ratios: Flt/(Flt+Pyr) vs BaA/(BaA+Chr), and Flt/(Flt+Pyr) vs InP/(InP+BgP)

Table 3.3 PCA analysis of PM-bound PAHs in two sampling stages

PAHs (Percent of variance)	2018-2019 (n=9)			2020-2023 (n=21)		
	PC1 (62.6%)	PC2 (20.9%)	PC3 (8.2%)	PC1 (73.5%)	PC2 (17.1%)	PC3 (5.5%)
Ace	**0.152**	-0.436	-0.011	**0.310**	-0.117	-0.074
Fl	0.209	**0.370**	-0.465	0.189	**0.514**	0.277
Phe	0.176	0.398	**0.457**	0.235	-0.075	**0.762**
Flt	**0.272**	0.254	0.198	0.033	**0.657**	0.098
Pyr	**0.293**	-0.277	-0.156	**0.318**	-0.014	-0.155
BaA	**0.284**	0.007	-0.538	**0.308**	-0.149	0.161
Chr	**0.308**	-0.248	0.115	**0.311**	0.113	-0.134
BbF	0.274	**0.360**	-0.061	0.261	**0.343**	-0.230
BkF	**0.336**	0.128	0.077	**0.313**	0.111	-0.075
BaP	**0.326**	-0.187	-0.173	**0.280**	-0.283	0.218
DbA	0.231	-0.355	**0.310**	**0.301**	-0.119	-0.118
BgP	**0.340**	-0.036	0.053	**0.312**	-0.156	-0.006
InP	**0.324**	0.057	0.265	**0.294**	-0.035	-0.374

3.3.4 Health risk assessment

The PM-bound PAHs health risk was estimated from three routes of inhalation, ingestion, and dermal exposure, and the carcinogenic risk caused by PAHs was the sum of these exposure pathways. Here, the cancer risk peaked in 2019 (1.1E-7 for children and 4.0E-7 for adults), after which there was a significant decrease (50% for children and 48% for adults, respectively) in 2020 due to improved air pollution conditions as result of COVID-19 outbreak control (**Table 3.4**). However, the cancer risk in 2021 rebounded to the same level as before the outbreak (6.4E-8 in 2021 vs. 6.2E-8 in 2018 for children, and 2.5E-7 vs. 2.4E-7 for adults), because the concentrations of several PAHs with larger toxicity equivalency factors (TEFs) instead increased (69.3%

`

increasing for Chr, 65.2% for BbF, 50.1% for BkF, 56.6% for BgP, and 53.4% for InP, respectively) though the overall PAHs concentration continued to show a decreasing trend. On the one hand, the elevated concentrations of multiple PAHs pollutants may be due to the long duration of a single sampling period, which amplifies the significant differences in PAHs pollution under different air pollution conditions, while on the other hand, the hosting of the Tokyo Olympics (23 July to 8 August 2021) and the gradual resumption of the public's daily life after the coronavirus vaccination is also a potential factor that cannot be ignored in contributing to the increase in pollutant concentrations [50], [65].

Overall, the risk of exposure to PM-bound PAHs is below the threshold of 10^{-6} for both children and adults, indicating a relatively low cancer risk. The cancer risk via inhalation pathway was in the range of 10^{-9} to 10^{-8} for children and adults, which was one order of magnitude lower than the risk via ingestion and dermal those had the same order of magnitude. This phenomenon was consisted with earlier research results, which indicated that ingestion and dermal exposure routes have a large contribution to the PM-bound PAHs cancer risk for both children and adults [36], [66], [67]. Most people wear masks to prevent the spread of the epidemic, which significantly reduces cancer risk via the inhalation pathway, but intake and dermal exposure ways are easily overlooked. Removing the mask while eating would increase the risk of PAHs intake via both the inhalation and ingestion pathways, and hand-washing behaviors promoted to reduce the spread of COVID-19 also neglect the routine cleaning of other exposed skin. Moreover, with the termination of the anti-epidemic policy, the level of PAHs contamination in the atmosphere will increase along with the resumption of economic and social activities. In the post-epidemic era, if it needs to wear masks and how to protect against PM-bound PAHs ingested through ingestion and dermal intake will remain a great health challenge. Especially, the threat of COVID-19 still remains, the damage for the respiratory system from air pollutants such as PAHs can make it more difficult for COVID-19 patients' recovery and lead to more severe and lethal of this

`

disease [68].

Table 3.4 Inhalation, ingestion, dermal and total cancer risks for children and adults

Year	Children (1-16)				Adults (17-70)			
	inhalation	ingestion	dermal	Cancer risk	inhalation	ingestion	dermal	Cancer risk
2018	2.2E-09	2.7E-08	3.3E-08	6.2E-08	2.5E-08	7.7E-08	1.4E-07	2.4E-07
2019	3.7E-09	4.5E-08	5.6E-08	1.1E-07	4.2E-08	1.3E-07	2.3E-07	4.0E-07
2020	1.9E-09	2.3E-08	2.9E-08	5.5E-08	2.2E-08	6.8E-08	1.2E-07	2.1E-07
2021	2.2E-09	2.8E-08	3.4E-08	6.4E-08	2.5E-08	8.0E-08	1.4E-07	2.5E-07
2022	1.4E-09	1.7E-08	2.1E-08	4.0E-08	1.6E-08	4.9E-08	8.8E-08	1.5E-07

3.4 Summary

The global outbreak of COVID-19 has had a dramatic impact on human behavior, and severe restrictions have significantly impacted regional air quality while reducing the risk of transmission. This study investigated the variation of PAHs concentration in cyclone-collected powdered PM samples in Yokohama, Japan from 2018 to 2023. Obviously, the annual average ∑PAHs concentration decreased from 20.66 ng/mg (2019) to 13.17 ng/mg (2020), 11.80 ng/mg (2021), and 11.49 ng/mg (2022), which showed a significant decline trend after COVID-19 outbreaking in Japan from 2020. And, there was a clear correlation between the concentration of PM-bound PAHs and the number of daily COVID-19 confirmed cases and the implementation of states of emergency declarations. Meanwhile, the correlation between PAHs concentration and meteorological conditions showed that under strong solar radiation, PAHs photochemically reacted with gaseous pollutants such as O_3 and NO_2 to increase AOD and aerosol loading, resulting in more severe photochemical pollution. Combined with the source identification results, the main sources of PAHs before and after the COVID-19 outbreak did not change much, and were still dominated by incomplete fossil fuel combustion emissions. Moreover, due to the improvement in air pollution conditions

`

during the period of limiting COVID-19 transmission, the health risk of PM-bound PAHs for children and adults also showed a significant reduction, decreased 50% for children and 48% for adults, respectively from 2019 to 2020. Strict social activity restriction policies during the epidemic strongly ameliorated atmospheric PM-bound PAHs pollution and reduced the human health risk of PM exposures significantly. This suggests that a wide-area policy approach can be effective in controlling regional air pollution, which provides deeper insights into public health policy-making.

3.5 References

[1] "Worldometers Info." [Online]. Available: https://www.worldometers.info/coronavirus/#countries

[2] "MHLW," Ministry of Health, Labour and Welfare. [Online]. Available: https://www.mhlw.go.jp/stf/covid-19/kokunainohasseijoukyou.html#h2_1

[3] A. Iwasaki and N. D. Grubaugh, "Why does Japan have so few cases of COVID-19?," *EMBO Mol. Med.*, vol. 12, no. 5, p. e12481, May 2020, doi: 10.15252/emmm.202012481.

[4] MHLW, "Avoid Three C's." [Online]. Available: https://www.mhlw.go.jp/content/000645566.pdf

[5] MHLW, "SoEs." [Online]. Available: https://www.mhlw.go.jp/content/10900000/000620796.pdf

[6] L. Di Domenico, G. Pullano, C. E. Sabbatini, P.-Y. Boëlle, and V. Colizza, "Impact of lockdown on COVID-19 epidemic in Île-de-France and possible exit strategies," *BMC Med.*, vol. 18, no. 1, p. 240, Dec. 2020, doi: 10.1186/s12916-020-01698-4.

[7] P.-Y. Liu, S. He, L.-B. Rong, and S.-Y. Tang, "The effect of control measures on COVID-19 transmission in Italy: Comparison with Guangdong province in China," *Infect. Dis. Poverty*, vol. 9, no. 1, p. 130, Dec. 2020, doi: 10.1186/s40249-020-00730-2.

[8] E. Naumann *et al.*, "COVID-19 policies in Germany and their social, political, and psychological consequences," *Eur. Policy Anal.*, vol. 6, no. 2, pp. 191–202, Dec. 2020, doi: 10.1002/epa2.1091.

[9] M. Martínez-Garcia, E. Sansano-Sansano, A. Castillo-Hornero, R. Femenia, K. Roomp, and N. Oliver, "Social isolation during the COVID-19 pandemic in Spain: a population study," *Sci. Rep.*, vol. 12, no. 1, p. 12543, Jul. 2022, doi: 10.1038/s41598-022-16628-y.

[10] V. Romano, M. Ancillotti, D. Mascalzoni, and R. Biasiotto, "Italians locked down: people's responses to early COVID-19 pandemic public health measures," *Humanit. Soc. Sci. Commun.*, vol. 9, no. 1, p. 342, Sep. 2022, doi:

`

10.1057/s41599-022-01358-3.
[11] M. J. Ju, J. Oh, and Y.-H. Choi, “Changes in air pollution levels after COVID-19 outbreak in Korea,” *Sci. Total Environ.*, vol. 750, p. 141521, Jan. 2021, doi: 10.1016/j.scitotenv.2020.141521.
[12] Q. Liu *et al.*, “Spatiotemporal impacts of COVID-19 on air pollution in California, USA,” *Sci. Total Environ.*, vol. 750, p. 141592, Jan. 2021, doi: 10.1016/j.scitotenv.2020.141592.
[13] A. F. Skirienė and Ž. Stasiškienė, “COVID-19 and Air Pollution: Measuring Pandemic Impact to Air Quality in Five European Countries,” *Atmosphere*, vol. 12, no. 3, p. 290, Feb. 2021, doi: 10.3390/atmos12030290.
[14] T. Feng, H. Du, Z. Lin, X. Chen, Z. Chen, and Q. Tu, “Green recovery or pollution rebound? Evidence from air pollution of China in the post-COVID-19 era,” *J. Environ. Manage.*, vol. 324, p. 116360, Dec. 2022, doi: 10.1016/j.jenvman.2022.116360.
[15] I. Arpaci, S. Kilicarslan, O. Aslan, and I. Ozturk, “Air pollution in marmara region before and during the COVID-19 outbreak,” *Environ. Monit. Assess.*, vol. 195, no. 6, p. 764, Jun. 2023, doi: 10.1007/s10661-023-11377-5.
[16] H. M. Adly and S. A. K. Saleh, “Evaluation of Carcinogenic Polyaromatic Hydrocarbon Levels in Airborne Particulates Associated with Long-Term Exposure throughout the COVID-19 Pandemic in Makkah, Saudi Arabia,” *Int. J. Environ. Res. Public. Health*, vol. 18, no. 23, p. 12745, Dec. 2021, doi: 10.3390/ijerph182312745.
[17] R. M. Prats, B. L. Van Drooge, P. Fernández, E. Marco, and J. O. Grimalt, “Changes in Urban Gas-Phase Persistent Organic Pollutants During the COVID-19 Lockdown in Barcelona,” *Front. Environ. Sci.*, vol. 9, p. 650539, Apr. 2021, doi: 10.3389/fenvs.2021.650539.
[18] M. H. Rabin, Q. Wang, W. Wang, and C. E. Enyoh, “Pollution Characteristics, Source Apportionment, and Health Risk of Polycyclic Aromatic Hydrocarbons (PAHs) of Fine Street Dust during and after COVID-19 Lockdown in Bangladesh,” *Processes*, vol. 10, no. 12, p. 2575, Dec. 2022, doi: 10.3390/pr10122575.
[19] J. Feng *et al.*, “Effects of COVID-19 Control Measures on the Concentration and Composition of PM2.5-Bound Polycyclic Aromatic Hydrocarbons in Shanghai,” *Atmosphere*, vol. 14, no. 1, p. 95, Jan. 2023, doi: 10.3390/atmos14010095.
[20] B. Woodby, M. M. Arnold, and G. Valacchi, “SARS-CoV-2 infection, COVID-19 pathogenesis, and exposure to air pollution: What is the connection?,” *Ann. N. Y. Acad. Sci.*, vol. 1486, no. 1, pp. 15–38, Feb. 2021, doi: 10.1111/nyas.14512.
[21] J. De La Fuente *et al.*, “Good and bad get together: Inactivation of SARS-CoV-2 in particulate matter pollution from different fuels,” *Sci. Total Environ.*, vol. 844, p. 157241, Oct. 2022, doi: 10.1016/j.scitotenv.2022.157241.
[22] T. Okuda, R. Isobe, Y. Nagai, S. Okahisa, K. Funato, and K. Inoue, “Development of a High-Volume PM2.5 Particle Sampler Using Impactor and Cyclone Techniques,” *Aerosol Air Qual. Res.*, vol. 15, no. 3, pp. 759–767, 2015, doi:

`

10.4209/aaqr.2014.09.0194.
[23] T. Okuda *et al.*, "Development of a High-Volume Simultaneous Sampler for Fine and Coarse Particles using Virtual Impactor and Cyclone Techniques," *Asian J. Atmospheric Environ.*, vol. 12, no. 1, pp. 78–86, Mar. 2018, doi: 10.5572/ajae.2018.12.1.078.
[24] W. Jing *et al.*, "Characterization of Elemental Composition and Valence State of Cyclone-collected Aerosol Particles Using EDXRF and XAFS at Three Sites in Japan," *Asian J. Atmospheric Environ.*, vol. 16, no. 2, pp. 40–58, Jun. 2022, doi: 10.5572/ajae.2021.137.
[25] "NEO." [Online]. Available: https://neo.gsfc.nasa.gov/view.php?datasetId=MODAL2_E_AER_OD&year=2023
[26] "JMA-Yokohama meteorological station." [Online]. Available: https://www.data.jma.go.jp/obd/stats/etrn/view/mb5daily_s1.php?prec_no=46&block_no=47670&year=2018&month=4&day=24&view=p1
[27] "JMA-Tokyo meteorological station." [Online]. Available: https://www.data.jma.go.jp/obd/stats/etrn/view/mb5daily_s1.php?prec_no=44&block_no=47662&year=2018&month=4&day=24&view=p1
[28] "Real-time Air Quality Index-Chidori, Ota, Tokyo Station." [Online]. Available: https://aqicn.org/city/japan/otaku/tamakihachitorichidori/
[29] "EPA." [Online]. Available: https://www.airnow.gov/aqi/aqi-calculator/
[30] B. Fang *et al.*, "PM2.5-Bound Polycyclic Aromatic Hydrocarbons: Sources and Health Risk during Non-Heating and Heating Periods (Tangshan, China)," *Int. J. Environ. Res. Public. Health*, vol. 17, no. 2, p. 483, Jan. 2020, doi: 10.3390/ijerph17020483.
[31] X. Guo, F. Chen, J. Lu, and W. Zhang, "Seasonal variation, sources, and risk assessment of PM2.5-bound PAHs in Nantong, China: A pre- and post-COVID-19 case study," *Front. Environ. Sci.*, vol. 10, p. 947705, Aug. 2022, doi: 10.3389/fenvs.2022.947705.
[32] W. Liu *et al.*, "Variation of pollution sources and health effects on air pollution before and during COVID-19 pandemic in Linfen, Fenwei Plain," *Environ. Res.*, vol. 213, p. 113719, Oct. 2022, doi: 10.1016/j.envres.2022.113719.
[33] I. C. T. Nisbet and P. K. LaGoy, "Toxic equivalency factors (TEFs) for polycyclic aromatic hydrocarbons (PAHs)," *Regul. Toxicol. Pharmacol.*, vol. 16, no. 3, pp. 290–300, Dec. 1992, doi: 10.1016/0273-2300(92)90009-X.
[34] "U.S. EPA," Exposure Factors Handbook 2011 Edition (Final Report). U.S. Environmental Protection Agency, Washington, DC, EPA/600/R-09/052F. [Online]. Available: https://cfpub.epa.gov/ncea/risk/recordisplay.cfm?deid=236252
[35] J. Wang, N. B. Geng, Y. F. Xu, W. D. Zhang, X. Y. Tang, and R. Q. Zhang, "PAHs in PM2.5 in Zhengzhou: concentration, carcinogenic risk analysis, and source apportionment," *Environ. Monit. Assess.*, vol. 186, no. 11, pp. 7461–7473, Nov.

`

2014, doi: 10.1007/s10661-014-3940-1.
[36] M. Gope, R. E. Masto, J. George, and S. Balachandran, “Exposure and cancer risk assessment of polycyclic aromatic hydrocarbons (PAHs) in the street dust of Asansol city, India,” *Sustain. Cities Soc.*, vol. 38, pp. 616–626, Apr. 2018, doi: 10.1016/j.scs.2018.01.006.
[37] L. Wang *et al.*, “Polycyclic aromatic hydrocarbons in atmospheric PM2.5 and PM10 in the semi-arid city of Xi’an, Northwest China: Seasonal variations, sources, health risks, and relationships with meteorological factors,” *Atmospheric Res.*, vol. 229, pp. 60–73, Nov. 2019, doi: 10.1016/j.atmosres.2019.06.014.
[38] “Tokyo.” [Online]. Available: https://www.hokeniryo.metro.tokyo.lg.jp/kansen/corona_portal/index.html
[39] L. Zhang *et al.*, “Impact of the COVID-19 Outbreak on the Long-range Transport of Particulate PAHs in East Asia,” *Aerosol Air Qual. Res.*, vol. 20, no. 10, pp. 2035–2046, 2020, doi: 10.4209/aaqr.2020.07.0388.
[40] T. Kubo, W. Bai, M. Nagae, and Y. Takao, “Clear Declining Behaviors and Causes in Atmospheric Polycyclic Aromatic Hydrocarbon Concentrations at the West End of Japan from 2017 to 2021,” *Appl. Sci.*, vol. 12, no. 21, p. 10963, Oct. 2022, doi: 10.3390/app122110963.
[41] K. Hayakawa *et al.*, “Long term trends in atmospheric concentrations of polycyclic aromatic hydrocarbons and nitropolycyclic aromatic hydrocarbons: A study of Japanese cities from 1997 to 2014,” *Environ. Pollut.*, vol. 233, pp. 474–482, Feb. 2018, doi: 10.1016/j.envpol.2017.10.038.
[42] W. Wang *et al.*, “Industrial Source Contributions and Health Risk Assessment of Fine Particle-Bound Polycyclic Aromatic Hydrocarbons (PAHs) during Spring and Late Summer in the Baoshan Area, Shanghai,” *Processes*, vol. 9, no. 11, p. 2016, Nov. 2021, doi: 10.3390/pr9112016.
[43] N. Tang *et al.*, “Atmospheric behaviors of polycyclic aromatic hydrocarbons at a Japanese remote background site, Noto peninsula, from 2004 to 2014,” *Atmos. Environ.*, vol. 120, pp. 144–151, Nov. 2015, doi: 10.1016/j.atmosenv.2015.08.090.
[44] W.-J. Hong *et al.*, “Distribution, Fate, Inhalation Exposure and Lung Cancer Risk of Atmospheric Polycyclic Aromatic Hydrocarbons in Some Asian Countries,” *Environ. Sci. Technol.*, vol. 50, no. 13, pp. 7163–7174, Jul. 2016, doi: 10.1021/acs.est.6b01090.
[45] T. F. Bidleman, W. Neil. Billings, and W. T. Foreman, “Vapor-particle partitioning of semivolatile organic compounds: estimates from field collections,” *Environ. Sci. Technol.*, vol. 20, no. 10, pp. 1038–1043, Oct. 1986, doi: 10.1021/es00152a013.
[46] A. A. Chudnovsky, H. J. Lee, A. Kostinski, T. Kotlov, and P. Koutrakis, “Prediction of daily fine particulate matter concentrations using aerosol optical depth retrievals from the Geostationary Operational Environmental Satellite (GOES),” *J. Air Waste Manag. Assoc.*, vol. 62, no. 9, pp. 1022–1031, Sep. 2012, doi: 10.1080/10962247.2012.695321.
[47] Y. Qi, J. Ge, and J. Huang, “Spatial and temporal distribution of MODIS and

`

MISR aerosol optical depth over northern China and comparison with AERONET," *Chin. Sci. Bull.*, vol. 58, no. 20, pp. 2497–2506, Jul. 2013, doi: 10.1007/s11434-013-5678-5.

[48] M. Ghahremanloo, Y. Lops, Y. Choi, and S. Mousavinezhad, "Impact of the COVID-19 outbreak on air pollution levels in East Asia," *Sci. Total Environ.*, vol. 754, p. 142226, Feb. 2021, doi: 10.1016/j.scitotenv.2020.142226.

[49] K. Papachristopoulou, I.-P. Raptis, A. Gkikas, I. Fountoulakis, A. Masoom, and S. Kazadzis, "Aerosol optical depth regime over megacities of the world," *Atmospheric Chem. Phys.*, vol. 22, no. 24, pp. 15703–15727, Dec. 2022, doi: 10.5194/acp-22-15703-2022.

[50] M. A. Zoran, R. S. Savastru, D. M. Savastru, and M. N. Tautan, "Peculiar weather patterns effects on air pollution and COVID-19 spread in Tokyo metropolis," *Environ. Res.*, vol. 228, p. 115907, Jul. 2023, doi: 10.1016/j.envres.2023.115907.

[51] J. M. Mitchell, "The Effect of Atmospheric Aerosols on Climate with Special Reference to Temperature near the Earth's Surface," *J. Appl. Meteorol.*, vol. 10, no. 4, pp. 703–714, Aug. 1971, doi: 10.1175/1520-0450(1971)010<0703:TEOAAO>2.0.CO;2.

[52] R. Greenwald, M. H. Bergin, J. Xu, D. Cohan, G. Hoogenboom, and W. L. Chameides, "The influence of aerosols on crop production: A study using the CERES crop model," *Agric. Syst.*, vol. 89, no. 2–3, pp. 390–413, Sep. 2006, doi: 10.1016/j.agsy.2005.10.004.

[53] X. Xia *et al.*, "Aerosol optical properties and radiative effects in the Yangtze Delta region of China," *J. Geophys. Res.*, vol. 112, no. D22, p. D22S12, Nov. 2007, doi: 10.1029/2007JD008859.

[54] Y. J. Kaufman and R. S. Fraser, "Light Extinction by Aerosols during Summer Air Pollution," *J. Clim. Appl. Meteorol.*, vol. 22, no. 10, pp. 1694–1706, Oct. 1983, doi: 10.1175/1520-0450(1983)022<1694:LEBADS>2.0.CO;2.

[55] J. Wang, "Intercomparison between satellite-derived aerosol optical thickness and PM $_{2.5}$ mass: Implications for air quality studies," *Geophys. Res. Lett.*, vol. 30, no. 21, p. 2095, 2003, doi: 10.1029/2003GL018174.

[56] K.-M. Wai *et al.*, "Aerosol pollution and its potential impacts on outdoor human thermal sensation: East Asian perspectives," *Environ. Res.*, vol. 158, pp. 753–758, Oct. 2017, doi: 10.1016/j.envres.2017.07.036.

[57] M. S. Ali-Taleshi, A. Riyahi Bakhtiari, M. Moeinaddini, S. Squizzato, S. Feiznia, and D. Cesari, "Single-site source apportionment modeling of PM2.5-bound PAHs in the Tehran metropolitan area, Iran: Implications for source-specific multi-pathway cancer risk assessment," *Urban Clim.*, vol. 39, p. 100928, Sep. 2021, doi: 10.1016/j.uclim.2021.100928.

[58] Y. Wang *et al.*, "Source apportionment of polycyclic aromatic hydrocarbons (PAHs) in the air of Dalian, China: Correlations with six criteria air pollutants and meteorological conditions," *Chemosphere*, vol. 216, pp. 516–523, Feb. 2019, doi: 10.1016/j.chemosphere.2018.10.184.

`

[59] T. Wang *et al.*, "Pollution characteristics, sources and lung cancer risk of atmospheric polycyclic aromatic hydrocarbons in a new urban district of Nanjing, China," *J. Environ. Sci.*, vol. 55, pp. 118–128, May 2017, doi: 10.1016/j.jes.2016.06.025.

[60] Z. Pilková, E. Hiller, L. Filová, and Ľ. Jurkovič, "Sixteen priority polycyclic aromatic hydrocarbons in roadside soils at traffic light intersections (Bratislava, Slovakia): concentrations, sources and influencing factors," *Environ. Geochem. Health*, Oct. 2021, doi: 10.1007/s10653-021-01122-7.

[61] W.-L. Ma, Y.-F. Li, H. Qi, D.-Z. Sun, L.-Y. Liu, and D.-G. Wang, "Seasonal variations of sources of polycyclic aromatic hydrocarbons (PAHs) to a northeastern urban city, China," *Chemosphere*, vol. 79, no. 4, pp. 441–447, Apr. 2010, doi: 10.1016/j.chemosphere.2010.01.048.

[62] N. Hazarika, A. Srivastava, and A. Das, "Quantification of particle bound metallic load and PAHs in urban environment of Delhi, India: Source and toxicity assessment," *Sustain. Cities Soc.*, vol. 29, pp. 58–67, Feb. 2017, doi: 10.1016/j.scs.2016.11.010.

[63] J. Yang, W. Xu, and H. Cheng, "Seasonal Variations and Sources of Airborne Polycyclic Aromatic Hydrocarbons (PAHs) in Chengdu, China," *Atmosphere*, vol. 9, no. 2, p. 63, Feb. 2018, doi: 10.3390/atmos9020063.

[64] W. Xing *et al.*, "Variations in traffic-related polycyclic aromatic hydrocarbons in PM2.5 in Kanazawa, Japan, after the implementation of a new vehicle emission regulation," *J. Environ. Sci.*, vol. 121, pp. 38–47, Nov. 2022, doi: 10.1016/j.jes.2021.08.046.

[65] A. Hirata, S. Kodera, Y. Diao, and E. A. Rashed, "Did the Tokyo Olympic Games enhance the transmission of COVID-19? An interpretation with machine learning," *Comput. Biol. Med.*, vol. 146, p. 105548, Jul. 2022, doi: 10.1016/j.compbiomed.2022.105548.

[66] W. Wang *et al.*, "Polycyclic aromatic hydrocarbons (PAHs) in urban surface dust of Guangzhou, China: Status, sources and human health risk assessment," *Sci. Total Environ.*, vol. 409, no. 21, pp. 4519–4527, Oct. 2011, doi: 10.1016/j.scitotenv.2011.07.030.

[67] Y. Jiang, X. Hu, U. J. Yves, H. Zhan, and Y. Wu, "Status, source and health risk assessment of polycyclic aromatic hydrocarbons in street dust of an industrial city, NW China," *Ecotoxicol. Environ. Saf.*, vol. 106, pp. 11–18, Aug. 2014, doi: 10.1016/j.ecoenv.2014.04.031.

[68] J. L. Domingo and J. Rovira, "Effects of air pollutants on the transmission and severity of respiratory viral infections," *Environ. Res.*, vol. 187, p. 109650, Aug. 2020, doi: 10.1016/j.envres.2020.109650.

`

Chapter 4: Protective Effect of Astaxanthin Enriched in Japanese Raw Fish Diet Against PM-bound PAHs Induces Cell Damage

This study aims to verify the protective effect of astaxanthin, an antioxidant enriched in deep-sea fish that is a favorite in the Japanese diet, on A549 cells exposed to PAHs. The inhibitory effect of ATX on the production of harmful intermediates in the exposed cells was quantified by exposing A549 cells to the PAHs standard solution containing ATX solution and examining the cell viability, ROS, and expression of inflammatory cytokines. Finally, actual aerosol samples collected by the cyclone were used to simulate and verify the protective effect of ATX on lung cells under actual exposure conditions.

4.1 Introduction

Polycyclic aromatic hydrocarbons (PAHs), which are generated during incomplete combustion with the structure of two or more benzene rings or cyclopentadiene, are a typical organic contaminant adsorbed in PM [1]–[3]. The damage caused by PAHs to cells consists of two main aspects. On the one hand, PAHs can activate aryl hydrocarbon receptor (AhR) and induce reactive oxygen species (ROS) formation through AhR-dependent induction of cytochrome P450 (CYP) isoforms including CYP1A1, CYP1A2, and CYP1B1 [4]–[7]. Particularly, oxidative stress is often accompanied by inflammation [4], [8]. Oxidative stress and excessive ROS can induce cell inflammation and DNA damage resulting in cell death by activating several signaling pathways such as NF-kB, PI3K/Akt, il-6/AKT/SATA3, and Notch1 in various of cells [9]–[12]. On the other hand, mitochondria, which is the main site for ROS production in cellular, could be activated directly by the contaminants and produce more free radicals to enhance the NF-kB signaling pathway resulting in stronger inflammation reaction, previous study

`

has shown that BaP induces excessive free radical production in the body's mitochondria with triggering lesions in mice [13]. Moreover, Benzo[b]fluoranthene (BbF) can disrupt mitochondrial membrane potential directly to induce apoptosis in human airway epithelial cells [14]. As mentioned in the Hill et al. [15] research that air pollutants might promote inflammatory changes in the lung tissue microenvironment that permit pre-existing mutated clones to expand then cause cancer rather than directly inducing DNA damage strangely. "It's that sustained inflammation that becomes chronic that is essential to get these mutated cells to grow into tumours."

Hill et al. [15] research shown that treating mice with an antibody that blocks IL-1β reduced their incidence of lung cancer, but "it is not feasible to treat all of them with IL-1β blocking drugs - it would be expensive, and the drugs could cause unwanted side effects in otherwise healthy people." Instead, researchers suggested that simple dietary interventions that combat inflammation might be able to reduce the risk of some cancers. For example, Sánchez-Martín et al. [16] thought eating honey which has natural antioxidants such as polyphenols can protect human-derived cells against DNA strand breaks and oxidative DNA damage effects induced by BaP. Bulanda et al. [17] believes that by adding antioxidant-rich dried fruits (prunes, apricots, and cranberries) and eating them can effectively reduce the PAHs concentration produced during the pork grilling as well as the harmful effects on humans. These studies have attempted to reduce the amount of ROS produced by PAHs in cells through the intake of antioxidants in food to avoid inflammatory reactions.

However, these dietary recommendations do not fit well with the Japanese diet. Japanese people like to eat raw fish, especially deep-sea fish, and the cooking style is bland instead of using too much oil. Fish meat is rich in astaxanthin (ATX). ATX is a kind of antioxidant which has very high reactivity and can inhibit oxidation. High-temperature cooking will denature astaxanthin and lose its antioxidant activity, so raw food and lighter cooking methods will retain the most possible astaxanthin in food but also reduce the production of PAHs during the cooking process. This provides a new

`

choice for us to try to reduce the cellular damage of PAHs through food intake of antioxidants.

Astaxanthin is a keto-carotenoid within a group of chemical compounds known as terpenes. Astaxanthin has two chiral centers at the 3- and 3'- positions resulting in three unique stereoisomers (3S,3'S, 3S,3'R meso, and 3R,3'R) (**Fig. 4.1**). While all three stereoisomers are present in nature, relative distribution varies considerably from one organism to another. Synthetic astaxanthin contains a mixture of all three stereoisomers, in approximately 1:2:1 proportion, which has the less antioxidative property. Oppositely, natural astaxanthin contained in salmon and algae is mainly (3S,3'S)-isomer, which has stronger antioxidant properties [18], [19].

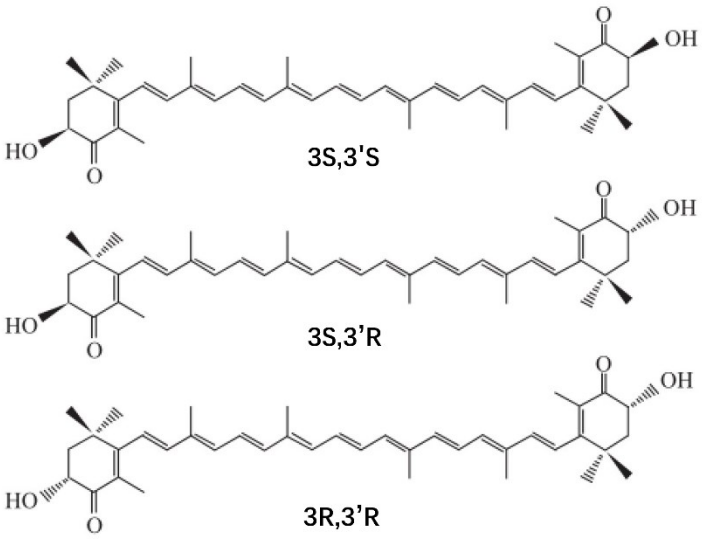


Fig. 4.1 Structures of astaxanthin stereoisomers [20]

The special structure of astaxanthin allows it to span the bilayer phospholipid layer of the cell, and the functional groups at its ends can absorb the unpaired electrons from free radicals, thus reacting with free radicals and effectively reducing their activity [21], [22]. Besides, astaxanthin can also act against inflammation. Naguib et al. [23] reported that astaxanthin has higher antioxidant activity compared to various carotenoids such as lutein, lycopene, α-carotene and β-carotene. The results of animal experiments shown that astaxanthin in *H. pluvialis* offered the best protection to free radicals in rats

`

followed by β-carotene and lutein [24]. Park et al. [25] pointed out astaxanthin can reduce the inflammation marker of DNA oxidative damage thus enhancing immune response in young healthy adult female human subjects. In the field of PM exposure protection research, Yin et al. [26] showed that ATX can alleviate histomorphological changes, oxidative stress, and inflammation in ATX-treated groups of rats compared with $PM_{2.5}$-exposed groups, concluded that ATX can alleviate lung injury after $PM_{2.5}$ exposure by inhibiting ferroptosis and apoptosis. ATX has a potentially beneficial effect on $PM_{2.5}$ exposure in the brain by suppressing PM2.5-induced neuroinflammation by regulating Akt phosphorylation in BV-2 microglial cells reported by Kim et al [12].

The focus of this study was to explore the protective role of ATX against the adverse effects of exposure of A549 cells to standard solutions of PAHs, and to determine its contribution to the effects on cell viability, ROS, and expression of inflammatory cytokines after exposure. Finally, simulations using actual aerosol samples collected by cyclone were used to validate the protective effect of ATX on lung cells exposed to air pollution under real-world conditions. The results of this in vitro experiment will provide an economically viable potential countermeasure for subsequent human health protection from air pollution exposure.

4.2 Materials and methods

4.2.1 Chemical reagents

Acetonitrile (ACN, HPLC grade) and dimethyl sulfoxide (DMSO, cell culture sure) were purchased from Fujifilm Wako Pure Chemical Co. (Fujifilm, Tokyo, Japan).

Sixteen PAHs mixture standard in a DCM: MeOH solution (1:1, v/v) were purchased from AccuStandard (200 μg/ml, 1 ml, AccuStandard, Inc., New Haven, CT, USA). The 200 μg/ml standard solution was diluted in ACN into low concentrations as 10, 20, and 50 ng/ml.

Astaxanthin was purchased from Selleckchem (Selleck Chemicals LLC, USA), and

`

the solid reagent was dissolved in DMSO then using the MEM cell culture medium to dilute different concentrations of 1, 5, 10, 50, 100, and 200 μg/ml.

4.2.2 A549 cell culture

For in vitro assay, the A549 cells, which were derived from a type II-like human alveolar epithelial carcinoma, were cultured in minimum essential medium (MEM) with Earle's salts and L-Glutamine (Gibco, Thermo Fisher Scientific, USA) with 5% CO_2 at 37 ℃. The medium contained 10% fetal bovine serum (FBS) (Cosmo Bio Co., Ltd, Tokyo, Japan) and 1% penicillin-streptomycin (PS) solution (×100) (Fujifilm, Osaka, Japan). For cell sub-culturing, they were washed with phosphate-buffered saline (PBS) (Gibco, Thermo Fisher Scientific, USA) and harvested by 0.25w/v% trypsin-1mmol/L EDTA·4Na solution with phenol red (Fujifilm, Osaka, Japan). The cells harvested from the sterile plastic flask were centrifuged to remove the lysate, and the collected cells were mixed with new medium and incubated for 72 h for subsequent experiments.

4.2.3 Cell viability

The cell viability of A549 cells were assessed by the water-soluble tetrazolium-1 (WST-1) assay (Premix WST-1 cell proliferation assay system, Takara, Shiga, Japan). A549 cells were incubated into 96-well plates at a density of 2500 cells/well in a volume of 100 μl medium, then treated with different doses of PAHs and astaxanthin solutions in 96-well culture plate at different exposure time. Then 10 μl WST-1 solution was added to each well, and the cells were incubated for another 1 h at 5% CO_2 and 37℃. The absorbance at 450nm is recorded, and the reference wavelength is 630 nm on MPR-A100 microplate reader (AS ONE CO., Osaka, Japan). Cell viability is expressed as a percentage of the blank control and calculated by **Eq. 4.1**.

$$\boldsymbol{Cell\ viability}\ (\%) = \frac{(Abs_{sample\ 450nm} - Abs_{sample\ 630nm}) - (Abs_{sample\ blank\ 450nm} - Abs_{sample\ blank\ 630nm})}{(Abs_{ctrl\ 450nm} - Abs_{ctrl\ 630nm}) - (Abs_{ctrl\ blank\ 450nm} - Abs_{ctrl\ blank\ 630nm})} \quad (4.1)$$

`

4.2.4 Reactive oxygen species (ROS)

Fluorescent probe 2′,7′-dichlorofluorescin diacetate (DCFH-DA) fluorogenic probe (CM-H2DCFDA, Thermo Fisher Scientific, USA) was used to measure the intracellular levels of reactive oxygen species (ROS) exposed to different contaminant concentrations. A549 cells were cultured with a concentration of 2500 cells/well at the special bottom transparent 96-well plate for 72 h at 5% CO2 and 37℃. Removed the cell medium then added 70 μl of 5 μmol/ml DCFH-DA solution per well, which was diluted using colorless MEM medium with 1% PS, and cultured for 30 min at 5% CO2 and 37℃. Removed DCFH-DA probe solution and used PBS solution to wash cells three times, removed the washing solution, added the exposure substance, and detected the fluorescence signal intensity (emission and excitation wavelength, 495nm/529nm) after exposure 0h, 2h, ..., and *i*h on Infinite F Nano^{+} plate reader (TECAN CO., Kanagawa, Japan). All experimental operations were performed in dark condition. The ROS level was identified as the percentage of fluorescence of the blank group detected after exposure 0h and calculated by **Eq. 4.2**.

$$\boldsymbol{ROS\ level}\ (\%) = \frac{Fluorescence_{\ ih\ sample}}{Fluorescence_{\ 0h\ blank}} \tag{4.2}$$

4.2.5 RT-PCR

Total RNA was extracted from the cultured A549 cells exposed to PAHs and ATX solutions with NucleoSpin RNA assay kit (Macherey-Nagel GmbH & Co., Germany) according to the manufacturer's instructions. Reverse transcription of total RNA to cDNA was performed with the two-step RT-PCR method with the instruction of PrimeScript RT reagent kit (Takara, Shiga, Japan). The first step was reversed transcribing the total RNA in each sample into cDNA using GeneAtlas (Astec Co., Ltd, Fukouka, Japan), and the second step was using the quantitative real-time PCR (qPCR) to determine the transcript levels of the target inflammation gene's transcript with the TB Green Premix Ex Taq II (Tli RNaseH Plus) RT-PCR kit (Takara, Shiga, Japan) on

`

Gene Detection Device GVP-9600 (Shimadzu, Japan). The PCR reaction conditions were: initial denaturation at 95 ℃ for 30 sec, 95 ℃ for 5 sec, 60 ℃ for 30 sec and 50 cycles. In this study, β-actin was used as internal reference, and $2^{-\Delta\Delta Ct}$ method was used to calculate the relative target inflammation factor expression (**Table 4.1**).

Table 4.1 Primer sequences

Gene	Reverse primers	Forward primers
IL-6	*5'-TGTCCTGCAGCCACTGGTTC*	*5'-AAGCCAGAGCTGTGCAGATGAGTA*
IL-8	*5'-TGTGGTCCACTCTCAATCACTCTC*	*5'-CACTGTGTGTAAACATGACTTCCAA*
β-actin	*5'-CTAAGTCATAGTCCGCCTAGAAGCA*	*5'-TGGCACCCAGCACAATGAA*

4.2.6 Atmospheric aerosol samples

Two cyclone-collected powder aerosol samples, that were used for ATX protection effect practical validation experiments, named sample 1 and sample 2, and the samples information were listed in **Table 4.2**. Actual aerosol samples were collected at the same method introduced in **section 3.2.1**. PAHs concentration were detected using the HPLC/FLD system mentioned in **Chapter 2**, and concentration of metal pollutants were analyzed using energy-dispersive X-ray fluorescence (EDXRF) method which we will introduced in **Chapter 5**.

`

Table 4.2 Sampling information and main contaminants concentration of two aerosol samples

	Sample 1	Sample 2
Sampling data	2020/12/10-2021/1/6	2021/9/8-11/25
∑PAHs (ng/mg)	24.67	10.50
Metals (ppmw)		
Cr	389.7	1736.1
Mn	849.0	1152.6
Fe	33769.5	40442.0
Ni	207.4	830.7
Cu	384.8	746.8
Zn	1799.6	70504.8
Pb	125.9	385.0

4.2.7 Statistical analysis

All data are expressed as the mean ± standard deviation (SD) (n=6). The paired samples t-test was used to analyze the significant comparison of different exposed groups by the Origin software (version OriginPro 2018C). A value of $p < 0.05$ was considered statistically significant.

4.3 Results and discussion

4.3.1 Harmful effects of ATX on cells viability

It is necessary to verify whether astaxanthin is harmful to the cells before using it for cell protection caused by PAHs exposure. Moreover, since astaxanthin is insoluble in water and can only be dissolved in DMSO, it must be dissolved in DMSO and then diluted to different concentrations using cell culture medium and used for exposure

`

experiments. Meanwhile, high concentrations of DMSO have an inhibitory effect on cell growth, so it is necessary to ensure that the concentration of DMSO in the solution is not higher than 1‰ at the time of dilution and to set up a blank control with the corresponding concentration of DMSO during the experiment.

The concentrations of ATX used for cell exposure were 1, 5, 10, 50, 100, and 200 μg/ml. The solution was prepared by dissolving 2 mg of ATX in 1 ml of DMSO, adding 9 ml of cell culture medium to form a 200 μg/ml solution, and diluting in steps to obtain other concentrations. Next, 1 ml of DMSO was dissolved in 9 ml of culture medium to obtain a solution with a corresponding DMSO concentration of 10% and diluted to obtain a control reagent with the corresponding DMSO concentration (0.5‰, 2.5‰, 5‰, 2.5%, and 5%, v/v). The corresponding solution was added to A549 cells and determining the cell viability after exposed 24 h using WST-1 assay.

The experiments results are shown in **Fig. 4.2** and **Fig. 4.3**. It resulted that concentration of DMSO in the culture medium below 2.5% (v/v) had no significant effect on cell survival, and the average survival rate of cells after 24h of exposure was higher than 80%. However, high concentrations of DMSO significantly can affect the cell survival rate. This is similar to the conclusion of existing studies, which means that high concentrations of DMSO have the effect of inhibiting cell proliferation and promoting apoptosis [27].

Fig. 4.3 shown that when the ATX concentration in the culture medium was 100 μg/ml and 200 μg/ml (corresponding to DMSO concentrations of 5% and 10%), the cell survival rate decreased sharply. However, the effect of ATX solution on cell survival is not only due to DMSO. The low concentration of ATX solution containing DMSO was at a very low concentration. In contrast, the survival rate of cells was more stable under the exposure conditions with ATX concentration of 10 μg/ml.

`

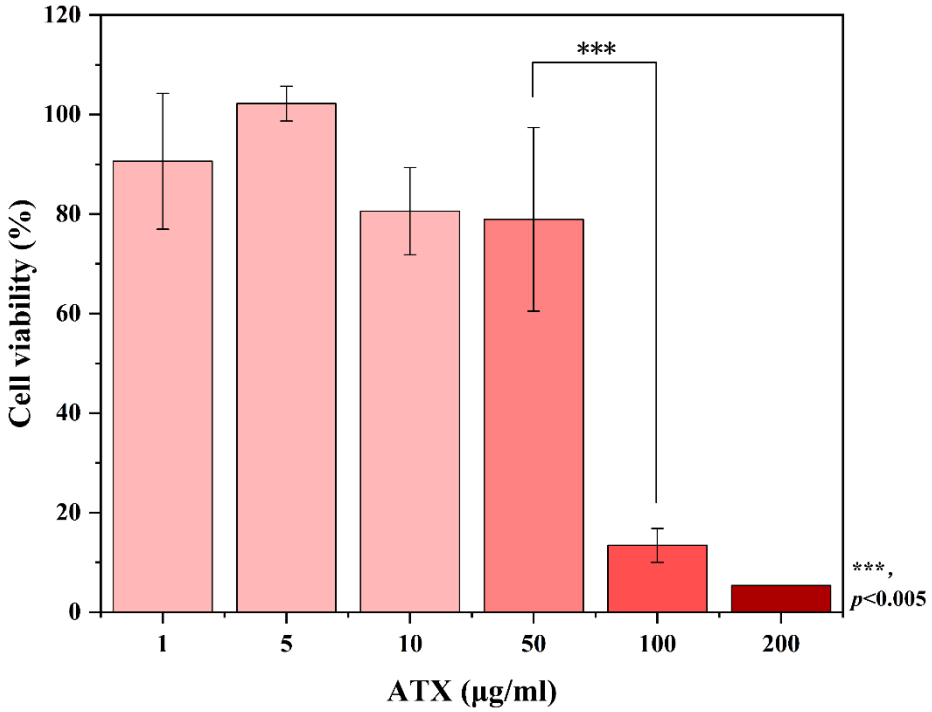


Fig. 4.2 A549 cell survival rate exposed to different concentration ATX solutions

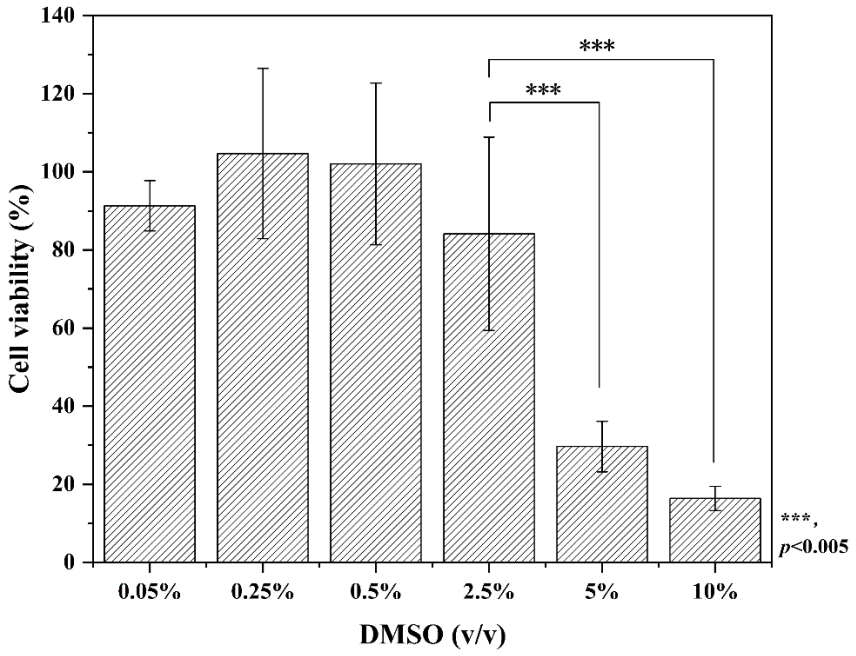


Fig. 4.3 A549 cell survival rate exposed to corresponding concentration DOSM solutions

4.3.2 Cell hazard testing for PAHs solutions

The concentrations of PAHs used for cell exposure were 10, 20, and 50 ng/ml. The solution was prepared by diluting 0.5 ml of 1 μg/ml PAHs standard solution to 9.5 ml of cell culture medium to form a 50 ng/ml solution, and diluting in steps to obtain other concentrations. However, the standard PAHs solution was formulated using acetonitrile, so it was also necessary to prepare a corresponding volume concentration of acetonitrile solution (5%, 2.5%, and 1.25%) for exposure, which was used to rule out the possibility that cell death might be due to acetonitrile. The results shown in **Fig. 4.4**. The positive control was 10% DMSO solution (v/v).

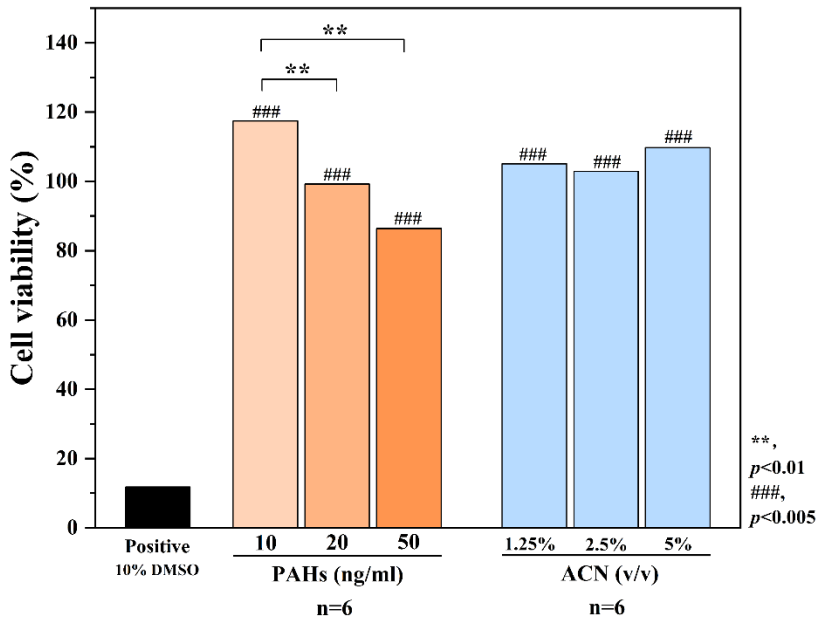


Fig. 4.4 Cell viability of PAHs exposure and corresponding ACN

p<0.005, compared with positive control; ** p<0.01, compared with different PAHs solutions

The exposure results showed that the ACN used to formulate the standard solution of PAHs had no effect on cell growth (the average value of cell viability was 104%), so much so that the tendency of the cell viability exposed to different concentrations of PAHs solutions to show a significant decrease with increasing exposure concentration is evidence that PAHs are indeed detrimental to the cell activity. Although 50 ng/ml PAHs solution significantly reduces cell survival, there is still a significant difference

relative to the positive control, indicating that its cell-damaging effect is not obvious enough. Therefore, it is also necessary to determine the cellular hazardous results of higher concentrations of PAHs solutions to obtain a more obvious cellular damage effect, so that better experimental results might be obtained in the subsequent experiments to verify the protection of ATX.

4.3.3 Protection effect of ATX for PAHs exposed A549 cells

The mixture of different concentration ATX and PAHs were exposed to A549 cells and tested the cell survival rate after 24h and 48h exposure. The cell viability results were shown in **Fig. 4.5** and **Fig. 4.6**.

The 24 h exposure results did not follow our expectations which the cell survival rate increases following exposing to the high concentration of ATX. Instead, it seems like ATX has the opposite effect which decreases the cell survival. But the 48 h exposing results indicate a significantly increasing trend of cell survival rate with the exposure concentration of ATX when exposed in the PAHs solution of 100 ng/ml. The reason for this result may be due to the lag in the protective effect of ATX on exposed cells. This is because ATX does not reduce the harmful effects of pollutants on cells by reacting to consume PAHs. It is only after the cells have been invaded by the pollutant and ROS are generated that ATX can protect the cells by reacting to consume the generated ROS, rather than protecting them from the pollutant by adding ATX to the cell culture medium in advance.

`

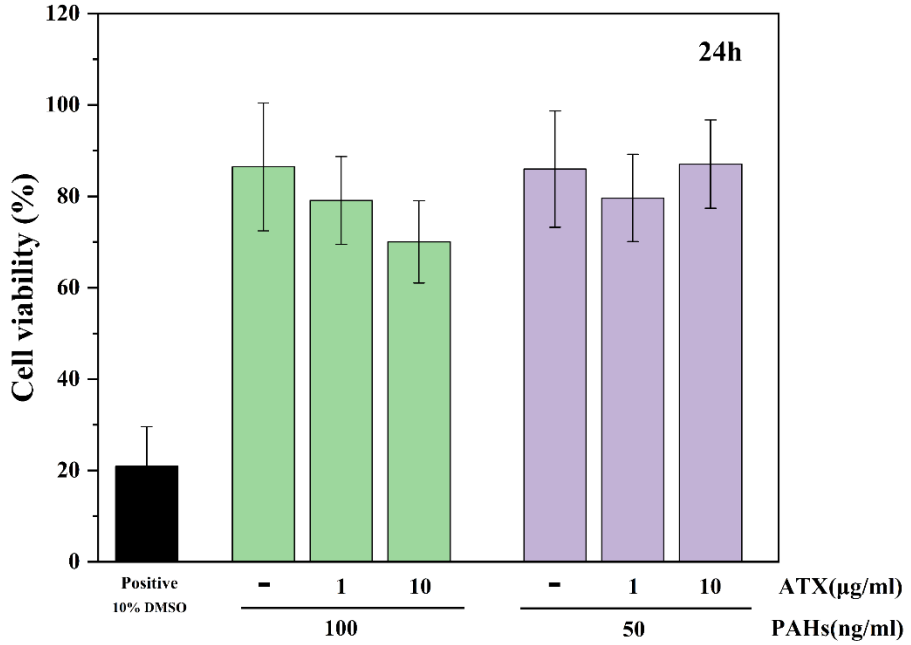


Fig. 4.5 Cell viability effect of ATX on PAHs-exposed A549 cells for 24 h

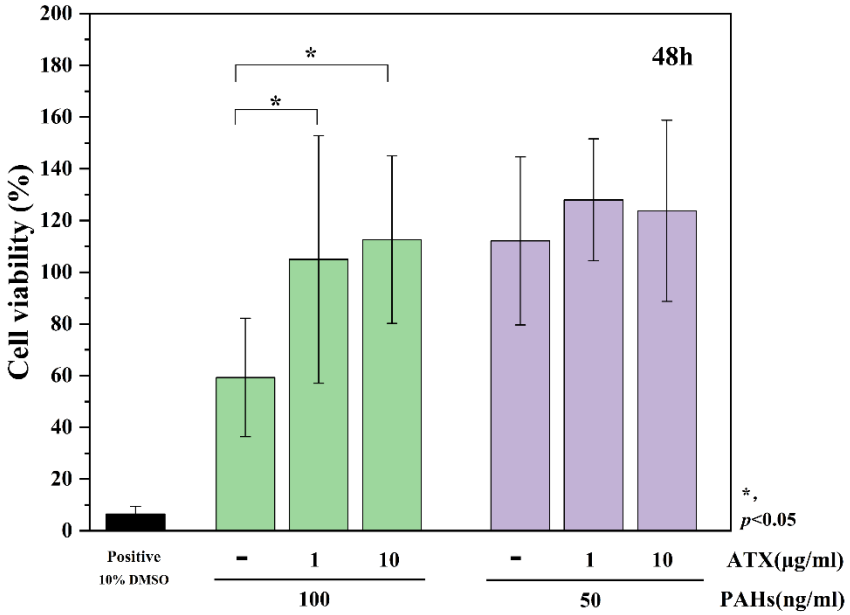


Fig. 4.6 Cell viability effect of ATX on PAHs-exposed A549 cells for 48 h

4.3.4 ATX cell protection validation experiments

There is a significant increasing trend of cell survival following the increasing concentration of ATX with the exposure condition of 100 ng/ml PAHs after 48 h, but the similar trend was not found in the 24 h exposed experiment.

`

PAHs concentration: 100 ng/ml

ATX concentration: 1 μg/ml, 10 μg/ml

Cel sampling time: sampling once per 6 h for 48 h

Detecting parameters: ROS, RT-PCR

Experimental steps:

Different concentrations of PAHs mixed with ATX solution were exposed to A549 cells, and cell samples were collected every 6 h for 48 h. After the pretreatment of liquid nitrogen freezing, mRNA from eight cell samples was uniformly extracted to determine the trend of inflammatory cytokine expression (IL-6) using RT-PCR.

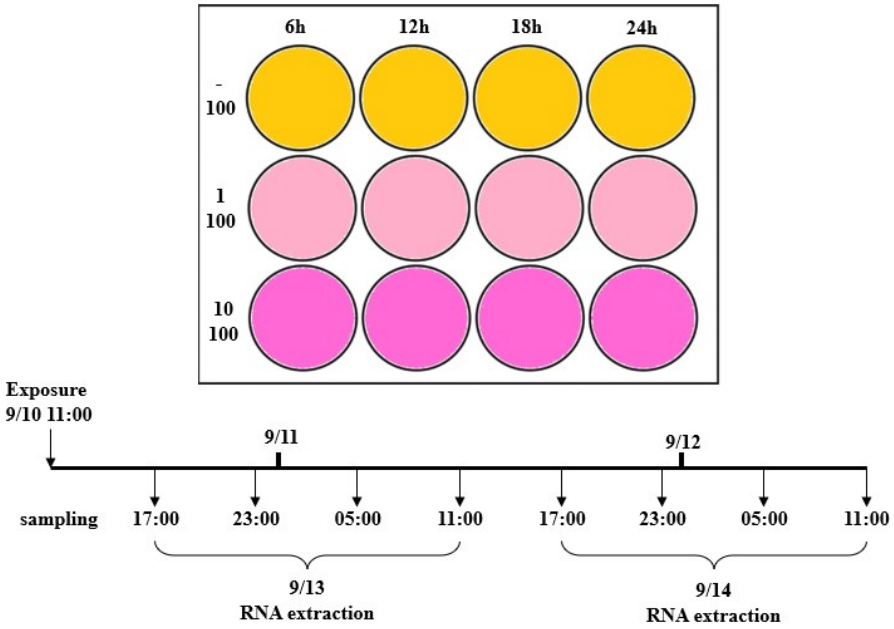


Fig. 4.7 Experimental process schematic

The results of the rt-PCR assay are shown in **Fig. 4.8**, which shows that the relative expression of IL-6 reached a maximum value at the 30th hour, followed by a rapid decline. This result basically proved our previous speculation that PAHs first generate ROS by stimulating the signaling pathway, thus causing an intracellular inflammatory response, and then ATX will play a role in eliminating the inflammation to protect the cells. Inflammatory cytokines are not significantly produced before 24 h after exposure to the pollutant, and therefore cell survival is not significantly affected until then, which

`

is consistent with the results of the previous survival validation experiments, i.e., cell survival did not show a consistent correlation with the concentration of the added pollutant after 24 h of exposure, whereas a clear concentration-dependent feature appeared in the 48 h result.

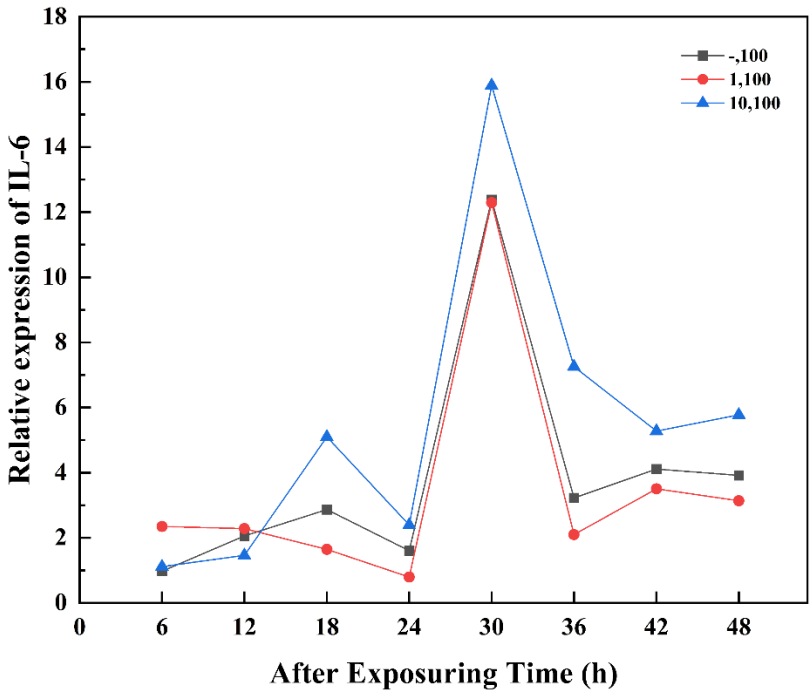


Fig. 4.8 Changing trend of relative expression of IL-6 in different exposure time samples

4.3.5 ROS

The ROS experiments were performed using colorless MEM cell cultures configured with samples for exposure, with sample parameters as shown in **Table 4.3**. Fluorescence intensity was detected at different time intervals after the addition of contaminants and the relative concentration of ROS was calculated, the detecting results shows in **Fig. 4.9**.

`

Table 4.3 Cell exposure experiments parameters

	ATX (μg/ml)	PAH (ng/ml)
-,100	×	
1,100	1	100
10,100	10	
Control	just MEM cell culture fluid + 1%PS	
Positive	3% H_2O_2 solution	

The positive control group stimulated the cells to produce a large amount of ROS just after being added to the cells (**Fig. 4.9**). Then the concentration of ROS gradually decreased with the increase of the incubation time, and significantly reduced and finally remained unchanged after 6 h. This was because cells in positive control group had died after 6 h. The ROS content in the cells of the experimental group remained basically unchanged in the first 6 h, and with the increase of culture time, the ROS concentration in the exposed group containing only PAHs began to increase, which may be due to the fact that the reproduction cycle of A549 cells is about 22 h, and the cells need to take up the nutrients from the external culture medium in the process of cell proliferation, and the PAHs in the culture medium enter into the cell interior and stimulate the cells to produce ROS. In contrast, the ROS concentration in the ATX-exposed group also showed a rising trend at 24 h but was not significant, and remained essentially unchanged during the subsequent incubation time, a result that suggests that ATX reacts with ROS produced inside the cells and protects the cells from oxidative stress damage. **Fig. 4.10** compares the relative concentration of ROS in the cells collected at 2h, 24h, and 48h after samples exposure, we can see that concentration of ROS in the experimental group with the addition of ATX showed a significant decrease compared to the exposure group without ATX, which more intuitively proves the protective effect of ATX on PAHs-exposed cells.

`

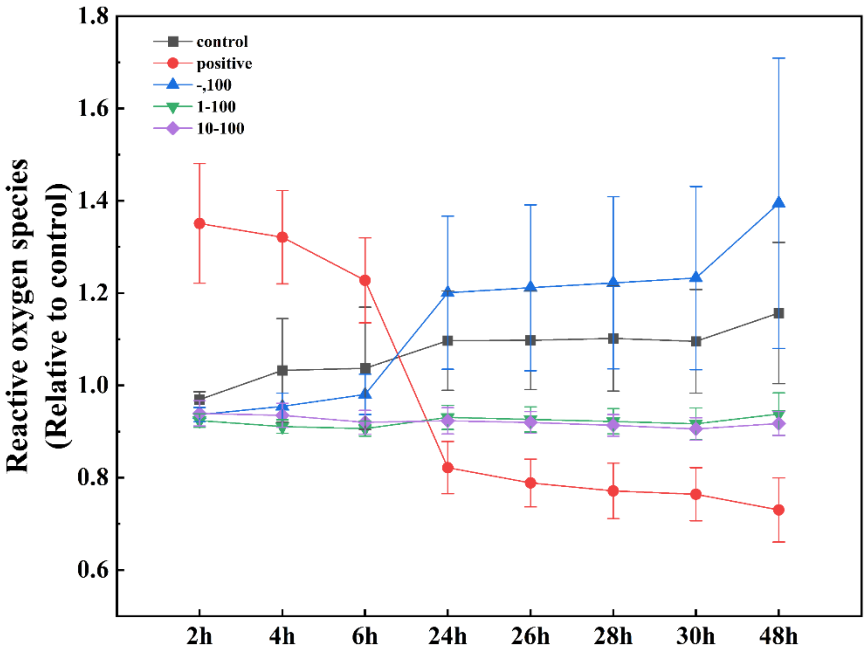


Fig. 4.9 ROS relative concentration at different detecting time

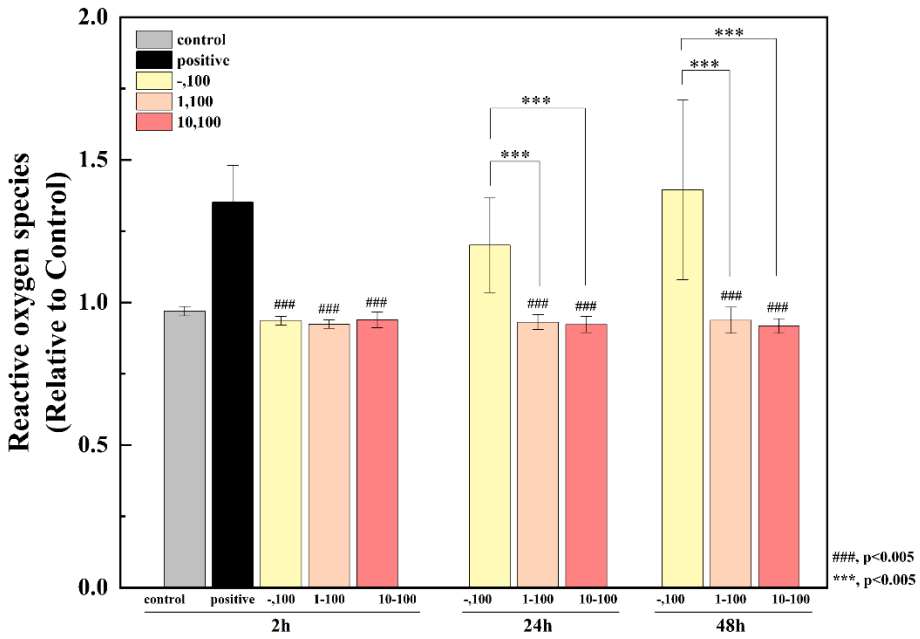


Fig. 4.10 ROS relative concentration of cell exposure experiments at 2h, 24h, and 48h (n=12). ### p<0.005, compared with positive control at 2h

On the one hand, the ability of ATX to inhibit ROS production in cells is thought to be related to its unique chemical structure. The functional groups at its ends can absorb the unpaired electrons from free radicals, and the singlet oxygen-capturing ability of

natural ATX is 6000 times of vitamin C, 800 times of coenzyme Q, and 100 times of vitamin E [22], [28]. Thus, ATX can reduce intracellular ROS content by providing an electronic burst of singlet oxygen and blocking free radical reactions. On the other hand, ATX inhibits mitochondrial damage thereby reducing the production of ROS, which are normally produced by electron transfer chains (ETCs) in the mitochondrial cristae and released into the cellular matrix [29]. When stimulated by external pollutants, mitochondria produce large amounts of ROS, resulting in an imbalance in ROS levels. Excessive ROS leads to disruption of the mitochondrial bilayer and decoupling of membrane-bound complexes, and the damaged mitochondria release more ROS into the cytoplasm, which then triggers a cascade reaction leading to apoptosis or DNA damage [28], [30], [31].

4.3.6 ATX protection effect for actual aerosol exposure to A549 cell

Exposure cell experiments using standard solutions of PAHs have demonstrated that ATX significantly reduces the expression of ROS and inflammatory cytokines generated by PAHs exposure and thus reduces the mortality of A549 cells. However, the actual particulate matter inhaled by humans is more complex than standard chemical exposures. Atmospheric aerosol particles are a mixture of chemicals such as PAHs, water-soluble ions, and metals, and the combination-effect of these pollutants can multiply PM biotoxicity. Therefore, it is necessary to verify the effectiveness of ATX in protecting cells exposed to actual aerosol samples to confirm the feasibility of its use for real-life pollution protection.

`

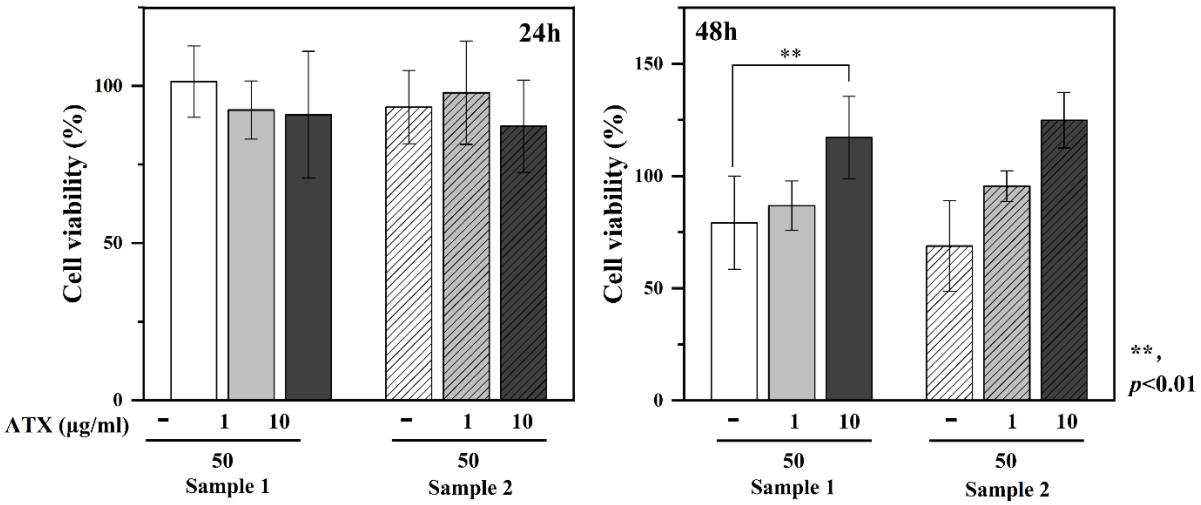


Fig 4.11 Cell survival rate of A549 cells exposed to different sample combinations after 24 h and 48 h

Fig. 4.11 represents the survival of A549 cells after exposure to different sample combinations for 24 h and 48 h. The blank groups only added media solutions containing two particulate matter samples (50 μg/ml), and the experimental groups were a mixture of particulate matter samples with two concentrations of ATX (1 μg/ml and 10 μg/ml). Similar as the results of the viability assay for A549 cells exposed directly to the PAHs standard solution and its mixture with the ATX solution (Section 4.3.3), the same hysteresis was observed for the viability of cells exposed to the actual samples. Briefly, there was no significant difference in cell survival between the blank and experimental groups after 24 h of exposure, but the 48 h results showed a significant difference in cell survival in the experimental group with the addition of the high concentration of ATX solution as compared to the control group (especially exposed to sample 1), indicating that ATX did express a protective effect on A549 cells exposed to aerosol samples. Cell survival in the experimental group after 48h of exposure to sample 2 failed to be statistically significant due to the large relative error of the assay results (n=4), but a trend of increased survival relative to the control group was observed, suggesting that ATX also has a delayed protective effect on the cells exposed to sample 2.

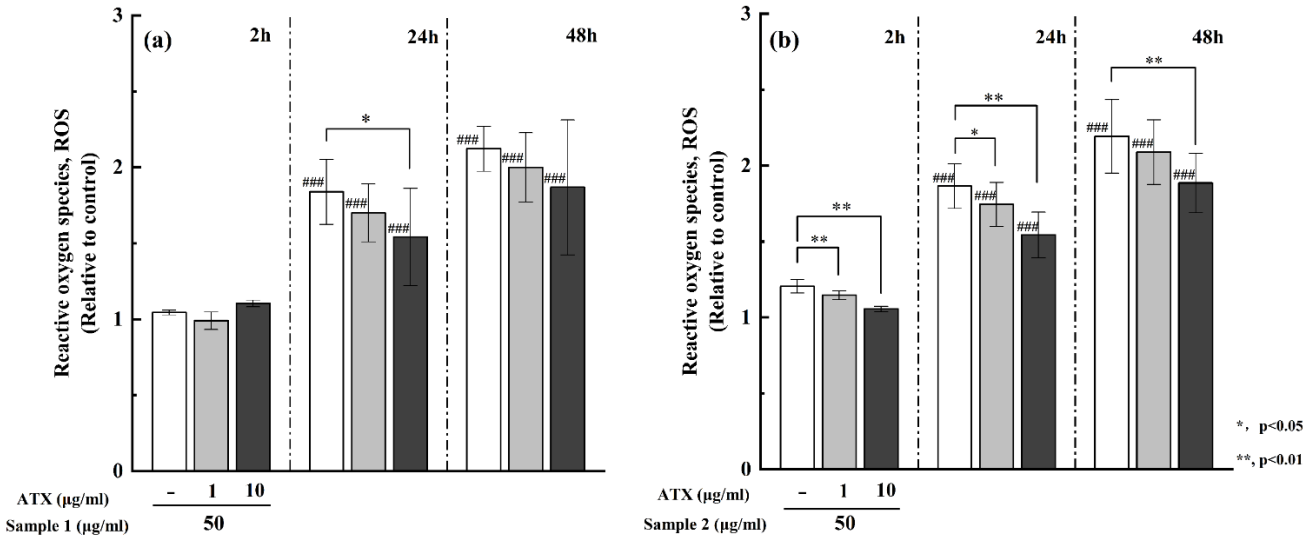


Fig. 4.12 ROS concentration after exposed 2h, 24h, and 48h of (a) sample 1 and (b) sample 2. ### $p<0.005$, compared with corresponding blank group at 2h

The trend of ROS concentration in cells after exposure can help us better understand the protective mechanism of ATX on cells (**Fig. 4.12**). The experimental results showed that the concentration of ROS in the cells of all exposure groups increased significantly after 24 h and 48 h of exposure relative to the initial phase. This is the reason that the actual sample is a complex mixture of multiple pollutants, not only the PAHs attached to the particulate matter, but also other pollutants such as metals can induce the cells to produce ROS, and in this case, even with a high concentration of ATX solution (10 μg/ml), only part of the induced ROS can be removed. However, we also saw that the concentration of ROS in the cells of the experimental group with added ATX was still significantly decreased relative to the blank group, indicating that ATX did reduce the production of ROS in the cells.

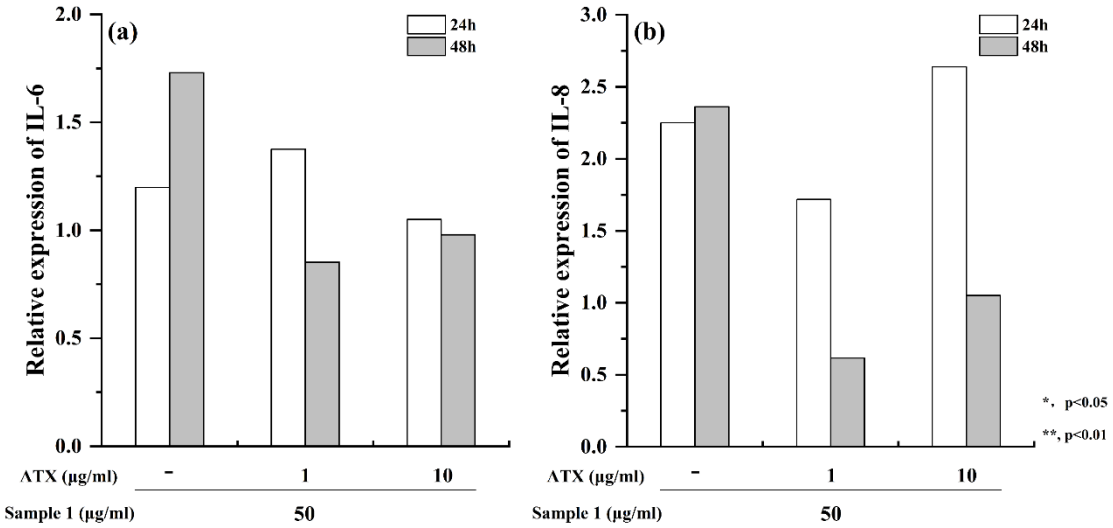


Fig. 4.13 Inflammation factors concentration of (a) IL-6 and (b) IL-8 exposed to sample 1 and mixture of ATX after 24h and 48h

The 48 h results of the experimental group of Sample 1 exposed to a high concentration of ATX solution did not show statistically significant results compared to the blank group due to the large error in the assay results (**Fig. 4.12(a)**), so in order to prove that the ATX added in the experimental group did have an inhibitory effect on the intracellular ROS as well as on the subsequent inflammatory production, we examined the changes in the concentration of the two inflammatory cytokines, IL-6 and IL-8, in the cells of both the blank group and the experimental groups exposed to sample 1.

Fig. 4.13(a) shows that the relative expression of IL-6 in the cells of the blank group exposed for 48 h was elevated by 44%, the concentration of IL-6 in the experimental group to which a low concentration of ATX was added decreased by 38%, and the decrease in the concentration of IL-6 in the experimental group to which a high concentration of ATX was added was not significant. In contrast, for the inflammatory cytokine IL-8, there was a significant decrease in IL-8 concentrations in the experimental groups to which ATX was added (64% and 60% for two groups, respectively) (**Fig. 4.13(b)**). Overall, the expression of inflammatory cytokines in the cells of the experimental group with the addition of ATX were all reduced relative to the blank group. Still, the inhibitory effect of ATX on different inflammatory cytokines was not the same, so this may be this is the reason why the expression of the

concentration of the two inflammatory cytokines did not show a decreasing trend with the concentration of ATX increase.

Unlike in vitro cell exposure experiments conducted solely using standard solutions of PAHs, cell experiments using actual aerosol samples are more complex. Aerosolized particulate matter suspensions contain large amounts of insoluble material. Unlike the soluble components that enter the cell interior, these particulate components enter the cell primarily through phagocytosis and endocytosis [32]. Large amounts of cellular endocytosis of ultrafine particulate matter might lead to a decrease in the rigidity of the cell membrane, and therefore may cause severe physical damage to the cell membrane, which in turn increases the penetration of PM into the cell [33]–[35]. It has been shown that diesel exhaust particulate matter (DPM) can be ingested by cells through phagocytosis and clathrin-mediated endocytosis [36]. DPM that invades cells accumulates in the cell thereby causing membrane damage including membrane potential disturbance, plasma membrane disruption and increased fluidity. The polar-nonpolar-polar symmetric structure of ATX can cross the cell membrane to effectively increase the membrane stiffness, reduce the membrane fluidity, and hinder the diffusion of free radicals within the membrane. Thus, in addition to the previously discussed ability of ATX to inhibit intracellular oxidative stress by protecting mitochondria and reacting directly with ROS, ATX can also rescue actual aerosol sample-induced cell membrane disruption by maintaining the integrity and stability of the cell membrane, resulting in protecting the cell.

4.4 Summary

PAHs induce the production of ROS in cells, resulting in inflammation and DNA damage leading to cell death, therefore, reducing the production of ROS in exposed cells through the intake of a certain amount of antioxidant substances in food is one of the possible ways to protect cells from the hazards of particulate matter exposure. In

`

this study, we chose astaxanthin, an antioxidant enriched in deep-sea fish that is a favorite in the Japanese diet, to investigate its protective effect on A549 cells after PAHs exposure. Firstly, we eliminated the interference of results caused by organic solvents through a series of pre-experiments, and then selected the most suitable experimental conditions. On this basis, we measured the survival rate, ROS and inflammatory cytokine production of the blank group cells exposed to PAHs standard solution only and the control group cells added with two different concentrations of ATX solution. The results of the experiments showed that there was no significant difference in the survival of the control cells after 24h of exposure as well as in the production of ROS and inflammatory cytokines compared to the blank group. On the contrary, significant differences were observed in the cell samples 48h after exposure in the control group cells compared to the blank group. This result suggests that the protective effect of ATX on cells has a lagging effect, that is, even in the control cells with ATX, the cells are still stimulated by PAHs to produce ROS and inflammatory cytokines, and then ATX reacts with the intermediates produced to reduce the damage caused by them, thus achieving the purpose of protecting the cells. Subsequent experimental results using ambient aerosol samples to verify the actual protective effect of ATX support this conjecture. Cells exposed to both aerosol samples showed a significant increase in survival with the addition of ATX solution and a significant decrease in intracellular ROS as well as in the expression of the inflammatory cytokines IL-6 and IL-8. However, the addition of ATX did not prevent the prior production of harmful intermediates by the exposed cells.

4.5 References

[1] W. Wang *et al.*, “Industrial Source Contributions and Health Risk Assessment of Fine Particle-Bound Polycyclic Aromatic Hydrocarbons (PAHs) during Spring and Late Summer in the Baoshan Area, Shanghai,” *Processes*, vol. 9, no. 11, p. 2016, Nov. 2021, doi: 10.3390/pr9112016.

[2] B. Fang *et al.*, “PM2.5-Bound Polycyclic Aromatic Hydrocarbons: Sources and

`

Health Risk during Non-Heating and Heating Periods (Tangshan, China)," *IJERPH*, vol. 17, no. 2, p. 483, Jan. 2020, doi: 10.3390/ijerph17020483.

[3] Y. Song, Y. Zhang, R. Li, W. Chen, C. K. A. Chung, and Z. Cai, "The cellular effects of PM2.5 collected in Chinese Taiyuan and Guangzhou and their associations with polycyclic aromatic hydrocarbons (PAHs), nitro-PAHs and hydroxy-PAHs," *Ecotoxicology and Environmental Safety*, vol. 191, p. 110225, Mar. 2020, doi: 10.1016/j.ecoenv.2020.110225.

[4] H. Wang *et al.*, "Cytotoxicity and inflammatory effects in human bronchial epithelial cells induced by polycyclic aromatic hydrocarbons mixture," *J Appl Toxicol*, vol. 41, no. 11, pp. 1803–1815, Nov. 2021, doi: 10.1002/jat.4164.

[5] N. Yamashita *et al.*, "Aryl hydrocarbon receptor counteracts pharmacological efficacy of doxorubicin via enhanced AKR1C3 expression in triple negative breast cancer cells," *Biochemical and Biophysical Research Communications*, vol. 516, no. 3, pp. 693–698, Aug. 2019, doi: 10.1016/j.bbrc.2019.06.119.

[6] C. F. A. Vogel, L. S. Van Winkle, C. Esser, and T. Haarmann-Stemmann, "The aryl hydrocarbon receptor as a target of environmental stressors – Implications for pollution mediated stress and inflammatory responses," *Redox Biology*, vol. 34, p. 101530, Jul. 2020, doi: 10.1016/j.redox.2020.101530.

[7] S. Marvanová *et al.*, "Benzo[b]naphtho[d]thiophenes and naphthylbenzo[b]thiophenes: Their aryl hydrocarbon receptor-mediated activities and environmental presence," *Science of The Total Environment*, vol. 879, p. 162924, Jun. 2023, doi: 10.1016/j.scitotenv.2023.162924.

[8] Y. Sun *et al.*, "Gas-PM2.5 partitioning, health risks, and sources of atmospheric PAHs in a northern China city: Impact of domestic heating," *Environmental Pollution*, vol. 313, p. 120156, Nov. 2022, doi: 10.1016/j.envpol.2022.120156.

[9] H. Xu *et al.*, "Inter-annual variability of wintertime PM 2.5 chemical composition in Xi'an, China: Evidences of changing source emissions," *Science of The Total Environment*, vol. 545–546, pp. 546–555, Mar. 2016, doi: 10.1016/j.scitotenv.2015.12.070.

[10] J. Wang *et al.*, "Effects of N-acetylcysteine on oxidative stress and inflammation reactions in a rat model of allergic rhinitis after PM2.5 exposure," *Biochemical and Biophysical Research Communications*, vol. 533, no. 3, pp. 275–281, Dec. 2020, doi: 10.1016/j.bbrc.2020.09.022.

[11] J. He *et al.*, "Environmental dose of 16 priority-controlled PAHs mixture induce damages of vascular endothelial cells involved in oxidative stress and inflammation," *Toxicology in Vitro*, vol. 79, p. 105296, Mar. 2022, doi: 10.1016/j.tiv.2021.105296.

[12] R.-E. Kim, C. Y. Shin, S.-H. Han, and K. J. Kwon, "Astaxanthin Suppresses PM2.5-Induced Neuroinflammation by Regulating Akt Phosphorylation in BV-2 Microglial Cells," *IJMS*, vol. 21, no. 19, p. 7227, Sep. 2020, doi: 10.3390/ijms21197227.

[13] M. Gao *et al.*, "Mitochondrial decay is involved in BaP-induced cervical damage,"

`

Free Radical Biology and Medicine, vol. 49, no. 11, pp. 1735–1745, Dec. 2010, doi: 10.1016/j.freeradbiomed.2010.09.003.

[14] Q. Bao, S. Zhao, Y. Liu, Y. Yao, J. You, and J. Xiong, "Benzo[b]fluoranthene induced oxidative stress and apoptosis in human airway epithelial cells via mitochondrial disruption," *J of Applied Toxicology*, vol. 43, no. 7, pp. 1083–1094, Jul. 2023, doi: 10.1002/jat.4445.

[15] W. Hill *et al.*, "Lung adenocarcinoma promotion by air pollutants," *Nature*, vol. 616, no. 7955, pp. 159–167, Apr. 2023, doi: 10.1038/s41586-023-05874-3.

[16] V. Sánchez-Martín *et al.*, "Protective Effect of Thyme and Chestnut Honeys Enriched with Bee Products against Benzo(a)pyrene-Induced DNA Damage," *IJERPH*, vol. 19, no. 24, p. 16969, Dec. 2022, doi: 10.3390/ijerph192416969.

[17] S. Bulanda and B. Janoszka, "Polycyclic Aromatic Hydrocarbons (PAHs) in Roasted Pork Meat and the Effect of Dried Fruits on PAH Content," *IJERPH*, vol. 20, no. 6, p. 4922, Mar. 2023, doi: 10.3390/ijerph20064922.

[18] M. Guerin, M. E. Huntley, and M. Olaizola, "Haematococcus astaxanthin: applications for human health and nutrition," *Trends in Biotechnology*, vol. 21, no. 5, pp. 210–216, May 2003, doi: 10.1016/S0167-7799(03)00078-7.

[19] S. Fakhri, F. Abbaszadeh, L. Dargahi, and M. Jorjani, "Astaxanthin: A mechanistic review on its biological activities and health benefits," *Pharmacological Research*, vol. 136, pp. 1–20, Oct. 2018, doi: 10.1016/j.phrs.2018.08.012.

[20] S. Yang, T. Zhang, J. Xu, X. Li, Q. Zhou, and C. Xue, "Chiral Separation and Analysis of Astaxanthin Stereoisomers in Biological Organisms by High-Performance Liquid Chromatography," *Food Science*, vol. 8, pp. 139–144, 2015, doi: 10.7506/spkx1002-6630-201508025.

[21] H. P. McNulty, J. Byun, S. F. Lockwood, R. F. Jacob, and R. P. Mason, "Differential effects of carotenoids on lipid peroxidation due to membrane interactions: X-ray diffraction analysis," *Biochimica et Biophysica Acta (BBA) - Biomembranes*, vol. 1768, no. 1, pp. 167–174, Jan. 2007, doi: 10.1016/j.bbamem.2006.09.010.

[22] R. Ambati, S.-M. Phang, S. Ravi, and R. Aswathanarayana, "Astaxanthin: Sources, Extraction, Stability, Biological Activities and Its Commercial Applications—A Review," *Marine Drugs*, vol. 12, no. 1, pp. 128–152, Jan. 2014, doi: 10.3390/md12010128.

[23] Y. M. A. Naguib, "Antioxidant Activities of Astaxanthin and Related Carotenoids," *J. Agric. Food Chem.*, vol. 48, no. 4, pp. 1150–1154, Apr. 2000, doi: 10.1021/jf991106k.

[24] A. Ranga Rao, R. L. Raghunath Reddy, V. Baskaran, R. Sarada, and G. A. Ravishankar, "Characterization of Microalgal Carotenoids by Mass Spectrometry and Their Bioavailability and Antioxidant Properties Elucidated in Rat Model," *J. Agric. Food Chem.*, vol. 58, no. 15, pp. 8553–8559, Aug. 2010, doi: 10.1021/jf101187k.

`

[25] J. S. Park, J. H. Chyun, Y. K. Kim, L. L. Line, and B. P. Chew, “Astaxanthin decreased oxidative stress and inflammation and enhanced immune response in humans,” *Nutr Metab (Lond)*, vol. 7, no. 1, p. 18, Dec. 2010, doi: 10.1186/1743-7075-7-18.

[26] B. Yin *et al.*, “Astaxanthin alleviates fine particulate matter ($PM_{2.5}$)-induced lung injury in rats by suppressing ferroptosis and apoptosis,” *Food Funct.*, vol. 14, no. 24, pp. 10841–10854, 2023, doi: 10.1039/D3FO03641C.

[27] X.-G. Cao, X.-X. Li, Y.-Z. Bao, N.-Z. Xing, and Y. Chen, “Responses of Human Lens Epithelial Cells to Quercetin and DMSO,” *Invest. Ophthalmol. Vis. Sci.*, vol. 48, no. 8, p. 3714, Aug. 2007, doi: 10.1167/iovs.06-1304.

[28] Y. Nishida, E. Yamashita, and W. Miki, “Quenching Activities of Common Hydrophilic and Lipophilic Antioxidants against Singlet Oxygen Using Chemiluminescence Detection System,” *Carotenoid Science*, vol. 11, pp. 16–20, 2007, doi: 10.11501/10996240.

[29] C. L. Quinlan, I. V. Perevoshchikova, M. Hey-Mogensen, A. L. Orr, and M. D. Brand, “Sites of reactive oxygen species generation by mitochondria oxidizing different substrates,” *Redox Biology*, vol. 1, no. 1, pp. 304–312, 2013, doi: 10.1016/j.redox.2013.04.005.

[30] Z.-W. Zhang, X.-C. Xu, T. Liu, and S. Yuan, “Mitochondrion-Permeable Antioxidants to Treat ROS-Burst-Mediated Acute Diseases,” *Oxidative Medicine and Cellular Longevity*, vol. 2016, pp. 1–10, 2016, doi: 10.1155/2016/6859523.

[31] S. Kim and H. Kim, “Inhibitory Effect of Astaxanthin on Oxidative Stress-Induced Mitochondrial Dysfunction-A Mini-Review,” *Nutrients*, vol. 10, no. 9, p. 1137, Aug. 2018, doi: 10.3390/nu10091137.

[32] H. Geng, Z. Meng, and Q. Zhang, “In vitro responses of rat alveolar macrophages to particle suspensions and water-soluble components of dust storm PM2.5,” *Toxicology in Vitro*, vol. 20, no. 5, pp. 575–584, Aug. 2006, doi: 10.1016/j.tiv.2005.09.015.

[33] E. Santa-Helena *et al.*, “From air to heart: Particle pollution (PM2.5) and induced injury on cardioblast cells,” *Atmospheric Pollution Research*, vol. 12, no. 4, pp. 152–159, Apr. 2021, doi: 10.1016/j.apr.2021.03.001.

[34] J. G. Joseph and A. P. Liu, “Mechanical Regulation of Endocytosis: New Insights and Recent Advances,” *Adv. Biosys.*, vol. 4, no. 5, p. 1900278, May 2020, doi: 10.1002/adbi.201900278.

[35] T. Harayama and H. Riezman, “Understanding the diversity of membrane lipid composition,” *Nat Rev Mol Cell Biol*, vol. 19, no. 5, pp. 281–296, May 2018, doi: 10.1038/nrm.2017.138.

[36] T. Wang *et al.*, “Astaxanthin protected against the adverse effects induced by diesel exhaust particulate matter via improving membrane stability and anti-oxidative property,” *Journal of Hazardous Materials*, vol. 456, p. 131684, Aug. 2023, doi: 10.1016/j.jhazmat.2023.131684.

`

`

Chapter 5: Characterization of elemental compositions and valence states of cyclone-collected aerosol particles using EDXRF and XAFS at three sites in Japan

This chapter is based on the manuscript submitted for publication in Asian Journal of Atmospheric Environment (AJAE) (Jing W.D., Saito K., Sugimoto K., Okamoto T., Saito H., Nishita-Hara C., Hara K., Hayashi M., Hasegawa S., Okuda T. Characterization of elemental compositions and valence states of cyclone-collected aerosol particles using EDXRF and XAFS at three sites in Japan, accepted on 29 March 2022 [1]) with some addition. This study aims to verify the feasibility of EXDRF and XAFS method in detecting the concentration and valence composition of metal components in cyclone-collected powder form aerosol samples. The rapid detection of metal concentration and valence state in cyclone samples can be used in subsequent research to explore the role of changes in metal valence states in particulate matter in the degradation/photooxidation of PAHs on PM surface.

5.1 Introduction

Particulate matter (PM) pollution is a serious issue worldwide. $PM_{2.5}$ (particle diameter < 2.5μm) contributed to more than 4.3 million premature deaths worldwide in 2015 [2]. Exposure to high PM concentrations can cause adverse health effects including decreased lung function and cardiovascular and respiratory diseases [3]–[5].

Metals are important components in PM that can produce reactive oxygen species (ROS) including hydroxyl radicals in vivo, which are more toxic and cause pro-oxidant and proinflammatory effects on the respiratory system [6]–[8]. The biological toxicity and carcinogenicity of heavy metals can vary for different valence states. For example, Cr(III) poses little or no threat to human health, while Cr(VI) is toxic and potentially carcinogenic [9], [10]. Vanadium(V) species (e.g., V_2O_5) are particularly toxic and have mutagenic effects. Cohen et al. [11] compared several forms of vanadium and

`

demonstrated that the vanadate [V(V)] species had the greatest biological effects. Therefore, the valence states of metals should also be measured in addition to the metal concentrations in PM samples. In this study, we used energy-dispersive X-ray fluorescence (EDXRF) to analyze element concentrations in atmospheric PM, which allows rapid and non-destructive detection for elements concentration in a sample, and X-ray absorption fine structure (XAFS) spectroscopy, X-ray absorption near-edge structure (XANES) spectra mainly, to analyze the valence states of target metals in the PM samples [12]–[14].

Previous studies typically collected PM samples using filters made from different materials (such as quartz fiber or PTFE) with a low/high volume air sampler [15]–[17]. However, in vivo / in vitro studies that used filters to collect PM may not reflect realistic biological reactions of health effects. Firstly, high volume sampler, which is widely used for filter-samples collection, doesn't offer the separation collection of gas and particle-phase in general, gaseous compounds may be adsorbed to quartz fiber filters, thus resulting in a positive bias in the measured particle-phase concentration [18], [19]. The study pointed that volatile organics may adsorb onto filter materials in the high volume sampler and undergo subsequent on-filter oxidation and sulfation resulting in the formation of both organic acids and organosulfates [20]. Additionally, the extraction of $PM_{2.5}$ collected by filters can alter particle properties. There are potential extraction artifacts such as compositional biases in the extracted PM, volatilization losses, and contamination with filter material [21], [22]. Besides, particles collected and entangled in the filters are difficult to be removed without contaminating by the filter materials, and thus not suited for the following exposure experiments. Therefore, powder samples collected using a cyclone without filters are superior to aerosol samples adsorbed on a filter for studying cellular exposure and PM toxicity.

Cyclonic separation with an impactor enables the collection of $PM_{2.5}$ in “powder form” [23]–[25]. PM is classified by an impactor, enters the cyclone device, and is collected at an inner wall of the cyclone and an attached bottle. Honda et al. [26] studied

`

the performance of two kinds of particles collected by cyclonic separation and filtration methods in cell exposure experiments. $PM_{2.5}$ collected using cyclonic separation has more significant effects for secreting of interleukins 6 and 8 (IL-6, IL-8) from airway epithelial cells, and expressing of the cluster of differentiation 86 (CD86) and dendritic and epithelial cells 205 (DEC 205) on antigen-presenting cells, comparing with the effects of filter-collected $PM_{2.5}$. Besides, powder samples collected by cyclone increased inflammatory cytokine levels and induced lung inflammation in vivo. The results suggested that crude $PM_{2.5}$ collected using cyclonic separation caused stronger biological responses than filter-collected $PM_{2.5}$. It was possibly due to the co-existence of particles in the exposure experiment had a significant effect rather than the exposure of extracts of particles without particles themselves. Another study compared the cytotoxicity and inflammatory potential of $PM_{2.5}$ collected by a cyclone from three Asian cities, by measuring cytokines such as interleukin (IL)-6 and IL-8 [27]. Ogino et al. [28], [29] administered a mixture of powder particles and saline intranasally to NC/Nga mice for five consecutive days, collected bronchoalveolar lavage fluid (BALF) from the mice, and analyzed them for airway hyperresponsiveness (AHR). The studies showed that $PM_{2.5}$ increased AHR and cell numbers of eosinophils in BALF, and that $PM_{2.5}$ collected by the cyclone system could induce asthma-like airway inflammation. A recent study analyzed lung sections of mice that underwent tracheal injection of particles in a crude PM dispersion liquid [30]. The results showed that PM exposure increased the expression of angiotensin-converting enzyme 2 (ACE2) and transmembrane protease serine-type 2 (TMPRSS2) in alveolar cells and macrophages, which are required for the entry of severe acute respiratory syndrome coronavirus 2 (SARS-CoV-2) into host cells, thereby demonstrating that PM exposure may adversely affect the manifestation and progression of COVID-19. These studies have shown that powder particles collected by the cyclone have better operability than filtration in cell exposure experiments and in vivo experiments.

Another advantage of cyclone-collected aerosol particles is that the pelletized

`

powder form of particles is suitable for XAFS analysis. In contrast, aerosol particles layer on the filter which collected by filtration method would be too thin that it is difficult to obtain amount of XAFS signals relative to the background noise [14].

The objectives of this research were to (i) measure the content of metal elements in powder aerosol samples of different sizes collected by a cyclone using EDXRF; (ii) understand the characteristics of the valence states of target metals by XAFS, and (iii) identify the sources of target metals at three sampling sites in Japan based on the source identification models. These results can provide more detailed information for understanding the correlation between the contamination properties of heavy metals in atmospheric PM samples and their oxidation potential in further cell exposure experiments.

5.2 Experimental

5.2.1 Sample collection

We collected aerosol samples at three sites in Japan: Fukuoka University (FU), Keio University (KO), and the Center of Environmental Science in Saitama (SA). **Fig. 5.1** shows the locations of the sites. Fukuoka University (33.550°N, 130.364°E) is in Fukuoka Prefecture in southwestern Japan, which is close to the East Asian continent. This unique location is suitable for observing the effects of long-range transport on air pollution. Keio University (35.555°N, 139.656°E) is located in Kanagawa Prefecture on the east coast of mainland Japan. Kanagawa Prefecture is part of the Tokyo metropolitan area, has the largest port in the country, and is one of the four major industrial zones in Japan. The Center of Environmental Science in Saitama (CESS) (36.086°N, 139.560°E) is in an inland area with high agricultural and industrial production. These three sampling sites have different sources of air pollutants due to different geographical locations and industrial activities.

We used a high-flow simultaneous sampling system that combined the virtual impactor and cyclone to collect atmospheric PM at a flow rate of 1,200 L/min. Particles

`

with diameters smaller than 2.5 μm were classified as fine particles (PF) and particles with diameters larger than 2.5 μm were classified as coarse particles (PC). Details of the particle collection instrument are provided in our previous studies [23], [25]. **Table 5.1** shows the mass of PM during the sampling period and the meteorological conditions (JMA, 2021) at the sampling sites.

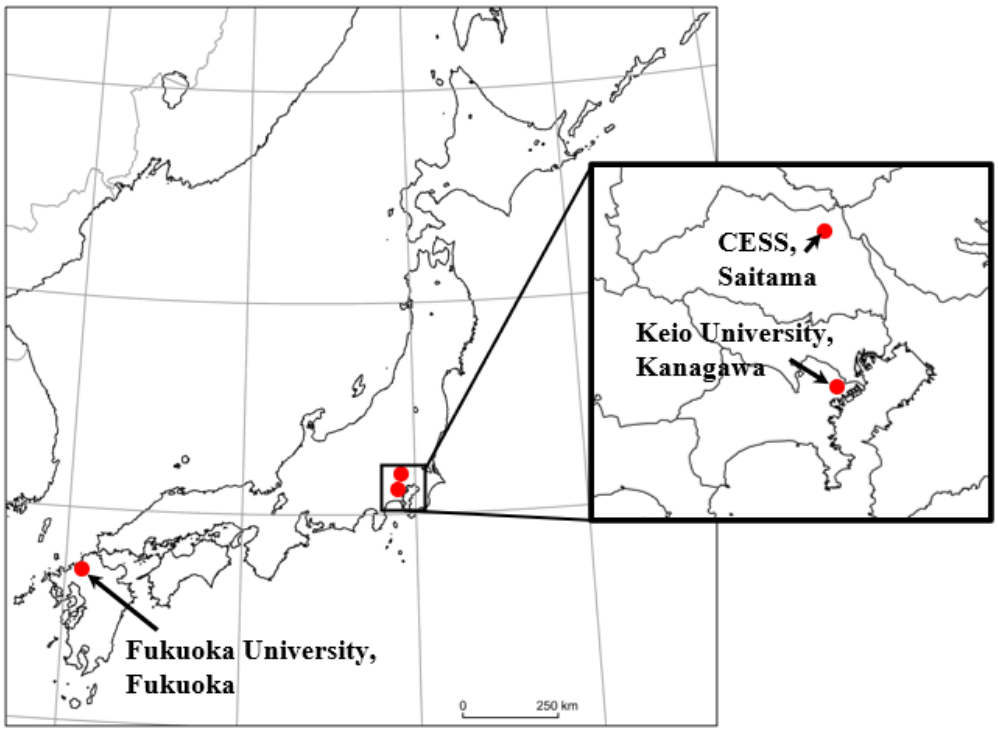


Fig. 5.1 Location map of sampling sites

5.2.2 EDXRF analysis

We measured element concentrations in the atmospheric PM by using an EDXRF analyzer (EDXL 300, Rigaku Corp., Japan) [25], [31] with a solid-state detector (SSD). The 20 mg of powder samples mixed with 300 mg of cellulose were pressed into pellets of Φ13 mm × 0.5 mmt by 50 kN pressure for testing. Standard material of urban aerosol particles (CRM#28) with known metal contents was also pelleted and analyzed for calibration. The pelletized samples were analyzed by EDXRF in approximately 1 Pa of vacuum, and the analysis time was 15 min per a sample. The quantification was achieved with a fundamental parameter coupled with O-Balance method. The ratio of measured and certified values for each element (n=5) was generally in the range of 0.8-

1.2, and measurement precision, represented as the coefficient of variation (=standard deviation / mean), was less than 20% [25].

`

Table 5.1 Amount of collected particles and meteorological data during the sampling period for three sampling sites

	Date	Season	Volume (m^3)	Fine particles (mg)	Coarse particles (mg)	Total rainfall [a] (mm)	Average relative humidity (%)	Average sunshine duration (h)
Kanagawa (KO)	2/15~3/10	Winter	42648.0	434.0	619.2	26.5 (2/16-3/10)	56.4	5.8
	5/10~6/06	Spring	51614.2	238.0	267.3	97.5 (5/11-6/5)	70.8	10.9
	7/14~8/07	Summer	47068.5	115.4	105.3	176 (7/16-8/10)	65.6	4.1
	10/18~11/16	Autumn	56424.1	172.5	75.4	446 (10/16-11/15)	74.5	4.7
Saitama (SA)	2/17~3/15	Winter	49054.6	290.4	212.9	13.5 (2/16-3/15)	46.0	6.3
	5/10~6/06	Spring	50639	200.4	133.5	50.5 (5/11-6/5)	62.6	7.3
	7/14~8/07	Summer	44848.6	95.8	54.1	69.0 (7/16-8/10)	74.8	3.6
	10/20~11/15	Autumn	48454.2	148.7	118.5	323 (10/21-11/15)	67.6	5.7
Fukuoka (FU)	2/16~3/21	Winter	61613.2	182.5	92	42.0 (2/16-3/20)	59.9	5.6
	5/11~6/08	Spring	52442.5	167.7	136.8	65.5 (5/11-6/10)	63.8	9.1
	7/21~8/17	Summer	50631.3	97.5	55.5	53.5 (7/21-8/15)	75.6	8.3
	10/19~11/16	Autumn	52280.6	195.8	55.4	65.5 (10/21-11/15)	69.6	6.1

All meteorological data were obtained from JMA, 2021. For KO, rainfall data were from the Hiyoshi monitoring station, while relative humidity and sunshine duration data were from Yokohama station. For SA, rainfall and sunshine duration data were from Kuki station, and relative humidity was from Kumagaya station. For FU, meteorological data were from Fukuoka station.

[a] The date in parentheses indicates the statistical date of the station.

5.2.3 XAFS spectra analysis

We mainly used XANES to probe the valence states of the absorbing atoms, which were measured at the Kyushu Synchrotron Light Research Center (SAGA-LS) using

`

Beam Line 11 (BL-11). This ensured the quality of the continuous spectrum by performing the XAFS measurement on synchrotron radiation [14]. The valence states of target metals in the PC sample collected in the winter at FU could not be determined, as a large proportion of this sample was used for other experiments and the remaining amount was not enough.

XANES is a fine structure in the absorption spectrum that appears in the narrower energy range (−10 eV to +40 eV) near the absorption edge. Absorbance increases sharply at a certain energy value in the XAFS spectrum, which is referred to as the absorption edge. In this study, the midpoint of the rising edge of the absorption peak was uniformly defined as the absorption edge of the samples, while the pre-edge and post-edge lines were drawn with the energy range of −150 eV to +30 eV with the absorption edge as the center point. The absorbance on the pre-edge line was 0 ($E_0 = 0$), and the absorbance on the post-edge line was 1 ($E_1 = 1$). The absorption peak was located above the post-edge line, so its absorbance was greater than 1.

Metallic standard compounds (Mn, MnO, MnO_2, Fe, FeO, Fe_3O_4, Fe_2O_3(α, γ), FeOOH, Cu, Cu_2O, CuO, $CuCl_2$, $CuSO_4$, CuS, Zn, ZnO, $Zn(OH)_2$, $ZnFe_2O_4$, $ZnSO_4$, and $Zn(NO_3)_2$) were used to carry out the chemical speciation for each metallic compound by using the linear combination fitting (LCF) method. Each standard compound was mixed well with boron nitride (BN) for 20 min in a mortar, then it was pressed into a pellet similar as the aerosol samples. For XAFS spectra analysis, we measured the XAFS spectra of the standards substances with the different valence of the target metal at first, and then performed a linear fit using the least-squares method after obtaining the XAFS spectra of the target elements in the sample to calculate the valence ratio of the target metal in the sample. Normalization of the experimental data and the linear fitting calculation using the least-squares method for valence ratio were done using Athena software (ver. 0.9.26), and the detailed procedures are described in a previous paper [14]. The R-factors, which were generally used for the evaluation of fitting results, ranged 0.01-0.06 for Mn (except for SA-winter-PC, 0.28), smaller than

`

0.002 for Fe, 0.002-0.007 for Cu, and 0.002-0.02 for Zn. For Zn speciation, since the spectra for ZnO and $Zn(OH)_2$, and also $ZnSO_4$ and $Zn(NO_3)_2$, were very similar, we used only Zn, ZnO, $ZnFe_2O_4$, and $ZnSO_4$ for the LCF analysis.

5.2.4 Indices of source identification

Enrichment factors (EFs) were used to evaluate the air quality in terms of heavy metals and indicate the contribution of anthropogenic emissions to the atmosphere. Here, EFs are defined as

$$EF = \frac{C_i^{PM}/C_X^{PM}}{C_i^{crust}/C_X^{crust}} \quad (5.1)$$

where C_i^{PM} is the concentration of element i in the PM samples, and C_X^{PM} is the concentration of X as a reference element in the PM samples. C_X^{crust} indicates the assumption that the dominant source of X in PM originated from the natural crust. C_i^{crust} is the average elemental concentration in the crust. In this equation, we used the average chemical profile of continental crust data from Taylor [32] and chose Ti as the reference element instead of Al because the source of Ti in aerosol samples is more stable and Al is influenced by anthropogenic emissions. An EF of <10 suggests that crustal sources are mainly natural, and an EF of >10 suggests strong enrichment from non-crustal sources [33], [34].

Principal component analysis (PCA) was used to identify likely sources of the metallic elements. We normalized all data using the *z*-score method before analysis, and we rejected factors that contributed less than 5% to the variance.

Cluster analysis (CA) was used to indicate the potential emitting sources of the different metals in the samples detected by EDXRF and XAFS. We combined CA and PCA results for greater confidence in the source identification. The grouping of CA results was chosen on the base of a dendrogram using the average linkage method with Euclidean distances. We used Origin software (version: OriginPro 2018C) to perform these analyses.

`

5.3 Results and discussion

5.3.1 Metallic element concentration in aerosol particles

Table 5.2 presents the concentrations of nine metallic elements in aerosol particles detected by EDXRF. Note that all data were expressed in the mass concentration (μg/g) in the original aerosol particles. The concentration of Ti ranged between 1062 and 3781 μg/g in KO, between 652 and 4172 μg/g in SA, and between 246 and 1681 μg/g in FU. In terms of seasonal variations, the concentration of Ti in all samples, except for PF collected in KO, tended to be higher in winter and spring and lower in summer and autumn. The concentrations of V and Ni were more constant, with overall average concentrations of 62 and 63 μg/g, respectively. The overall average concentration of Pb in KO samples (158.8 μg/g) were much higher than in SA and FU samples (59.3 and 69.6 μg/g). The characteristic concentration distributions of V, Ni, and Pb in the different sized particles were similar, higher in PF compared with PC in samples from SA and FU, while we observed the opposite in the KO samples.

Cr, Cu, and Mn are highly related elements with oxidative potential, which is a measure for the toxicity of atmospheric PM [35]–[37]. Fe and Zn also have a relatively high association with oxidation capacity [7], [38], [39], and they were present at relatively high atmospheric concentrations (**Table 5.2**). Therefore, we selected these five elements as the target elements to further investigate their pollution properties and chemical characteristics.

5.3.1.1 Cr

The concentration of Cr in PC and PF collected in KO and FU was constant, with averages of 114 ± 42 μg/g and 50 ± 32 μg/g in all samples from the two locations, respectively. In contrast, the concentration of Cr in PF collected in SA in summer reached 1033 μg/g, which was much higher than in the other samples. The high Cr concentration may have resulted from local emissions during the sampling period. Comparison of the results of other samples showed that the concentration of Cr was not

`

higher in PF than in PC. Therefore, this high concentration of Cr was irregular, and the data from this sampling time was removed in subsequent analyses.

5.3.1.2 Mn

The concentrations of Mn in the samples from KO ranged between 399 and 1327 μg/g and were close to the soil background value (950 μg/g). Mn concentrations in SA and KO samples were similar, but the particle size distributions were different. In KO samples, Mn concentration was higher in PC than in PF, while the opposite was observed in SA samples. Additionally, Mn concentrations for the two particle sizes from both SA and KO were high in winter and spring. Mn concentration was even lower in samples from FU than in those from KO and SA during the same sampling period, especially in samples collected in summer (77.3 μg/g in PF and 59.4 μg/g in PC). Note that not only Mn but the other crustal elements such as Ti was also low in the concentration in aerosol samples collected in summer in FU.

5.3.1.3 Fe

The average concentration of Fe was the highest among the nine metallic elements across the three sites. Fe concentration was the highest in samples from KO (25114 μg/g), followed by SA (17330 μg/g) and FU (7683 μg/g). For samples from the same location, Fe concentration showed trends similar as those of Mn for both particle sizes and particle size concentration distributions.

5.3.1.4 Cu

Cu concentrations in all samples were relatively low except in PC of KO samples (713.6 μg/g on average). Cu concentrations were comparable in PC and PF in SA (203.2 vs. 131.7 μg/g) and FU samples (101 vs. 50.5 μg/g), while there were large differences for KO samples. Cu concentrations in the rest of the samples were higher in winter and spring, except for PF in KO samples.

`

5.3.1.5 Zn

Zn concentrations in PC and PF from KO samples were considerably different. Trend in Zn concentration was similar as that in Mn, Fe, and Cu. Zn concentration in PC from KO was high (3443 μg/g) compared with other samples from SA and FU (497 and 235 μg/g, respectively).

`

Table 5.2 Concentrations of heavy elements in aerosol particles detected by EDXRF (unit: μg/g)

			Ti	V	Cr	Mn	Fe	Ni	Cu	Zn	Pb
KO	Fine	Winter	2809	72.7	104	677	29142	62.9	264	859	58.4
	particles	Spring	1139	67.9	52.5	405	13773	43.2	152	567	51.4
		Summer	1215	89.7	114	413	14641	57.2	201	565	53.6
		Autumn	1494	74.9	102	519	17545	53.7	274	804	74.1
	Average		1664	76.3	93.1	503	18775	54.3	223	699	59.4
	EF		1.0	1.5	2.5	1.4	1.0	1.9	**10.7**	**26.4**	**12.1**
	Coarse	Winter	3227	102	154	866	38160	49.8	642	1710	140
	particles	Spring	3781	128	185	1327	53679	134	1279	7351	593
		Summer	1062	48.2	76.5	399	13966	32.6	403	3204	175
		Autumn	1749	85.1	126	555	20009	44.9	531	1507	126
	Average		2455	90.8	135	787	31453	65.3	714	3443	258
	EF		1.0	1.2	2.4	1.5	1.1	1.6	**23.3**	**88.2**	**35.6**
SA	Fine	Winter	2523	69.9	125	616	25277	64.2	162	896	81.3
	particles	Spring	4172	150	153	1171	44795	92.6	450	2064	178
		Summer	791	47.7	1033	289	10649	388	92.2	303	28.4
		Autumn	1342	27.2	323	473	10225	111	109	578	42.6
	Average		2207	73.6	200	637	22737	164	203	960	82.5
	EF		1.0	1.1	8.1[a]	1.3	1.0	4.4	7.4	**27.4**	**12.7**
	Coarse	Winter	1519	40.6	71.8	385	14011	21.0	160	447	27.9
	particles	Spring	1903	51.9	59.7	493	20370	41.2	155	865	75.1
		Summer	652	25.5	40.1	146	5425	11.2	94.2	258	15.8
		Autumn	1024	23.0	48.6	344	7884	17.6	118	418	25.2
	Average		1275	35.2	55.1	342	11922	22.7	132	497	36.0
	EF		1.0	0.9	1.9	1.2	0.8	1.1	8.3	**24.5**	9.6

Table 2 (Continued)

			Ti	V	Cr	Mn	Fe	Ni	Cu	Zn	Pb
FU	Fine	Winter	1357	85.3	86.9	438	13757	74.7	211	1142	241
	particles	Spring	1681	59.9	105	393	15933	74.1	105	559	94.8
		Summer	246	35.7	32.7	77.3	2195	17.6	34.0	225	36.8
		Autumn	484	20.4	31.2	87.7	4601	9.6	54.0	144	18.9
	Average		942	50.3	63.9	249	9121	44.0	101	518	98.0
	EF		1.0	1.7	3.0	1.2	0.9	2.7	8.6	**34.5**	**35.2**
	Coarse	Winter	-	-	-	-	-	-	-	-	-
	particles	Spring	1308	47.9	37.9	280	12548	28.8	85.7	327	55.3
		Summer	276	25.5	26.7	59.4	2313	6.9	25.5	152	17.9
		Autumn	420	35.7	32.4	103	3874	17.6	40.2	225	50.5
	Average		668	36.4	32.4	147	6245	17.8	50.5	235	41.2
	EF		1.0	1.8	2.1	1.0	0.8	1.6	6.1	**22.1**	**20.9**

All data were expressed in the mass concentration (μg/g) in the original aerosol particles.

- Not analyzed.

[a] Irregular data were eliminated during the calculation of EF for Cr in SA PF samples.

5.3.2 Valence state of target elements

The XAFS spectra for the standard materials, representative aerosol samples, and corresponding LCF results are shown in **Fig. 5.2**. The percentages of different valence states of target metals detected by XAFS are shown in **Fig. 5.3**. We only examined the valence states of Mn, Fe, Cu, and Zn, as those of Cr were explored in our previous study [14].

5.3.2.1 Mn

Mn (II) was the major component in all aerosol samples at averages of 60.9%, 73.8%, and 85.1% for KO, SA, and FU, respectively. Mn (0) was detected in some PC samples from KO and SA at under 10%. Mn (IV) accounted for a relatively large proportion of aerosol samples collected in KO and SA (37.6% and 25.8% on average), especially in samples collected in winter. These results were generally consistent with a previous study that reported the oxidation state of Mn in the aerosol or road dust samples were approximately 2.2-2.6 [40], [41].

5.3.2.2 Fe

The major valence state of Fe in the aerosol samples was Fe(III). The average proportions of Fe(III) in KO, SA, and FU samples were 70.4% (n = 8), 79.8% (n = 8), and 86.7% (n = 7), respectively. There was more Fe(II) in KO samples (23.5% average) than in SA samples (12.9% average) and FU samples (8.4% average). Fe(III) concentration was the highest but Fe(II) concentration was the lowest in FU samples. This may be because Fe(II), which was more reactive valence state than Fe(III), was oxidized during the long-range transport from the Asian continent. In contrast, there was more Fe(II) in SA and KO samples due to greater local emissions of aerosol particles containing Fe. Moreover, Fe(0) was not detected in five samples including PF from KO in autumn and PC from SA in spring. Fe(II) was not detected in PC from SA in summer and PF from FU in autumn.

`

5.3.2.3 Cu

Cu(II) was the main component of the particles at all locations and sizes. The average percentage of Cu(II) was 92.1% in KO, 88.0% in SA, and 99.4% in FU. The proportion of Cu(0) was larger in PC at KO (13.6% average) and SA (14.4% average), and it was only detected in PF from all FU samples collected in autumn. Cu(I) was not detected in any sample.

5.3.2.4 Zn

Zn(II) was the major chemical valance of Zn in all samples (98.8% in KO, 99.4% in SA, and 97.2% in FU). Chemical speciation results for Zn are presented in **Fig. 5.3**. The major Zn components were $ZnFe_2O_4$ and $ZnSO_4$. The proportion of $ZnFe_2O_4$ was higher than $ZnSO_4$ in all samples (54% vs 31.3% on average) except the fine particles collected in FU site (26.7% vs 65.3% on average). In addition, ZnO existed in all samples except the fine samples collected in spring and summer at FU but at a low amount (12.3% on average). Zn(0) was detected only in some particles and the average proportion in FU samples were three times than others (2.8% to 0.9%). Overall, the Zn chemical speciation results for FU were unique. Note that when we changed $ZnSO_4$ to $Zn(NO_3)_2$ as the standard spectrum for the LCF analysis, the result was very similar to the original result.

`

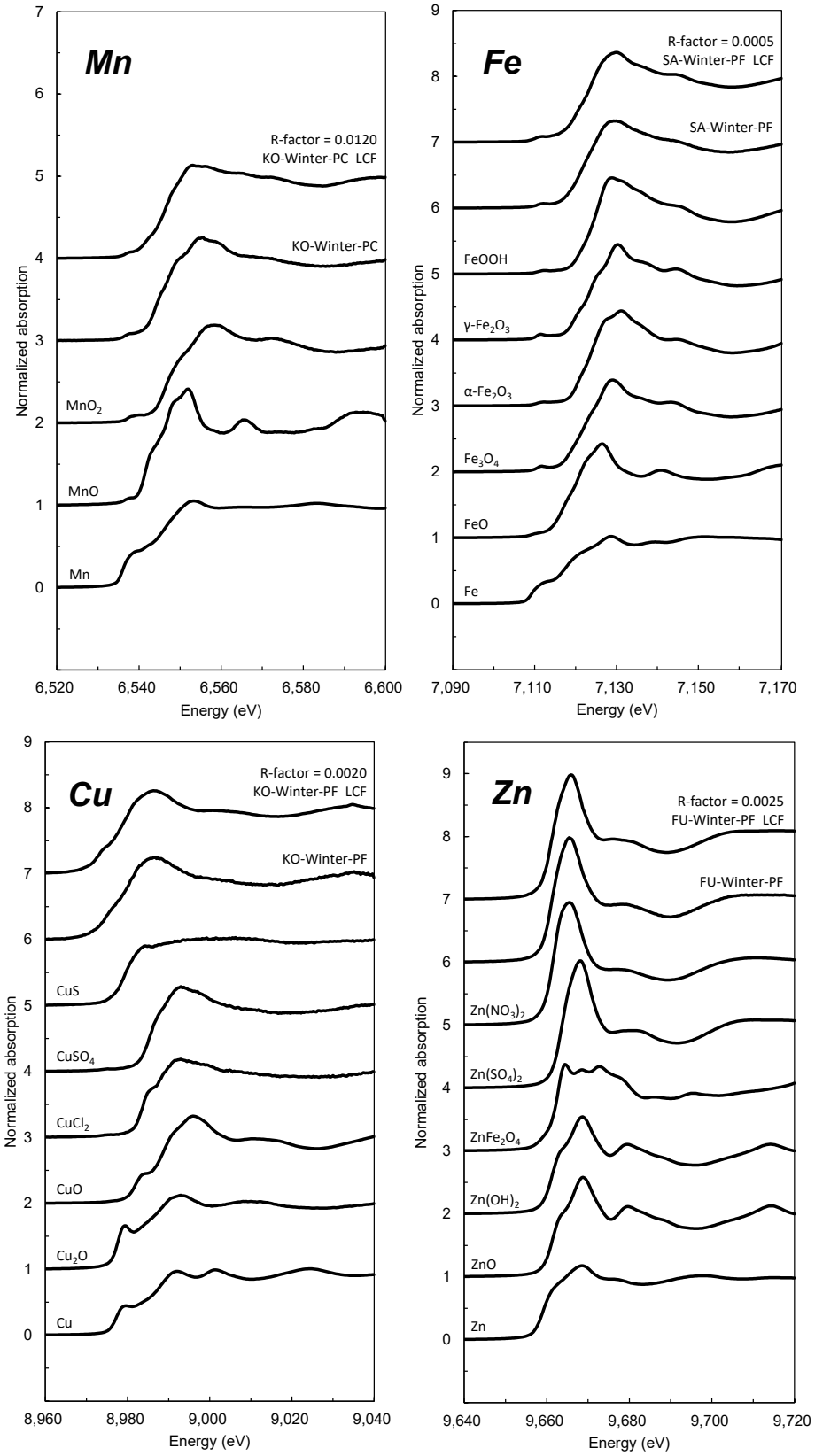


Fig. 5.2 The XAFS spectra of each element for the standard materials, representative aerosol samples, and corresponding linear combination fitting (LCF) results

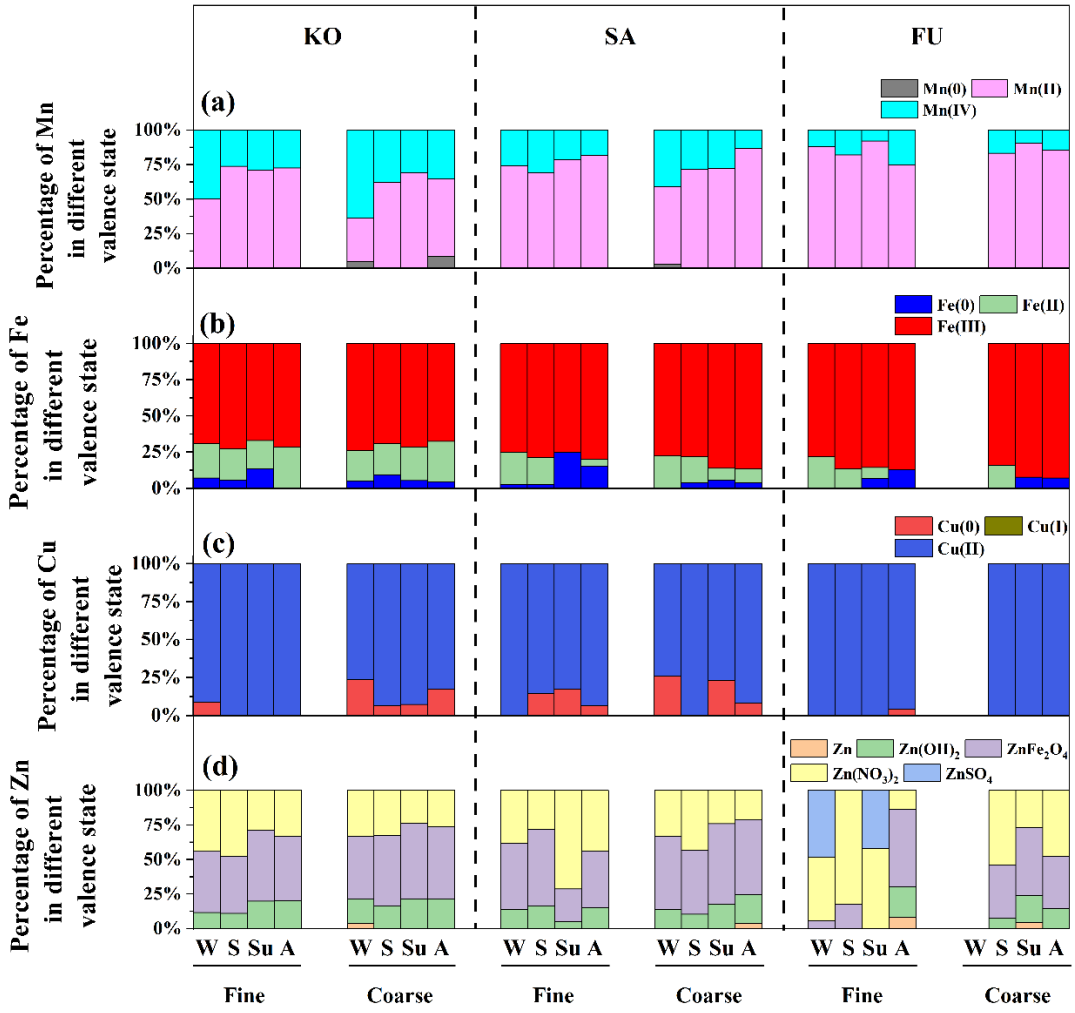


Fig. 5.3 Percentage composition of different valence states of target metals in fine and coarse particles at three sites

5.3.3 Source identification

EFs, correlation analysis, PCA, and CA were applied to identify the potential sources of metallic elements in aerosol samples from three sampling sites.

5.3.3.1 Enrichment factors (EFs)

EFs for metals in the particle samples were calculated by using the average concentrations to investigate the potential sources of metallic elements that were emitted from natural or anthropogenic sources. The results are summarized in **Table 5.2**.

The results showed that Ti, V, Cr, Mn, Fe, and Ni had EF values in the range of 0.8-

4.4, which suggests that these metals were derived from crustal contribution and part of anthropogenic influences. The EFs of Zn were higher than 10 in all samples at three sites. The values of Pb were also higher than 10 in all samples except for PC collected in the SA site. The EF values of Cu in the KO samples are also higher than 10 and those in the other two sampling sites are also much higher than the reference values as crustal sources. This suggests that the contribution of soil to these elements was much smaller than those of anthropogenic sources. Pb has been used in marker compounds for coal combustion and non-ferrous metal smelters [34], [42]. Additionally, the presence of Pb in atmospheric air is related to vehicular and industrial emissions (i.e., burning of fossil fuels) [43], [44]. Xu et al. [45] listed vehicular emissions as one of the main sources of Pb in the environment of Xi'an, China, even after the use of Pb-containing gasoline was prohibited. Zn is used to make automotive brakes and tire rubber (which contains 1% Zn as it acts an activation agent for the sulfurization of rubber), and Zn is also added to automobile engine oil [46], [47].

5.3.3.2 Correlation analysis

Fig. 5.3 shows the XAFS results on the valence states of the five trace metals in aerosol particles. The concentration of each valence state was calculated from its percentage and the total metal concentration from **Table 5.2**. These values were used in a correlation analysis to investigate the potential emission sources of aerosol particles at the three sites (**Table 5.3**). *Z*-score normalization was applied to all data to standardize different magnitudes into a uniform measure before correlation analysis. In addition, *t*-tests were performed to determine the statistical significance of the correlation analysis results (**Table 5.3**) to reduce calculation errors from the small number of samples (n = 4). Correlations between an element and its valence states are not discussed as they are not independent, since valence state concentrations were calculated using the element concentrations and valence state percentages.

The concentration of Cr in PF in summer SA samples may be anomalous, as

`

previously discussed. Therefore, we excluded the data for this sampling period to keep the data constant when performing the correlation analysis between Cr and other elements. These correlation coefficients are indicated in Table 3b by a gray background. However, these correlation coefficients are less accurate (e.g., R^2 = 1.000 between Cr(III) and Mn) because of the reduced sample size and will not be used for source analysis. Similarly, the correlation analysis of elements in FU PC samples was excluded because of the lack of EDXRF and XAFS data on FU PC samples collected in winter.

As shown in **Table 5.3**, there were significant correlations between Mn(IV) and Ti, and the correlation between Fe(II) and Fe(III) with Ti and Mn for all samples. Ti, Mn, and Fe are all typical crustal enrichment elements, and the EFs for both Mn and Fe were close to 1 (**Table 2**), which indicates that Mn and Fe mainly originated from the soil. There is research pointed that small-sized particles were emitted from vehicle exhausts as the result of engine combustion [48], and Lu et al. [49] stated that the principal source of Mn and Pb in street dust is automotive emissions. Therefore, the high correlations between Mn with Cu, Zn, and Pb in SA fine particles indicated that automotive emissions might be one anthropogenic source of Mn.

Zn is the largest metallic portion emitted from electric arc furnace dust, which can reach 7%-40% of total metal emissions. Vapor zinc is emitted out from the furnace as compounds like ZnO and $ZnFe_2O_4$ with other gaseous or particulate compounds generated during steelmaking reactions [50], while Mn is derived from franklinite ((Zn, Mn^{2+}, Fe^{2+}) (Fe^{3+}, Mn^{3+})$_2O_4$), and Cr is richer in the dust from stainless steelmaking than in that from carbon steelmaking [51], [52]. Manno et al. [53] stated that heavy metals such as Zn and Ni are highly abundant in urban areas and industrial sites, and major sources of V have been identified as combustion of residual fuel such as ships and refinery plants [54]–[56]. Therefore, the strong correlations between Zn, Mn, Fe, and Cr with Ni (R^2 = 0.8006-0.9752, p<0.05) and V (R^2 = 0.8143-0.9648, p<0.05) in aerosol particles at KO and FU sites indicates that they were likely emitted from industrial production in the Keihin and Kitakyushu industrial areas, where also are

`

important ports.

Cu and Zn are known as wear-generating elements, as Cu can be emitted from the wear of engine parts, fuel, and oil leakage [57], [58], while Zn can be derived from tire abrasion, brake wear, and corrosion of vehicle parts [59]. Previously deposited Pb in the soil may be re-suspended in road dust [60]–[64]. This explains the significant correlations between Cu(II), Zn(II), and Pb. Furthermore, a previous chemical characterization study of brake wear particles showed that Fe existed in both fine and coarse fractions, while TEM analysis revealed the presence of maghemite (γ-Fe_2O_3), magnetite (FeO-Fe_2O_3), and amorphous carbon in the nanoparticle fraction, as well as maghemite, magnetite, and hematite (α-Fe_2O_3) in the fine fraction [47]. Hence, the Fe produced by brake wear emissions from cars is mainly in the form of compounds. However, the correlation between Fe(II) and Fe(III) with Zn and Cu was not statistically significant due to the limitation of sample numbers in this study, so this anthropogenic contribution of Fe deserves further investigation.

`

Table 5.3 Pearson correlation analysis of valence state concentrations for different particle size samples

a. KO

Fine particles	Cr(0)	Cr(III)	Mn(II)	Mn(IV)	Fe(0)	Fe (II)	Fe (III)	Cu (II)	Zn(II)
Ti	**0.952***	0.091	0.401	**0.998****	0.461	0.945	**0.996****	0.483	0.816
V	-0.125	0.816	-0.298	-0.228	0.445	-0.348	-0.306	0.110	-0.320
Cr	0.328	**0.958***	0.312	0.351	0.397	0.356	0.328	0.699	0.406
Mn	0.858	0.158	0.598	**0.957***	0.272	**0.994****	**0.987***	0.647	0.926
Fe	0.943	0.112	0.428	**0.996****	0.442	**0.953***	**0.997****	0.511	0.833
Ni	0.742	0.702	0.309	0.751	0.610	0.681	0.717	0.647	0.623
Cu	0.425	0.608	0.870	0.600	-0.076	0.806	0.671	**0.981***	0.913
Zn	0.601	0.247	0.856	0.778	-0.075	**0.958***	0.855	0.841	**1.000****
Pb	-0.163	0.446	0.949	0.071	-0.641	0.436	0.198	0.884	0.675
Coarse particles									
Ti	0.843	0.860	0.690	**0.957***	0.861	**0.968***	**0.988***	0.780	0.532
V	0.861	0.924	0.747	0.853	0.854	**0.980***	0.936	0.817	0.533
Cr	0.876	0.910	0.725	0.873	0.844	**0.977***	0.941	0.800	0.511
Mn	0.684	**0.962***	0.874	0.837	**0.971***	**0.991****	**0.981***	0.931	0.751
Fe	0.734	0.923	0.811	0.897	0.943	**0.987***	**0.997****	0.882	0.686
Ni	0.439	**0.979***	**0.988***	0.594	**0.983***	0.909	0.855	**0.999****	0.906
Cu	0.522	**0.988***	**0.967***	0.673	**0.991****	0.947	0.903	**0.992****	0.869
Zn	0.045	0.802	0.948	0.338	0.890	0.679	0.655	0.923	**1.000****
Pb	0.223	0.902	**0.990***	0.455	**0.951***	0.798	0.757	**0.979***	**0.981***

`

Table 5.3 (Continued)

b. SA

Fine particles	Cr(0)	Cr(III)	Mn(II)	Mn(IV)	Fe(0)	Fe (II)	Fe (III)	Cu (II)	Zn(II)
Ti	0.863[a]	0.974	**0.977***	**0.982***	-0.638	**0.973***	**0.987***	**0.970***	**0.981***
V	0.900	0.989	0.912	**0.973***	-0.348	0.901	**0.980***	**0.972***	**0.955***
Cr	-0.286	-0.558	-0.517	-0.607	0.826	-0.896	-0.716	-0.558	-0.561
Mn	0.957	1.000	**0.998****	**0.993****	-0.536	0.914	**0.975***	**0.991****	**0.998****
Fe	0.853	0.969	**0.952***	**0.987***	-0.534	**0.967***	**0.999****	**0.977***	**0.975***
Ni	0.227	-0.072	-0.653	-0.532	0.938	-0.649	-0.525	-0.502	-0.569
Cu	0.970	0.998	**0.967***	**0.991****	-0.365	0.867	**0.971***	**0.997****	**0.988***
Zn	0.954	1.000	**0.993****	**0.997****	-0.500	0.913	**0.982***	**0.997****	**1.000****
Pb	0.928	0.997	**0.983***	**1.000****	-0.503	0.933	**0.993****	**0.997****	**0.997****
Coarse particles									
Ti	0.689	0.858	0.758	0.888	0.437	**0.968****	**0.987***	**0.969***	0.911
V	0.666	0.676	0.538	0.887	0.510	**0.965***	**0.964***	0.857	0.881
Cr	**0.971***	0.942	0.402	0.942	-0.199	0.857	0.699	0.661	0.470
Mn	0.562	0.883	0.910	0.751	0.417	0.851	0.915	**0.983***	0.883
Fe	0.629	0.766	0.715	0.863	0.541	0.964	**0.999****	**0.953***	0.943
Ni	0.368	0.612	0.808	0.671	0.754	0.839	**0.963***	**0.953***	**0.999****
Cu	0.882	**0.962***	0.614	**0.961***	0.095	**0.953***	0.874	0.852	0.709
Zn	0.329	0.606	0.840	0.635	0.767	0.812	0.950	**0.957***	**1.000****
Pb	0.264	0.509	0.780	0.590	0.829	0.778	0.927	0.912	**0.993****

Table 5.3 (Continued)

c. FU

Fine particles	Cr(0)	Cr(III)	Mn(II)	Mn(IV)	Fe(0)	Fe (II)	Fe (III)	Cu (II)	Zn(II)
Ti	0.666	**0.993****	0.927	**0.994****	-0.653	0.890	**0.999****	0.717	0.713
V	0.591	0.821	**0.953***	0.710	-0.834	**0.974***	0.755	0.933	**0.977***
Cr	0.767	**0.999****	0.938	**0.969***	-0.762	0.906	**0.985***	0.709	0.733
Mn	0.628	**0.964***	**0.998****	0.918	-0.748	**0.988***	0.940	0.884	0.894
Fe	0.644	**0.992****	0.946	**0.989***	-0.658	0.914	**0.996****	0.759	0.752
Ni	0.734	**0.976***	**0.986***	0.915	-0.823	**0.972***	0.942	0.825	0.857
Cu	0.272	0.726	0.904	0.667	-0.570	0.931	0.693	**1.000****	**0.982***
Zn	0.397	0.743	0.921	0.651	-0.696	**0.951***	0.689	**0.986***	**1.000****
Pb	0.336	0.686	0.886	0.590	-0.661	0.922	0.629	**0.985***	**0.996****

* $p<0.05$, ** $p<0.01$

[a] Correlation coefficient between contaminants without irregular data in SA samples collected in summer.

`

5.3.3.3 Principal component analysis (PCA) and cluster analysis (CA)

Table 5.4 shows the principal components (PC) of the valence states of target metals from XAFS. Eigenvalues, variance contributions, and cumulative variance are also presented. We also performed CA on target metal compounds for the three sites to better identify possible emission sources (**Fig. 5.4**). We performed PCA and CA for both particle sizes together because the number of samples was limited and because the irregular Cr concentration in PF collected in summer at SA had to be removed. The PCA and CA results for the three sites were different, even for KO and SA, which were relatively close geographically. This indicates that the emitting sources at each site were different and depended on their geographical location and regional characteristics.

Table 5.4 Varimax rotated factor loadings (only those with values ≥0.3 are listed) for XAFS data of target metals from three sites

Components	KO			SA		FU			
	PC1	PC2	PC3	PC1	PC2	PC1	PC2	PC3	PC4
Cr(0)		0.53			0.65				0.30
Cr(III)			0.76		0.45	0.35			
Mn(II)	0.33			0.39		0.38			
Mn(IV)	0.32	0.48		0.38		0.35		0.50	
Fe (0)	0.34				0.50			0.52	0.71
Fe (II)	0.36			0.36		0.37			
Fe (III)	0.37			0.39		0.35		0.43	
Cu (II)	0.36			0.38		0.34	0.36		0.33
Zn(II)	0.32			0.39		0.34			0.37
Eigenvalues	6.9	1.11	0.47	6.33	2.23	6.99	0.84	0.57	0.56
Variance	76.7%	12.3%	5.2%	70.4%	24.7%	77.7%	9.2%	6.3%	6.2%
Cumulative variance	76.7%	89.0%	94.2%	70.4%	95.1%	77.7%	86.9%	93.2%	99.4%

For KO, the PCA model extracted three PCs and explained up to 94% of the total variance. PC1 and PC2 contained the most pollutant components, as their combined cumulative variance contribution reached 89.0%. The components originally belonging to PC1 were grouped into one cluster with those of PC2 in the CA analysis results. As

previous discussion of emission sources of included factors, PC1 indicated the surface dust emission sources, including Cu(II) and Zn(II) generated from traffic brake wear, Mn(II), Fe(II), and Fe(III) from crustal soil. In combination with the CA results, Fe(II) and Fe(III) were also classified into the same cluster with Cr(0) and Mn(IV) in PC2, this means possible anthropogenic activities emitting such as fly ash generated from steel and marine industries in the Keihin industrial area. The PCA and CA results show that Cr(III) was unique, it was always grouped separately and the variance contribution was 5.2% for PCA. There were strong correlations between Cr(III) with V, Ni, Cu, and Pb (**Table 5.3(a)**). Ni and V are often considered to be tracers of ship emissions because both are major impurities in residual oil used by ocean-going vessels, and shipping facilities are considered an important source of airborne fine Ni and V in port areas [65], [66], while Cu and Pb are the main elements in fly ash from municipal waste incinerators, and the crystalline and non-crystalline forms of Cr and Cu can be incorporated into the spinel structure in fly ash particles [67]–[69]. Therefore, PC3 containing only Cr(III) can be considered to represent the combustion source such as fossil fuel burning and waste incineration.

At SA, the overall variance contribution of the two PCs was 95.1%. The PCA and CA results for the valence states were also consistent. This indicates that the sources of pollutants in this region were relatively stable, and the emission sources derived from the model results are sufficient to identify the largest sources of the target contaminants. The components of PC1 for SA and KO were similar. However, since Saitama Prefecture is an inland-type region with more developed agricultural production, the valence distribution of Mn and Fe, which mainly originate from the soil, maybe more related to the solidification process of toxic metals, which occurs in paddy soils during rice cultivation. On the one hand, the reduction of Mn(IV) to Mn(II) oxidizes As(III) to As(V), and oxidation of As(III) by Mn oxides likely leads to decreased As mobility in soil [70], [71]. On the other hand, Mn oxides would promote Fe(II) oxidation to Fe(III), thereby creating freshly precipitated Fe(III) hydroxides that could serve as efficient

sorbents for As [72], [73]. Some Mn-containing pesticides also contribute to the PM-bound Mn besides the soil re-suspension [74]. This might explain why the highest concentrations of Mn(II) and Fe(III) were found in SA samples in summer and autumn when rice harvesting can cause more soil dust to enter the atmosphere. PC2 including the Cr(0), Cr(III), and Fe(0) might indicate the industrial emission source around the sampling site.

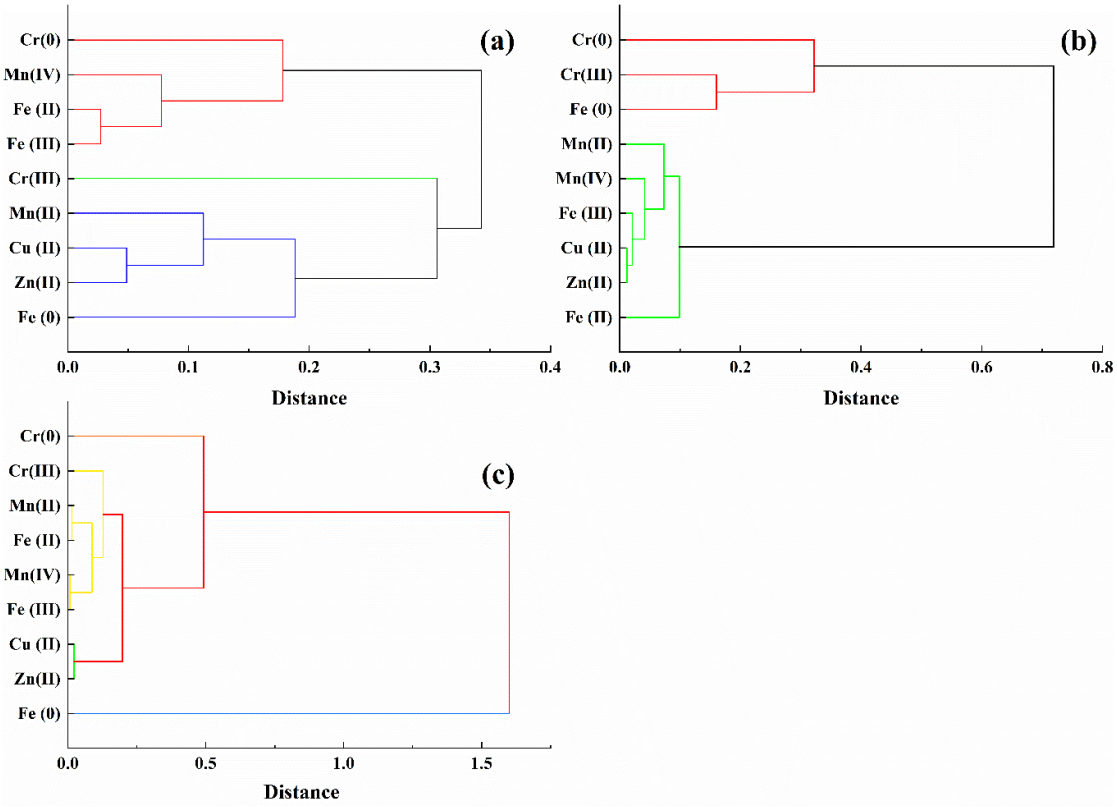


Fig. 5.4 Cluster analysis of target metal compounds from (a) KO, (b) SA, and (c) FU

For FU, the PCA results were complex. For example, Fe(0) and Cu(II) had relatively high loadings in different PCs, and their PCA and CA results differed significantly. This was probably due to the diverse industrial structure of the Fukuoka region and its proximity to the East Asian continent, which makes it susceptible to long-distance transport of pollutants from the continent. Therefore, the sources of pollutants are more complex. The small number of samples (n = 7) obtained at FU may be another reason

behind the large differences between the PCA and CA results. PCA is designed to capture the maximum amount of raw information and reduce the number of variables by extracting the main components of multivariate data, while CA groups variables that are close together into the same cluster in the dendrogram.

In terms of source identification of contaminants at FU, Cu(II) and Zn(II) were likely emitted from traffic brake wear. Cr(III), Mn(II), Mn(IV), Fe(II), and Fe(III) in aerosol particles were likely influenced by fly ash generated by steel production in the Kitakyushu industrial area, as previously discussed. Furthermore, the high correlation between Mn(II), Mn(IV), and Fe(III) with Ti indicate that they may have been from peri-urban agricultural production emissions. The CA results showed that Cr(0) and Fe(0) belonged to separate clusters, with low correlations between them and other pollutants but they were grouped in PC4 with Cu(II) and Zn(II) by PCA result. Kennedy et al. [75] presented that brake dust generated during the braking process wear of the brake discs/drums, which are commonly made of steel of alloys was enriched in Cr, Cu, Fe, and tin (Sn). This might indicate the unique sources for Cr(0) and Fe(0), such as the abrasion of metallic alloys on surfaces.

5.3.4 Potential contribution for PAHs photocatalytic and PM oxidative potential

Aerosol particles are complex systems containing multiple contaminants, and the synergistic effect between multiple contaminants will affect the contamination characteristics of PM-bound PAHs more significantly. **Fig. 5.5** shows the multivariate linear relationship between multiple contaminants in aerosol samples and the concentration of total PAHs obtained by fitting the multivariate linear regression model.

The negative coefficients of the metal components (Ti, Cr, Fe, and Cu) indicate a potential catalytic degradation effect on PAHs concentration on the surface of aerosol particulate matter. It has been shown that PAHs adsorb to highly active sites on the surface of mineral particulate matter, forming a stable adsorption state. The charge is

then transferred from the adsorbed PAHs to the metal oxide centers of the particulate matter and is stabilized in the interaction with the mineral surface to form ROS [76]–[78]. This just explains the positive coefficient of PAHs concentration on the DTT parameter. The DTT value is used to evaluate the oxidation potential of the particulate matter. Under light conditions, PAHs adsorbed on the surface of the particulate matter under transition metal-catalyzed oxidation generate a variety of oxygen-containing intermediates, which enhance the oxidation potential of the particulate matter [79]–[81]. However, there is no direct correlation between the strength of PAHs degradation and the oxidizing activity of the metal components, and adsorption on the surface of the particulate matter is still protective against the environmental presence of PAHs, which may explain why the *p*-values of these metal components in the model are not significant.

OLS Regression Results

Dep. Variable:	Total PAHs	R-squared:	0.917
Model:	OLS	Adj. R-squared:	0.390
Method:	Least Squares	F-statistic:	1.739
No. Observations:	23	Prob (F-statistic):	0.362
Df Residuals:	3	Log-Likelihood:	-48.579
Df Model:	19	AIC:	137.2
Covariance Type:	nonrobust	BIC:	159.9

	coef	std err	t	P>|t|	[0.025	0.975]
const	-80.0998	138.118	-0.580	0.603	-519.653	359.453
AOT	17.1138	41.965	0.408	0.711	-116.437	150.664
Rain	-0.0039	0.019	-0.208	0.849	-0.063	0.055
Temp	-1.4891	1.808	-0.824	0.471	-7.243	4.265
Humidity	1.4303	1.951	0.733	0.517	-4.779	7.640
weed	-13.7518	10.353	-1.328	0.276	-46.700	19.196
Insolation	6.1400	3.477	1.766	0.176	-4.926	17.205
O3	-1.9215	1.004	-1.915	0.151	-5.115	1.272
NO2	2.8859	1.830	1.577	0.213	-2.938	8.710
NO3-	-0.0004	0.001	-0.511	0.644	-0.003	0.002
NH4+	-0.0002	0.001	-0.172	0.875	-0.004	0.004
Ti	-0.0118	0.026	-0.451	0.683	-0.095	0.072
Cr	-0.0315	0.022	-1.433	0.247	-0.102	0.038
Mn	0.0590	0.049	1.209	0.313	-0.096	0.214
Fe	-5.366e-05	0.002	-0.035	0.974	-0.005	0.005
Cu	-0.0217	0.049	-0.440	0.690	-0.179	0.135
Zn	0.0066	0.005	1.401	0.256	-0.008	0.022
OC	1.796e-05	4.83e-05	0.372	0.735	-0.000	0.000
EC	-0.0002	0.000	-1.203	0.315	-0.001	0.000
DTT	3.9980	7.610	0.525	0.636	-20.221	28.217

Fig. 5.5 Results of multiple linear regression analysis

5.4 Summary

This study investigated the chemical compositions and valence states of elements in cyclone-collected particles from three sites in Japan. The average concentration of Fe was the highest among the nine metallic elements, and the ambient concentrations of Cu, Zn, and Pb far exceeded the background concentrations. XAFS results for the target metals showed that the major valence states were Cr(III), Mn(II), Fe(III), Cu(II), and Zn(II), followed by Cr(0), Mn(IV), Fe(II), Fe(0), and Cu(0). Cr(VI), Mn(0), and Zn(0) were detected in some samples, and Cu(I) was not detected in this study. Moreover, the source identification results from correlation analysis, PCA, and CA showed that the

potential emission sources of metallic contaminants differed significantly across the three sites and suggested influence from industrial activities and geographical location. The main contribution source of Mn and Fe is crustal soil. At KO and FU, which are metropolises near the sea and adjacent to industrial areas, the probably anthropogenic sources of metal contaminants such as Cr(III), Mn(II), Mn(IV), Fe(II), and Fe(III) are likely fly ash from steel production and fuel combustion in industrial areas. At SA, which is located inland with greater agricultural production, the dominant source is likely soil dust from agricultural production but this hypothesis needs further research. The main source of Cu(II) and Zn(II) in all three areas can be traffic brake wear. In addition, the source analysis model showed that the pollutants in FU exhibited cross-regional transport characteristics. The results of multiple linear regression modeling indicate that the metal components in the particulate matter can potentially affect the photocatalytic degradation of PAHs, which in turn generates a variety of oxygen-containing intermediates to enhance the oxidative potential of the particulate matter.

5.5 References

[1] W. Jing *et al.*, "Characterization of Elemental Composition and Valence State of Cyclone-collected Aerosol Particles Using EDXRF and XAFS at Three Sites in Japan," *Asian J. Atmospheric Environ.*, vol. 16, no. 2, pp. 40–58, Jun. 2022, doi: 10.5572/ajae.2021.137.

[2] M. D. Cohen *et al.*, "Pulmonary Immunotoxic Potentials of Metals Are Governed by Select Physicochemical Properties: Vanadium Agents," *J. Immunotoxicol.*, vol. 4, no. 1, pp. 49–60, Jan. 2007, doi: 10.1080/15476910601119350.

[3] Y. Sun *et al.*, "The impact of relative humidity on aerosol composition and evolution processes during wintertime in Beijing, China," *Atmos. Environ.*, vol. 77, pp. 927–934, Oct. 2013, doi: 10.1016/j.atmosenv.2013.06.019.

[4] A. Zanobetti *et al.*, "Associations between arrhythmia episodes and temporally and spatially resolved black carbon and particulate matter in elderly patients," *Occup. Environ. Med.*, vol. 71, no. 3, pp. 201–207, Mar. 2014, doi: 10.1136/oemed-2013-101526.

[5] M. H. Forouzanfar *et al.*, "Global, regional, and national comparative risk assessment of 79 behavioural, environmental and occupational, and metabolic risks or clusters of risks, 1990–2015: a systematic analysis for the Global Burden of Disease Study 2015," *The Lancet*, vol. 388, no. 10053, pp. 1659–1724, Oct.

2016, doi: 10.1016/S0140-6736(16)31679-8.
[6] D. Chirizzi *et al.*, “Influence of Saharan dust outbreaks and carbon content on oxidative potential of water-soluble fractions of PM2.5 and PM10,” *Atmos. Environ.*, vol. 163, pp. 1–8, Aug. 2017, doi: 10.1016/j.atmosenv.2017.05.021.
[7] D. Gao, K. J. Godri Pollitt, J. A. Mulholland, A. G. Russell, and R. J. Weber, “Characterization and comparison of PM_{2.5} oxidative potential assessed by two acellular assays,” *Atmospheric Chem. Phys.*, vol. 20, no. 9, pp. 5197–5210, May 2020, doi: 10.5194/acp-20-5197-2020.
[8] S. Taghvaee *et al.*, “Source apportionment of the oxidative potential of fine ambient particulate matter (PM2.5) in Athens, Greece,” *Sci. Total Environ.*, vol. 653, pp. 1407–1416, Feb. 2019, doi: 10.1016/j.scitotenv.2018.11.016.
[9] P. J. Sheehan, D. M. Meyer, M. M. Sauer, and D. J. Paustenbach, “Assessment of the human health risks posed by exposure to chromium-contaminated soils,” *J. Toxicol. Environ. Health*, vol. 32, no. 2, pp. 161–201, Feb. 1991, doi: 10.1080/15287399109531476.
[10] H. Sun, J. Brocato, and M. Costa, “Oral Chromium Exposure and Toxicity,” *Curr. Environ. Health Rep.*, vol. 2, no. 3, pp. 295–303, Sep. 2015, doi: 10.1007/s40572-015-0054-z.
[11] A. J. Cohen *et al.*, “Estimates and 25-year trends of the global burden of disease attributable to ambient air pollution: an analysis of data from the Global Burden of Diseases Study 2015,” *The Lancet*, vol. 389, no. 10082, pp. 1907–1918, May 2017, doi: 10.1016/S0140-6736(17)30505-6.
[12] F. E. Huggins and G. P. Huffman, “X-ray Absorption Fine Structure (XAFS) Spectroscopic Characterization of Emissions from Combustion of Fossil Fuels,” *Int. J. Soc. Mater. Eng. Resour.*, vol. 10, no. 1, pp. 1–13, 2002, doi: 10.5188/ijsmer.10.1.
[13] G. Zhang, “Atmospheric Particulate Matter Studied by Mössbauer Spectroscopy and XAFS,” *Hyperfine Interact.*, vol. 151/152, no. 1–4, pp. 299–306, 2003, doi: 10.1023/B:HYPE.0000020421.68173.55.
[14] Saito K., Okuda T., Hasegawa S., Nishita-Hara C., Hara K., and Hayashi M., “Chemical Speciation of Chromium in Atmospheric Particulate Matter Collected with Cyclone by XAFS Method.” Mar. 10, 2020. doi: 10.11298/taiki.55.27.
[15] K. Shimada *et al.*, “Concentrations of metallic elements in long-range-transported aerosols measured simultaneously at three coastal sites in China and Japan,” *J. Atmospheric Chem.*, vol. 75, no. 2, pp. 123–139, Jun. 2018, doi: 10.1007/s10874-017-9366-8.
[16] T. Sugiyama *et al.*, “Health effects of PM2.5 sources on children’s allergic and respiratory symptoms in Fukuoka, Japan,” *Sci. Total Environ.*, vol. 709, p. 136023, Mar. 2020, doi: 10.1016/j.scitotenv.2019.136023.
[17] P. Shahpoury *et al.*, “The influence of chemical composition, aerosol acidity, and metal dissolution on the oxidative potential of fine particulate matter and redox potential of the lung lining fluid,” *Environ. Int.*, vol. 148, p. 106343, Mar. 2021,

doi: 10.1016/j.envint.2020.106343.
[18] S. V. Hering *et al.*, "Comparison of Sampling Methods for Carbonaceous Aerosols in Ambient Air," *Aerosol Sci. Technol.*, vol. 12, no. 1, pp. 200–213, Jan. 1990, doi: 10.1080/02786829008959340.
[19] J. Parshintsev, J. Ruiz-Jimenez, T. Petäjä, K. Hartonen, M. Kulmala, and M.-L. Riekkola, "Comparison of quartz and Teflon filters for simultaneous collection of size-separated ultrafine aerosol particles and gas-phase zero samples," *Anal. Bioanal. Chem.*, vol. 400, no. 10, pp. 3527–3535, Jul. 2011, doi: 10.1007/s00216-011-5041-0.
[20] K. Kristensen, M. Bilde, P. P. Aalto, T. Petäjä, and M. Glasius, "Denuder/filter sampling of organic acids and organosulfates at urban and boreal forest sites: Gas/particle distribution and possible sampling artifacts," *Atmos. Environ.*, vol. 130, pp. 36–53, Apr. 2016, doi: 10.1016/j.atmosenv.2015.10.046.
[21] L. S. Van Winkle *et al.*, "Biological Dose Response to PM2.5: Effect of Particle Extraction Method on Platelet and Lung Responses," *Toxicol. Sci.*, vol. 143, no. 2, pp. 349–359, Feb. 2015, doi: 10.1093/toxsci/kfu230.
[22] C. Roper, L. S. Delgado, D. Barrett, S. L. Massey Simonich, and R. L. Tanguay, "PM2.5 Filter Extraction Methods: Implications for Chemical and Toxicological Analyses," *Environ. Sci. Technol.*, vol. 53, no. 1, pp. 434–442, Jan. 2019, doi: 10.1021/acs.est.8b04308.
[23] T. Okuda, R. Isobe, Y. Nagai, S. Okahisa, K. Funato, and K. Inoue, "Development of a High-Volume PM2.5 Particle Sampler Using Impactor and Cyclone Techniques," *Aerosol Air Qual. Res.*, vol. 15, no. 3, pp. 759–767, 2015, doi: 10.4209/aaqr.2014.09.0194.
[24] T. Okuda and R. Isobe, "Improvement of a High-volume Aerosol Particle Sampler for Collecting Submicron Particles through the Combined Use of a Cyclone with a Smoothened Inner Wall and a Circular Cone Attachment," *Asian J. Atmospheric Environ.*, vol. 11, no. 2, pp. 131–137, Jun. 2017, doi: 10.5572/ajae.2017.11.2.131.
[25] T. Okuda *et al.*, "Development of a High-Volume Simultaneous Sampler for Fine and Coarse Particles using Virtual Impactor and Cyclone Techniques," *Asian J. Atmospheric Environ.*, vol. 12, no. 1, pp. 78–86, Mar. 2018, doi: 10.5572/ajae.2018.12.1.078.
[26] A. Honda, T. Okuda, M. Nagao, N. Miyasaka, M. Tanaka, and H. Takano, "PM2.5 collected using cyclonic separation causes stronger biological responses than that collected using a conventional filtration method," *Environ. Res.*, vol. 198, p. 110490, Jul. 2021, doi: 10.1016/j.envres.2020.110490.
[27] P. H. Chowdhury *et al.*, "Effects of Ambient PM2.5 Collected Using Cyclonic Separator from Asian Cities on Human Airway Epithelial Cells," *Aerosol Air Qual. Res.*, vol. 19, no. 8, pp. 1808–1819, 2019, doi: 10.4209/aaqr.2019.01.0016.
[28] K. Ogino *et al.*, "PM2.5-induced airway inflammation and hyperresponsiveness in NC/Nga mice: PM2.5 INDUCES AIRWAY INFLAMMATION," *Environ. Toxicol.*, vol. 32, no. 3, pp. 1047–1054, Mar. 2017, doi: 10.1002/tox.22303.

[29] K. Ogino *et al.*, “Involvement of PM2.5-bound protein and metals in PM2.5-induced allergic airway inflammation in mice,” *Inhal. Toxicol.*, vol. 30, no. 13–14, pp. 498–508, Dec. 2018, doi: 10.1080/08958378.2018.1561769.

[30] T. Sagawa *et al.*, “Exposure to particulate matter upregulates ACE2 and TMPRSS2 expression in the murine lung,” *Environ. Res.*, vol. 195, p. 110722, Apr. 2021, doi: 10.1016/j.envres.2021.110722.

[31] T. Okuda *et al.*, “Rapid and Simple Determination of Multi-Elements in Aerosol Samples Collected on Quartz Fiber Filters by Using EDXRF Coupled with Fundamental Parameter Quantification Technique,” *Aerosol Air Qual. Res.*, vol. 13, no. 6, pp. 1864–1876, 2013, doi: 10.4209/aaqr.2012.11.0308.

[32] S. R. Taylor, “Abundance of chemical elements in the continental crust: a new table,” *Geochim. Cosmochim. Acta*, vol. 28, no. 8, pp. 1273–1285, Aug. 1964, doi: 10.1016/0016-7037(64)90129-2.

[33] I. F. Al-Momani, A. S. Daradkeh, A. T. Haj-Hussein, Y. A. Yousef, Q. M. Jaradat, and K. A. Momani, “Trace elements in daily collected aerosols in Al-Hashimya, central Jordan,” *Atmospheric Res.*, vol. 73, no. 1–2, pp. 87–100, Jan. 2005, doi: 10.1016/j.atmosres.2003.09.009.

[34] M. T. Ny and B.-K. Lee, “Size Distribution and Source Identification of Airborne Particulate Matter and Metallic Elements in a Typical Industrial City,” *Asian J. Atmospheric Environ.*, vol. 4, no. 1, pp. 9–19, Jun. 2010, doi: 10.5572/ajae.2010.4.1.009.

[35] S. W. See, Y. H. Wang, and R. Balasubramanian, “Contrasting reactive oxygen species and transition metal concentrations in combustion aerosols,” *Environ. Res.*, vol. 103, no. 3, pp. 317–324, Mar. 2007, doi: 10.1016/j.envres.2006.08.012.

[36] T. Szigeti, M. Óvári, C. Dunster, F. J. Kelly, F. Lucarelli, and G. Záray, “Changes in chemical composition and oxidative potential of urban PM2.5 between 2010 and 2013 in Hungary,” *Sci. Total Environ.*, vol. 518–519, pp. 534–544, Jun. 2015, doi: 10.1016/j.scitotenv.2015.03.025.

[37] N. A. H. Janssen *et al.*, “Oxidative potential of particulate matter collected at sites with different source characteristics,” *Sci. Total Environ.*, vol. 472, pp. 572–581, Feb. 2014, doi: 10.1016/j.scitotenv.2013.11.099.

[38] T. L. Stoiber, M. M. Shafer, and D. E. Armstrong, “Induction of reactive oxygen species in *chlamydomonas reinhardtii* in response to contrasting trace metal exposures: Induction of Reactive Oxygen Species IN *C. reinhardtii*,” *Environ. Toxicol.*, vol. 28, no. 9, pp. 516–523, Sep. 2013, doi: 10.1002/tox.20743.

[39] Y. Wang, M. J. Plewa, U. K. Mukherjee, and V. Verma, “Assessing the cytotoxicity of ambient particulate matter (PM) using Chinese hamster ovary (CHO) cells and its relationship with the PM chemical composition and oxidative potential,” *Atmos. Environ.*, vol. 179, pp. 132–141, Apr. 2018, doi: 10.1016/j.atmosenv.2018.02.025.

[40] F. Bardelli, E. Cattaruzza, F. Gonella, G. Rampazzo, and G. Valotto, “Characterization of road dust collected in Traforo del San Bernardo highway tunnel: Fe and Mn speciation,” *Atmos. Environ.*, vol. 45, no. 35, pp. 6459–6468,

Nov. 2011, doi: 10.1016/j.atmosenv.2011.07.035.
[41] A. Ohta *et al.*, "Chemical compositions and XANES speciations of Fe, Mn and Zn from aerosols collected in China and Japan during dust events," *Geochem. J.*, vol. 40, no. 4, pp. 363–376, 2006, doi: 10.2343/geochemj.40.363.
[42] T. Okuda *et al.*, "Trends in hazardous trace metal concentrations in aerosols collected in Beijing, China from 2001 to 2006," *Chemosphere*, vol. 72, no. 6, pp. 917–924, Jun. 2008, doi: 10.1016/j.chemosphere.2008.03.033.
[43] M. S. Hassanvand *et al.*, "Characterization of PAHs and metals in indoor/outdoor PM10/PM2.5/PM1 in a retirement home and a school dormitory," *Sci. Total Environ.*, vol. 527–528, pp. 100–110, Sep. 2015, doi: 10.1016/j.scitotenv.2015.05.001.
[44] D. D. Alves *et al.*, "Source apportionment of metallic elements in urban atmospheric particulate matter and assessment of its water-soluble fraction toxicity," *Environ. Sci. Pollut. Res.*, vol. 27, no. 11, pp. 12202–12214, Apr. 2020, doi: 10.1007/s11356-020-07791-8.
[45] H. M. Xu *et al.*, "Lead concentrations in fine particulate matter after the phasing out of leaded gasoline in Xi'an, China," *Atmos. Environ.*, vol. 46, pp. 217–224, Jan. 2012, doi: 10.1016/j.atmosenv.2011.09.078.
[46] A. Iijima *et al.*, "Particle size and composition distribution analysis of automotive brake abrasion dusts for the evaluation of antimony sources of airborne particulate matter," *Atmos. Environ.*, vol. 41, no. 23, pp. 4908–4919, Jul. 2007, doi: 10.1016/j.atmosenv.2007.02.005.
[47] T. Grigoratos and G. Martini, "Brake wear particle emissions: a review," *Environ. Sci. Pollut. Res.*, vol. 22, no. 4, pp. 2491–2504, Feb. 2015, doi: 10.1007/s11356-014-3696-8.
[48] P. A. Tanner, H.-L. Ma, and P. K. N. Yu, "Fingerprinting Metals in Urban Street Dust of Beijing, Shanghai, and Hong Kong," *Environ. Sci. Technol.*, vol. 42, no. 19, pp. 7111–7117, Oct. 2008, doi: 10.1021/es8007613.
[49] X. Lu, L. Wang, K. Lei, J. Huang, and Y. Zhai, "Contamination assessment of copper, lead, zinc, manganese and nickel in street dust of Baoji, NW China," *J. Hazard. Mater.*, vol. 161, no. 2–3, pp. 1058–1062, Jan. 2009, doi: 10.1016/j.jhazmat.2008.04.052.
[50] P. Oustadakis, P. E. Tsakiridis, A. Katsiapi, and S. Agatzini-Leonardou, "Hydrometallurgical process for zinc recovery from electric arc furnace dust (EAFD)," *J. Hazard. Mater.*, vol. 179, no. 1–3, pp. 1–7, Jul. 2010, doi: 10.1016/j.jhazmat.2010.01.059.
[51] M. Omran and T. Fabritius, "Effect of steelmaking dust characteristics on suitable recycling process determining: Ferrochrome converter (CRC) and electric arc furnace (EAF) dusts," *Powder Technol.*, vol. 308, pp. 47–60, Feb. 2017, doi: 10.1016/j.powtec.2016.11.049.
[52] T. Sofili, "Characterization of steel mill electric-arc furnace dust," *J. Hazard. Mater.*, vol. 109, no. 1–3, pp. 59–70, Jun. 2004, doi:

10.1016/j.jhazmat.2004.02.032.
[53] E. Manno, D. Varrica, and G. Dongarrà, “Metal distribution in road dust samples collected in an urban area close to a petrochemical plant at Gela, Sicily,” *Atmos. Environ.*, vol. 40, no. 30, pp. 5929–5941, Sep. 2006, doi: 10.1016/j.atmosenv.2006.05.020.
[54] M. Vallius, T. Lanki, P. Tiittanen, K. Koistinen, J. Ruuskanen, and J. Pekkanen, “Source apportionment of urban ambient PM2.5 in two successive measurement campaigns in Helsinki, Finland,” *Atmos. Environ.*, vol. 37, no. 5, pp. 615–623, Feb. 2003, doi: 10.1016/S1352-2310(02)00925-1.
[55] H. Agrawal, Q. G. J. Malloy, W. A. Welch, J. Wayne Miller, and D. R. Cocker, “In-use gaseous and particulate matter emissions from a modern ocean going container vessel,” *Atmos. Environ.*, vol. 42, no. 21, pp. 5504–5510, Jul. 2008, doi: 10.1016/j.atmosenv.2008.02.053.
[56] H. Agrawal, W. A. Welch, J. W. Miller, and D. R. Cocker, “Emission Measurements from a Crude Oil Tanker at Sea,” *Environ. Sci. Technol.*, vol. 42, no. 19, pp. 7098–7103, Oct. 2008, doi: 10.1021/es703102y.
[57] S. K. M. Hassan, “Metal concentrations and distribution in the household, stairs and entryway dust of some Egyptian homes,” *Atmos. Environ.*, vol. 54, pp. 207–215, Jul. 2012, doi: 10.1016/j.atmosenv.2012.02.013.
[58] J. Q. Yuen, P. H. Olin, H. S. Lim, S. G. Benner, R. A. Sutherland, and A. D. Ziegler, “Accumulation of potentially toxic elements in road deposited sediments in residential and light industrial neighborhoods of Singapore,” *J. Environ. Manage.*, vol. 101, pp. 151–163, Jun. 2012, doi: 10.1016/j.jenvman.2011.11.017.
[59] M. L. López, S. Ceppi, G. G. Palancar, L. E. Olcese, G. Tirao, and B. M. Toselli, “Elemental concentration and source identification of PM10 and PM2.5 by SR-XRF in Córdoba City, Argentina,” *Atmos. Environ.*, vol. 45, no. 31, pp. 5450–5457, Oct. 2011, doi: 10.1016/j.atmosenv.2011.07.003.
[60]F. Amato *et al.*, “Urban air quality: The challenge of traffic non-exhaust emissions,” *J. Hazard. Mater.*, vol. 275, pp. 31–36, Jun. 2014, doi: 10.1016/j.jhazmat.2014.04.053.
[61] H. Chen, X. Lu, L. Y. Li, T. Gao, and Y. Chang, “Metal contamination in campus dust of Xi’an, China: A study based on multivariate statistics and spatial distribution,” *Sci. Total Environ.*, vol. 484, pp. 27–35, Jun. 2014, doi: 10.1016/j.scitotenv.2014.03.026.
[62] X. Chen, M. Guo, J. Feng, S. Liang, D. Han, and J. Cheng, “Characterization and risk assessment of heavy metals in road dust from a developing city with good air quality and from Shanghai, China,” *Environ. Sci. Pollut. Res.*, vol. 26, no. 11, pp. 11387–11398, Apr. 2019, doi: 10.1007/s11356-019-04550-2.
[63] H. Jeong, K. Ra, K.-T. Kim, E.-S. Kim, S.-Y. Lee, and M.-S. Choi, “Tracing the Pollution Source Using Pb Isotopes in Sediments of the Coastal Region Surrounding the National Industrial Complex, Korea,” *J. Coast. Res.*, vol. 85, pp. 1456–1460, May 2018, doi: 10.2112/SI85-292.1.

[64] M. Taylor and N. Kruger, “Tyre Weights an Overlooked Diffuse Source of Lead and Antimony to Road Runoff,” *Sustainability*, vol. 12, no. 17, p. 6790, Aug. 2020, doi: 10.3390/su12176790.

[65] R. E. Peltier, S.-I. Hsu, R. Lall, and M. Lippmann, “Residual oil combustion: a major source of airborne nickel in New York City,” *J. Expo. Sci. Environ. Epidemiol.*, vol. 19, no. 6, pp. 603–612, Sep. 2009, doi: 10.1038/jes.2008.60.

[66] L. Tian *et al.*, “Shipping emissions associated with increased cardiovascular hospitalizations,” *Atmos. Environ.*, vol. 74, pp. 320–325, Aug. 2013, doi: 10.1016/j.atmosenv.2013.04.014.

[67] M. Takaoka, K. Shiota, G. Imai, and K. Oshita, “Emission of particulate matter 2.5 (PM2.5) and elements from municipal solid waste incinerators,” *J. Mater. Cycles Waste Manag.*, vol. 18, no. 1, pp. 72–80, Jan. 2016, doi: 10.1007/s10163-014-0314-2.

[68] C. H. Jung, T. Matsuto, N. Tanaka, and T. Okada, “Metal distribution in incineration residues of municipal solid waste (MSW) in Japan,” *Waste Manag.*, vol. 24, no. 4, pp. 381–391, Jan. 2004, doi: 10.1016/S0956-053X(03)00137-5.

[69] A. V. Dahlan, H. Kitamura, H. Sakanakura, T. Shimaoka, T. Yamamoto, and F. Takahashi, “Possible metal speciation in the fly ash produced from a fluidized bed incinerator of municipal solid waste.” Japan Society of Material Cycles and Waste Management, 2020. doi: 10.14912/jsmcwm.31.0_505.

[70] B. J. Lafferty, M. Ginder-Vogel, and D. L. Sparks, “Arsenite Oxidation by a Poorly Crystalline Manganese-Oxide 1. Stirred-Flow Experiments,” *Environ. Sci. Technol.*, vol. 44, no. 22, pp. 8460–8466, Nov. 2010, doi: 10.1021/es102013p.

[71] B. J. Lafferty, M. Ginder-Vogel, M. Zhu, K. J. T. Livi, and D. L. Sparks, “Arsenite Oxidation by a Poorly Crystalline Manganese-Oxide. 2. Results from X-ray Absorption Spectroscopy and X-ray Diffraction,” *Environ. Sci. Technol.*, vol. 44, no. 22, pp. 8467–8472, Nov. 2010, doi: 10.1021/es102016c.

[72] K. Ehlert, C. Mikutta, and R. Kretzschmar, “Effects of Manganese Oxide on Arsenic Reduction and Leaching from Contaminated Floodplain Soil,” *Environ. Sci. Technol.*, vol. 50, no. 17, pp. 9251–9261, Sep. 2016, doi: 10.1021/acs.est.6b01767.

[73] X. Xu, C. Chen, P. Wang, R. Kretzschmar, and F.-J. Zhao, “Control of arsenic mobilization in paddy soils by manganese and iron oxides,” *Environ. Pollut.*, vol. 231, pp. 37–47, Dec. 2017, doi: 10.1016/j.envpol.2017.07.084.

[74] J. Sysalová, I. Sýkorová, M. Havelcová, J. Száková, H. Trejtnarová, and B. Kotlík, “Toxicologically important trace elements and organic compounds investigated in size-fractionated urban particulate matter collected near the Prague highway,” *Sci. Total Environ.*, vol. 437, pp. 127–136, Oct. 2012, doi: 10.1016/j.scitotenv.2012.07.030.

[75] P. Kennedy and G. Jennifer, “Preliminary examination of trace elements in tyres, brake pads, and road bitumen in New Zealand. Prepared for Ministry of Transport, New Zealand, Infrastructure Auckland.,” Ministry of Transport, New Zealand,

Infrastructure Auckland, 2003.

[76] J. Zhu, M. Sheng, J. Shang, Y. Kuang, X. Shi, and X. Qiu, "Photocatalytic Role of Atmospheric Soot Particles under Visible-Light Irradiation: Reactive Oxygen Species Generation, Self-Oxidation Process, and Induced Higher Oxidative Potential and Cytotoxicity," *Environ. Sci. Technol.*, vol. 56, no. 12, pp. 7668–7678, Jun. 2022, doi: 10.1021/acs.est.2c00420.

[77] S. Zhao, H. Jia, G. Nulaji, H. Gao, F. Wang, and C. Wang, "Photolysis of polycyclic aromatic hydrocarbons (PAHs) on Fe3+-montmorillonite surface under visible light: Degradation kinetics, mechanism, and toxicity assessments," *Chemosphere*, vol. 184, pp. 1346–1354, Oct. 2017, doi: 10.1016/j.chemosphere.2017.06.106.

[78] P. Wang, "Degradation of Polycyclic Aromatic Hydrocarbons on Montmorillonite and Formation Mechanism of Environmental Persistent Free Radicels," Kunming University, 2019.

[79] M. Li, F. Bao, Y. Zhang, W. Song, C. Chen, and J. Zhao, "Role of elemental carbon in the photochemical aging of soot," *Proc. Natl. Acad. Sci.*, vol. 115, no. 30, pp. 7717–7722, Jul. 2018, doi: 10.1073/pnas.1804481115.

[80] C. Chen, W. Ma, and J. Zhao, "Semiconductor-mediated photodegradation of pollutants under visible-light irradiation," *Chem. Soc. Rev.*, vol. 39, no. 11, p. 4206, 2010, doi: 10.1039/b921692h.

[81] G. Fang, C. Liu, Y. Wang, D. D. Dionysiou, and D. Zhou, "Photogeneration of reactive oxygen species from biochar suspension for diethyl phthalate degradation," *Appl. Catal. B Environ.*, vol. 214, pp. 34–45, Oct. 2017, doi: 10.1016/j.apcatb.2017.05.036.

Chapter 6: General conclusions and future outlook

6.1 General conclusions

This thesis developed a QuEChERS extraction method for rapid extraction of PAHs from powder aerosol samples based on the cyclone sampler, analyzed the pollution characteristics and human exposure risk of PAHs in atmospheric particulate matter in Japan during the COVID-19 epidemic, investigated the feasibility of ameliorating the PAHs exposure risk to humans through daily dietary intake, and finally, verified the concentration and valence properties of metal components attached to powder form aerosol samples.

In Chapter 1, the background and purpose of this paper are described. The definition and environmental effect of particulate matter were introduced, followed by general information on PM-bound polycyclic aromatic hydrocarbons (PAHs) including the substance properties, detecting, and emitting characteristics, and health toxicity. Pointing out the problems of conventional filter-particle collection method and PAHs extraction operation, and carrying out targeted research based on cyclone sampling device.

In Chapter 2, the optimization of the QuEChERS (quick, easy, cheap, effective, rugged, and safe) extraction method for the determination of PAHs in powder-form environmental standard materials (SRM1944) was described, and proved it is also effective for analyzing PAHs in powder aerosol particle samples collected by cyclone. In this study, an I-optimal design response surface method combined with a desirability function were used to investigate the extraction effect of PAHs under different combinations of QuEChERS extraction factors. The 2-factor interaction (2FI) model combined with boundary conditions were used to determine the optimized conditions, resulting in acetonitrile/dichloromethane (7:1, v/v), Na_2SO_4/NaCl (1:1, w/w), and primary and secondary amine (PSA) as extraction solvents, extraction salts, and clean-up reagent, respectively. The optimized method showed good recoveries of PAHs for

SRM1944 and standard solution. The results for cyclone-collected ambient powder aerosol particles extracted by the optimized QuEChERS illustrated that this improved procedure has good PAHs extraction efficiency as the traditional Soxhlet method, while reducing hazardous organic solvents usage, experimental cost (per mg sample) by 97% and sample pretreatment time.

In Chapter 3, PM-bound polycyclic aromatic hydrocarbons (PAHs) pollution characteristics were investigated in 30 powder aerosol samples collected by the cyclone over a long period in Yokohama, Japan from 2018 to 2023. The results indicated that the annual average of ∑PAHs concentrations showed an increasing and an opposite decreasing trend before and after the COVID-19 outbreaking in Japan. Correlation analysis showed that besides the removal effect of PM-bound PAHs by conventional meteorological conditions (precipitation, temperature, humidity), gaseous pollutants such as O_3 and NO_2 reacted photochemically with PAHs under solar irradiation which might cause its photo-gradation. In addition, source identification showed the main stable source of PAHs was still the incomplete combustion of fossil fuel, although the Japanese government's epidemic prevention and control policies have reduced the emission of PAHs in the aerosol. Finally, the PAHs health exposure risk was calculated to assess the incremental lifetime cancer risk (ILCR) for children and adults.

In Chapter 4, astaxanthin, an antioxidant enriched in deep-sea fish which is a favorite in the Japanese diet, was used to investigate its protective effect on A549 cells after PAHs exposure. In this study, the survival rate, ROS and inflammatory cytokine production were measured between the blank group cells exposed to PAHs standard solution only and the control group cells added with two different concentrations of ATX solution. The results of the experiments showed that significant differences were observed in the cell samples 48h after exposure in the control group cells compared to the blank group, which is opposite to the detection results after 24 h exposure. Subsequent experimental results using ambient aerosol samples to verify the actual protective effect of ATX shown the same results. Cells exposed to both two aerosol

samples showed a significant increase in survival with the addition of ATX solution and a significant decrease in intracellular ROS as well as in the expression of the inflammatory cytokines IL-6 and IL-8. This suggests that the protective effect of ATX on cells has a lagging effect, that is, even in the control cells with ATX, the cells are still stimulated by PAHs to produce ROS and inflammatory cytokines, and then ATX reacts with the intermediates produced to reduce the damage caused by them, thus achieving the purpose of protecting the cells.

In Chapter 5, Energy dispersive X-ray fluorescence spectroscopy (EDXRF) and X-ray absorption fine structure (XAFS) spectroscopy were used to measure the concentrations of nine metallic elements (Ti, V, Cr, Mn, Fe, Ni, Cu, Zn, and Pb) and the valence states of five target elements (Cr, Mn, Fe, Cu, and Zn) in coarse and fine powder PM samples, which collected using the cyclone at Kanagawa, Saitama, and Fukuoka in Japan in 2017. The EDXRF results indicated that the average contents of Fe, Ti, and Zn were much higher than those of the other six elements in all samples. The XAFS results showed that the major valence states of the elements were Cr(III), Mn(II), Fe(III), Cu(II), and Zn(II). The source identification results showed that the sources of metal contaminants in the samples varied considerably between sampling sites and depended on the industrial structure and geographical location of the sampling area.

6.2 Future outlook

1. ***Improving the QuEChERS extraction method for PAHs extraction in both cyclone and filter samples***

The optimized QuEChERS extraction method mentioned in Chapter 2 aimed to be used for cyclone-collected powder form aerosol samples PAHs extraction. In our research, this developed method showed good extraction effects as the traditional Soxhlet method. However, the filter-collecting method is still the most used and most reliable particulate matter collection method. The optimized QuEChERS parameters

used for powder sample extraction cannot be used for filter samples directly because of the limitation of filter structure, for example, the filter can absorb the organic solvent used for extracting, and thus the volume of organic solvent usage needs to be reconfirmed. Therefore, in the next step work, it is necessary to study the applied QuEChERS method for filter samples' extraction to realize the same quick, high-effect, and low-cost extraction result as used for powder samples.

2. *Using multiple regression models and machine learning methods for pollution factors interaction analysis*

Particulate matter is a complex combination of mineral dust, inorganic ions and salts, metallic, organic substances, and water, even microorganisms. The organic contaminants adsorbed on PM interact and react with other components and the gaseous environment all the time, therefore, it is one-sided only to study the single linear correlation between a certain substance or factor and the target pollutant to explain the contribution or impact of this factor on the target substance. The multiple regression model considered the multiple interactions of the target contaminant with other potential factors not just the contribution of one factor to the target. Suppose all information of the one sample, such as the sampling time, the main social activities at the sampling period, meteorological parameters, and contaminants concentration can be collected and gathered into a huge database. In that case, the researchers can use machine learning methods to establish the multiple models between PM-bound pollutants and other human/non-human factors to help understand the interaction of each other deeply. Moreover, as the size of the database becomes larger and larger, the model established will become more and more accurate. Thus, with the help of collected information, we can use the model to predict the air pollution situation within a certain period, and then propose targeted protective measures in a foreseeable manner.

3. *The underlying mechanism of astaxanthin's protective effect on PAHs-damaged*

cells

Ingesting certain antioxidant substances through diet is a safe and feasible method to protect human cells from damage caused by inhaled particulate matter. From the research results in Chapter 4, we can see that astaxanthin does have a certain protective effect on PAHs-exposed cells. This intuitive result proves that our research direction is correct. However, the current research results are still relatively superficial, and more in-depth experiments are needed to explore the deep protective mechanism of astaxanthin on cells exposed to PAHs, such as how astaxanthin affects the cell growth statues, the nuclear factor-kappa B (Nf-kB) signaling pathway and the arylhydrocarbon receptor (AhR) signaling pathway to produce an impact, and further impact on the expression of inflammatory genes, thus establishing a clear PAHs protection process from food intake to molecular response and gene expression.

4. ***Degradation/photooxidation process of PAHs on the surface of particulate matter and the role of metal components in this process***

The degradation of PAHs on clay minerals such as montmorillonite, vermiculite, and kaolinite has been well studied. The transition metal elements (Fe, Cu, Zn, etc.) contained on the mineral dusts can act as photocatalysts to produce a photo-Fenton system even in the absence of H_2O, which enhances the photodegradation of PAHs under visible light irradiation. In addition, the presence of Fe^{3+} ions can also promote the photo-induced electron transfer between the mineral dust surface and PAHs, accelerating the photolytic activation process of PAHs. This kind of study generally collects soil samples continuously at different moments started from a certain experimental point, detects the PAHs concentration as well as the transition metal content and valence state, and then obtains the kinetic equation of the degradation of PAHs and its electron transfer process with the metal components. It is difficult to perform continuous PAHs degradation experiments on conventional PM samples like filter samples due to the limitation of the filter structure. Still, the cyclone samples bring

the feasibility for this study.

In Chapter 5 we have shown that the dusty aerosol samples collected by cyclone can be used for EDXAF and XAFS to detect the content and valence of the metal components contained therein, and cyclone aerosol samples themselves are the most typical samples of atmospheric particulate matter. Continuously sampling and detecting the changes in the pollution characteristics of PAHs and metal components in powder aerosol samples under different simulated environments (e.g., dry/humid visible light environment, dry/humid UV environment), can help us better understand the degradation kinetics of PAHs on the surface of aerosol particulate matter under different actual atmospheric conditions and the contribution of metal components in this process.

List of publications

Original papers related to this thesis

(1) Weidong Jing, Katsutomo Saito, Takuma Okamoto, Hibiki Saito, Kazuki Sugimoto, Chiharu Nishita-Hara, Keiichiro Hara, Masahiko Hayashi, Shuichi Hasegawa and Tomoaki Okuda. (2022). Characterization of Elemental Composition and Valence State of Cyclone-collected Aerosol Particles Using EDXRF and XAFS at Three Sites in Japan. Asian Journal of Atmospheric Environment, 16(2), 40-58. https://doi.org/10.5572/ajae.2021.137

(2) Jing Weidong, Nakano, K., Shen, Z., & Okuda, T. (2023). Optimization of the QuEChERS extraction method to determine Polycyclic Aromatic Hydrocarbons (PAHs) in powder aerosol particles collected by cyclone. Environmental Technology & Innovation, 31, 103141. https://doi.org/10.1016/j.eti.2023.103141

International conference presentation

Jing Weidong, Nakano Kohei, Shen Zhenxing, Okuda Tomoaki.

"Optimized QuEChERS Method for Effective Extraction of Polycyclic Aromatic Hydrocarbons (PAHs) in Powder Aerosol Particles Collected by Cyclone", Poster presentation at the 13rd Royal Society of Chemistry-Tokyo International Conference (RSC-TIC), September 7-8, 2023. Chiba, Japan.

ACKNOWLEDGMENTS

Firstly, I would like to give my sincere and hearty thanks and appreciation to my advisor, Prof. Okuda for his kindness, illuminating guidance and profound knowledge. It has been a great privilege and joy to study and research under his guidance and supervision. The relaxed research atmosphere allows me to explore any possible research, and Prof. Okuda's erudite professional knowledge and rigorous research attitude can point out problems in my research and provide more feasible suggestions. Without his previous advice and guidance, this study could not have been completed.

Secondly, I express my appreciation to Associate Prof. Tatsuhiro Mori, Dr. Chiharu Nishita, Dr. Ryosuke Mitani, and Dr. Muhammad Aiman bin Mohd Nor for supporting my research and giving important advice and comments in developing my thesis and defense presentation. And sincere gratitude also goes to Researcher Ms. Hiroko Yamanaka for her guidance and help during my experiments, and Prof. Shen Zhenxing for helping and giving important advice for my paper writing.

I would also like to thank my thesis committee: Prof. Daniel Citterio, Associate Prof. Satoko Fujioka, Associate Prof. Taisuke Banno, and my advisor Prof. Tomoaki Okuda. Thanks to them for asking important questions and insightful suggestions that allowed me to recognize the shortcomings of my research and make improvements.

I am also grateful to all my labmates that Mr. Yuki Kuruma, Miss Kako Ogane, Mr. Kohei Nakano, Miss Momo Terasaka, Miss Hina Nagayama, Mr. Hiroaki Tonai, Mr. Keisuke Masaki, Mr. Shoya Manabe, Miss Moeka Tsuzuku, Miss Karina Tsubakida, Mr. Ryuki Kato, Mr. Toma Kanai, Mr. Yoshiya Sasaki, Mr. Ryoji Mukai, and Miss Takano Kobayashi who accepted me to join them to provide me an opportunity to better understand different culture, and have kindly provided my assistance and companionship in the lab working and researching for this paper. Besides, I would also thank to my all fellow labmates who have graduated for being friends with me and giving me their help with my online studying.

I would like to thank Keio Leading-edge Laboratory of Science and Technology (KLL) Ph.D. Program Research Grant has supported my research, and thank Yamaoka Kenichi Memorial Scholarship Foundation for helping me complete my Ph.D. studies.

I also express my sincere gratitude to my friends that Ms. Yang Liu, Miss Gong Diqing, Miss Zhao Luqi, Mr. Chen Kaixu, Mr. Li Dong, and all the other friends. I am very honored to meet these friends, and I am very grateful for their help and care in my daily life and study. Thanks to my friends for exposing me to a more exciting world, for lending a helping hand when I fell into endless confusion and wandering, and for being a beam of light in my monotonous and boring life. "*The language of Friendship is not words, but meanings.*"

Finally, my cordial thanks also go to my family members. Thank you to my parents for their spiritual and financial support. The encouragement and motivation from my family is the driving force for me to keep moving forward. Thank you to my brother for helping me in life and providing me with new inspiration and direction in research. Finally, I would like to thank myself for persevering all the way. I hope that I can still maintain enough curiosity and desire to explore the world, and continue to move forward on the right path.

JING, Weidong

January, 2024